SAHC

Numerical Evaluation of the bearing capacity of the All Saints' Church walls in Broumov, CR

Evi Susanti

Czech Republic | 2017

ADVANCED MASTERS IN STRUCTURAL ANALYSIS
OF MONUMENTS AND HISTORICAL CONSTRUCTIONS

Master's Thesis

Evi Susanti

Numerical Evaluation of bearing capacity of the All Saint's Church walls in Broumov, CR

UNIVERSITAT POLITÈCNICA
DE CATALUNYA

Czech Technical University in Prague

Education and Culture

Erasmus Mundus

ADVANCED MASTERS IN STRUCTURAL ANALYSIS
OF MONUMENTS AND HISTORICAL CONSTRUCTIONS

Master's Thesis

Evi Susanti

Numerical Evaluation of the bearing capacity of the All Saints' Church walls in Broumov, CR

This Masters Course has been funded with support from the European Commission. This publication reflects the views only of the author, and the Commission cannot be held responsible for any use which may be made of the information contained therein.

Czech Republic | 2017

CZECH TECHNICAL UNIVERSITY IN PRAGUE
Faculty of Civil Engineering
Thákurova 7, 166 29 Prague 6, Czech Republic

MASTER'S THESIS PROPOSAL

study programme: Civil Engineering

study branch: Advanced Masters in Structural Analysis of Monuments and Historical Constructions

academic year: 2016/2017

Student's name and surname: Evi Susanti

Department: Department of Mechanics

Thesis supervisor: Prof.Ing. Pavel Kuklík, CSc.

Thesis title: Numerical bearing capacity of the All Saints' Church walls in Broumov, CR

Thesis title in English see above

Framework content:

-Analysis of bearing capacity of sectional and longitudinal wall section

-Assessment of extent of stressess in walls due to soil settlement using 2D and 3D FEM modelling

-Inspection of the church and estimation of material properties of structure and subsoil

Assignment date: 7/04/2017 Submission date: 06/07/2017

If the student fails to submit the Master's thesis on time, they are obliged to justify this fact in advance in writing, if this request (submitted through the Student Registrar) is granted by the Dean, the Dean will assign the student a substitute date for holding the final graduation examination (2 attempts for FGE remain). If this fact is not appropriately excused or if the request is not granted by the Dean, the Dean will assign the student a date for retaking the final graduation examination, FGE can be retaken only once. (Study and Examination Code, Art 22, Par 3, 4.)

The student takes notice of the obligation of working out the Master's thesis on their own, without any outside help, except for consultation. The list of references, other sources and names of consultants must be included in the Master's thesis.

.....
Master's thesis supervisor

.....
Head of department

Date of Master's thesis proposal take over: July 2017

.....
Student

This form must be completed in 3 copies – 1x department, 1x student, 1x Student Registrar (sent by department)

No later than by the end of the 2nd week of instruction in the semester, the department shall send one copy of BT Proposal to the Student Registrar and enter data into the faculty information system KOS.

This page is left blank on purpose.

DECLARATION

Name:	Evi Susanti
Email:	Evi.susanti.89@gmail.com

Title of the MSc Dissertation:	Numerical evaluation of the bearing capacity of the All Saints Church walls in Broumov, CR
Supervisor(s):	Prof. Ing. Pavel Kuklík, CSc.
Year:	2016/1017

I hereby declare that all information in this document has been obtained and presented in accordance with academic rules and ethical conduct. I also declare that, as required by these rules and conduct, I have fully cited and referenced all material and results that are not original to this work.

I hereby declare that the MSc Consortium responsible for the Advanced Masters in Structural Analysis of Monuments and Historical Constructions is allowed to store and make available electronically the present MSc Dissertation.

University:	Czech Technical University in Prague
Date:	03/07/17
Signature:	

This page is left blank on purpose.

ACKNOWLEDGEMENTS

I would like to acknowledge Prof. Ing. Pavel Kuklik for the enormous support he had provided over the past three months. I would also like to thank the Erasmus Mundus program that granted my scholarship thereby allowing me the privilege of this SAHC programme. The following people, Dr. Jan Záleský, Dr. Kateřina Kovářová and Dr. Martin Válek, have also been supporting me with invaluable source of information in their respective field of expertise. Lastly, I would also like to mention Alexandra and Dr. Petr Kabele for assisting with administrative matters with regards to the university and visa matters allowing me to focus on thesis during these periods.

This page is left blank on purpose.

ABSTRACT

The All Saints' Church is part of the Broumov group of churches which tells the legacy of Bohemian baroque architecture in the northern Bohemian area. Built by the famous Dientzenhofer family of architects, these churches had their glorious times through the numerous ruling powers in the area for 300 years of its life. Once glorified, the All Saints' Church has now fallen to despair from decades of neglect. This report summarizes a structural investigation, using ATENA 2D finite element (FEM) software, ATENA-Gid FEM software and Geo5 geotechnical FEM software, to assess the safety of the church walls with regards to damages it currently faces, in particular due to differential soil settlement and recommendations for proposal for further studies, in terms of additional proposed tests and monitoring, and proposed repair and strengthening methods. The study is started off by summary of findings from preliminary historical, geotechnical background studies. A brief report from preliminary investigation conduction in the site was explained. Several conclusions of possible sources of decay and damage of the church is deduced. The most important sources include presence of moisture and possible differential soil settlement as a result of uneven deterioration of subsoil. In order to investigate the extent of damage the differential soil settlement could cause; a series of FEM modelling was employed. The first set of models aim to assess the bearing capacity of the enclosure wall, which is the main structural element in the church. From these models, it was known that structure is able to sustain the vertical loads it is subjected to. Hence, the damages it suffers should not be due to the compression loads. The wall's mechanical properties are derived from these models as an input for the soil-structure interaction FEM models. The second set of models involve modelling the structure with the subsoil underneath it. The subsoil properties are estimated from visual inspection of the bore log samples extracted. Stresses on the walls due to differential soil settlement from 2D and 3D models were analysed and found to be rather significant that further more detailed studies should be conducted to ascertain the safety of the church and the need for further strengthening. The deterioration of both structural components and subsoil were taken into consideration in analysis of the bearing capacity of the structure, estimation of geotechnical parameters and soil-structure interaction modelling. Repair regime to control the presence of moisture surrounding the church proximity is proposed. Furthermore, proposal on additional tests and monitoring to obtain a more accurate mechanical properties of the wall's constituting materials is elaborated. Lastly, a few methods of foundation strengthening are discussed in view of potential need to strengthen the foundation in the future.

This page is left blank on purpose.

ABSTRAKT

Kostel Všech svatých je součástí Broumovské skupiny kostelů, která významně prezentuje bohatství české barokní architektury v severočeském regionu. Kostel byl postaven proslavenou rodinou architektů, Dientzenhoferů. Broumovská skupina prožívala zlaté časy v prvních tři sta letech své existence díky značnému vlivu církve v regionu Broumovska. Vlivem hektických historických událostí, byl kostel Všech svatých v posledních několika desítkách let zanedbáván. Diplomová práce shrnuje výsledky stavebního šetření a podává numerickou analýzu současného stavu. Pro výpočet byl využit konečně prvkový software ATENA 2D, software ATENA-Gid MKP a geotechnický software Geo5 MKP. Analýza byla zaměřena na spolehlivost a únosnost stěn kostela. Ukázalo se, že poškození, které prezentují trhliny jasně vykreslené ve zdech, bylo způsobeno nerovnoměrným sedáním základů. Práce se zabývá návrhem testů ke zjištění parametrů jednotlivých prvků stavby a doporučuje postup jejího sledování. Jsou v ní též doporučené způsoby oprav a posílení jednotlivých nosných prvků. Studie je zahájena souhrnem zjištění vycházejících předchozích historických a geotechnických skutečností. Uvádí stručnou zpráva z předběžného šetření na místě. Z tohoto jsou vyvozovány možné příčiny rozpadání a poškození. Mezi nejdůležitější příčiny patří přítomnost vlhkosti a rozdílné sedání zeminy v důsledku degradace podloží. Za účelem ověření rozsahu poškození byla provedena řada numerických testů pomocí MKP. První sada numerických byla zaměřena na zjištění únosnosti nosných stěn kostela. Výpočtem bylo zjištěno, že únosnost stěn je dostatečná a stěny bez problémů unesou svislé zatížení. Z toho vyplývá, že porušení stěn není způsobeno tlakovým zatížením. Druhá sada numerických modelů je zaměřena na interakci stavby s podložím. Mechanické vlastnosti zdí jsou odvozeny z první sady numerických modelů. Vlastnosti podloží jsou odhadnuty z vizuální prohlídky vyjmutých vzorků z vrtů. Napjatost ve stěnách v důsledku nerovnoměrného sedání byla ověřena pomocí 2D a 3D numerických modelů. Ukázalo se, že účinky nerovnoměrného sedání jsou významné. Pro budoucí bezpečnost a úspěšné zajištění stability stavby budou nutné další podrobnější studie. Při analýze únosnosti konstrukce byla zohledněna deteriorace kamenného zdiva, a to obou jeho složek, stejně tak jako zhoršení únosnosti základů v důsledku degradace základového zdiva i podloží. Je navrženo opatření, které povede ke kontrole vlhkosti v blízkosti kostela. Dále jsou navrženy dodatečné zkoušky a monitorování, což povede k přesnějšímu popisu mechanických vlastností jednotlivých materiálů tvořících stěnu. Nakonec je diskutováno několik metod nutných k budoucímu posílení základů.

This page is left blank on purpose.

RINGKASAN

Gereja All Saints' adalah bagian dari grup gereja Broumov yang menceritakan pengaruh arsitektur Barok Bohemia yang hebat dan sampai ke ujung Bohemia Utara. Dibangun oleh keluarga arsitek Dientzenhofer yang terkenal, gereja-gerja ini telah melalui waktu-waktu gemilangnya di bawah penguasa-penguasa yang berbeda dalam 300 tahun masa hidup gereja ini. Namun sekarang, gereja All Saints' ini telah mengalami beberapa kerusakan dikarenakan pemeliharaan yang kurang selama berpuluh-puluh tahun. Laporan ini meringkas investigasi structural mengenai tingkat keselamatan tembok gereja All Saints' ini terutama dalam bidang penuruan tanah yang tidak seimbang. Laporan ini diawali dengan ringkasan penemuan dari investigasi sejarah dan geoteknis dari gereja All Saints'. Laporan singkat ini dilanjutkan oleh beberapa kesimpulan mengenai sumber-sumber yang mungkin menyebabkan kerusakan pada gereja All Saints' ini. Sumber yang paling penting termasuk adanya kadar air yang tinggi dan penurunan tanah yang tidak seimbang disebabkan oleh kadar air yang tinggi di tanah. Untuk menginvestigasi sejauh apa penurunan tanah tidak seimbang ini bisa menyebabkan kerusakan pada gereja All Saints' ini, beberapa model FEM dianalisa. Sekumpulan model pertama bertujuan untuk menemukan daya tampung dari tembok gereja ini yang sangat heterogen. Dari model-model ini bisa disimpulkan bahwa kapasitas tembok ini dalam kompresi sangatlah cukup, makan kerusakan gereja kemungkinan bukan karena kurangnya kekuatan tembok. Lalu, dari model-model ini juga disimpulkan besarnya kekuatan dan modulus Youngs' dari tembok gereja ini untuk digunakan di model selanjutnya. Sekumpulan model yang kedua bertujuan untuk mengetahui seberapa besar tekanan pada tembok gereja yang disebabkan oleh penurunan tanah tidak seimbang. Tekanan pada tembok yang ditemukan lumayan besar. Di akhir laporan ini, beberapa kesimpulan dibuat termasuk ada perlunya untuk memperbaiki saluran air di gereja dan untuk mempelajari unsur-unsur bangunan dengan lebih teliti sehingga perkiraan parameter mekanis dari tembok dan tanah bisa dibuat dengan lebih akurat. Akhirnya, beberapa rekomendasi untuk kemungkinan pelajaran lebih lanjut dan perbaikan gereja diberikan.

This page is left blank on purpose.

TABLE OF CONTENTS

LIST OF FIGURES

LIST OF TABLES

This page is left blank on purpose.

LIST OF SYMBOLS

a	half of width of foundation (m)
A	cross sectional area of soil (m^2)
b	width of the foundation modelled (m)
c_1	soil matrix constant representing compressive deformability (MPa/m)
c_2	soil matrix constant representing shear deformability (MPa.m)
c_{1w}	Winkler Pasternak constants (MPa/m)
c_{2w}	Winkler Pasternak constants (MPa.m)
C_e	exposure coefficient (unitless)
C_t	thermal coefficient (unitless)
D	material stiffness matrix (kPa)
e	strain vector (unitless)
ε_c	strain of material at peak compressive stress (unitless)
ε_d	strain of material at failure compressive stress (unitless)
ε_o	strain of material at failure tensile stress (unitless)
ε_t	strain of material at peak tensile stress (unitless)
ε_x	strain components of the plane stress state in x-direction (unitless)
ε_y	strain components of the plane stress state in y-direction (unitless)
E	Young's modulus (GPa)
$E_{computer}$	Young's modulus to be modelled into the computer (GPa)
E_{sec}	secant Young's modulus (GPa)
E_T	Young's modulus at time T (GPa)
E_{ur}	unloading/reloading Young's modulus (GPa)
E_{wall}	Estimated material's actual Poisson ratio (GPa)
ε_{el}	elastic strain (unitless)
ε	strain (unitless)
f_c	peak compressive stress (MPa)
f_t	peak tensile stress (MPa)
F_s	vertical load (kN)
f_z	compressive stress experienced by soil (MPa)
G_f	fracture energy required to cause tensile failure (kN.m)
h	depth of soil excavation (m)
H	depth of influence zone (m)
H_w	total height of wall modelled (m)
I	second moment of area (m^4)
I_B	Boussinesq coefficient (unitless)
k	deformation modulus of soil (kN/m)

L	thickness of soil depth (m)
p	pressure (MPa)
q	surcharge (MPa)
Q	point load (kN)
r	horizontal distance of the point in study to the point load application (m)
s	stress vector (MPa)
s_L	snow load (MPa)
s_k	characteristic snow for a region (MPa)
σ_x	stress components of the plane stress state in x-direction (MPa)
σ_y	stress components of the plane stress state in y-direction (MPa)
σ_z	compressive stress (MPa)
t	time (s)
T	Tensile load (kN)
μ_i	snow load coefficient (unitless)
v	Poisson's ratio (unitless)
$v_{computer}$	Poisson's ratio to be modelled into the computer (unitless)
v_{wall}	Estimated material's actual Young's modulus (unitless)
dV	infinitesimal particles of volume (m^3)
w	crack width (m)
w_c	crack width at failure (m)
w_s	soil deformation/settlement (m)
X	reduction in length (m)
γ	unit weight of soil (kN/m^3)
γ_{xy}	shear stress components of the plane stress state in xy-direction (MPa)
z	depth of the point from the load application (m)

1. INTRODUCTION

Czech Republic is home to numerous important cultural heritages in Europe. History of human civilization on this land dates back to end of the fifth century when the Slavs arrived in the territory. However, it was not until the 14th century during the Premyslid dynasty that the Czech states reached the peak of its power. During this period, a lot of constructions started to spring around the country. The land had seen numerous shifts in the ruling power, but owing to its location, it has always remained an important part of European history and historical buildings continued to flourish over the years [1].

Unlike the current construction industry, builders from the past designed based on geometrical rules sanctioned by the experience and the observation of past successful structures. The first rational design approaches were formulated in the 17th century. However, these guidelines are very much generalized and knowledge of different types of construction material and subsoil was very limited. As a result, these historical buildings are typically under designed or over designed. The ones that have survived until now typically belong to the latter. Over the course of hundreds of years, however, accumulated stress from soil settlement, deterioration of materials and earthquakes create many problems in these buildings nowadays. In Czech Republic, the problem of deterioration of materials due to lack of maintenance is very prevalent; one of the reasons for this being the centralized state ownership of most properties during the communist regime [2]. As people were living in a property that they do not own, maintaining these buildings was deemed unnecessary. One such example is the Broumov group of churches that is the subject of study in this report.

The Broumov group of churches is built in the part of Czech Republic that has the most amazing rock formation. The rock formation consists of varied sandstone quality with a climate of high rainfall and cold weather [5]. Engineering in the past were not able to detect the correct soil type to design it against differential settlement. The current technology, though, has enabled engineers to obtain samples of the foundation and estimate the parameters needed to assess effect of soil settlement on the church. In addition, depending on the structure rigidity and the arrangement of the soil, the stress distribution on the soil and in turn its settlement and the stresses that are subjected to the structure will be different. In this paper, the soil structure interaction modelling will be performed and the deduction of this causing the cracks on the church walls will be assessed.

In addition, due to the church construction funded mostly by the local villagers which were not very well off, the walls of the church were constructed by various types of materials and the skills of the masons are not that high. The different skills of construction and the different types of construction materials around the church brings about lateral tension within the walls as different parts of the wall settle compresses in different manner with the same compressive force. Additionally, the different Poisson's ratios of the different material intensify this effect. The wall sections in transverse and longitudinal

directions will be modelled in this paper to analyse the effect of this lateral tension in the formation of cracks.

2. HISTORY

Before works on a cultural heritage is done, it is important to study the settings at which the building is built. These include the time period of the construction, the reigning power of the locality and the main figures involved in the construction such as the builder and the client. Understanding these aspects allows conservator to better apprehend the importance of the building, the construction techniques used in the construction, as well as possible sources of damage that happened in the past.

2.1 Bohemia

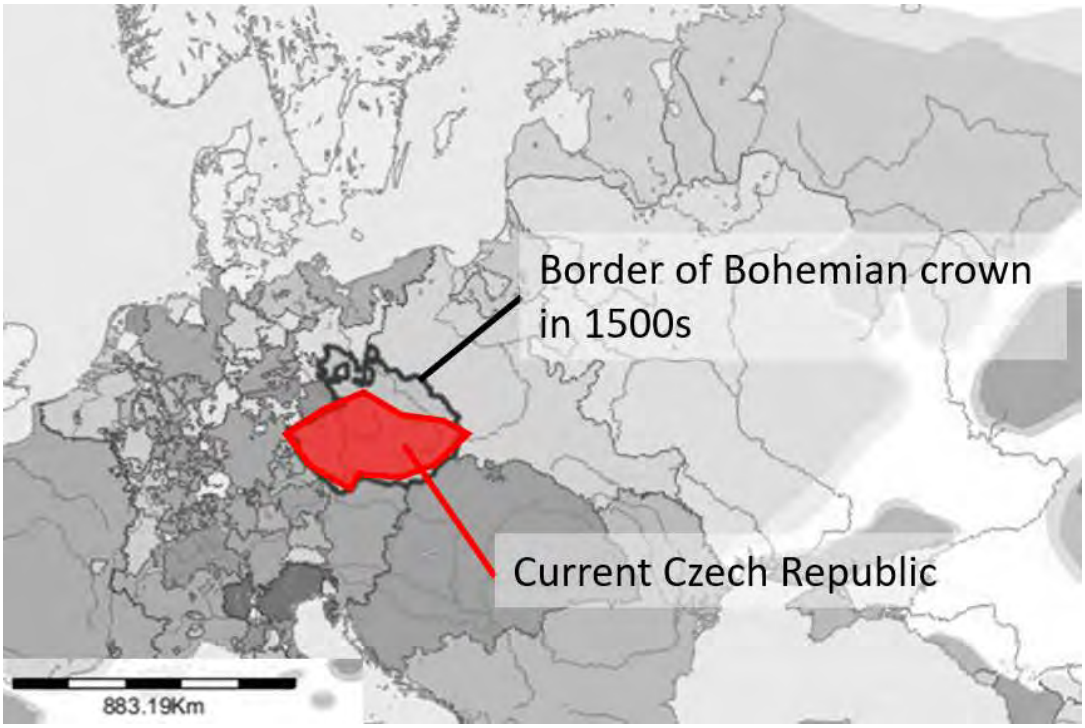

Figure 2.1. Map showing the current territory of Czech Republic and the Bohemian crown border in the 1500s [3]

As can be seen from Figure 2.1, the current Czech Republic boundary falls pretty much within Bohemian crown boundary in the 1500s, and so was the building that is studied in this report.

Bohemia's history goes as early as the ninth century dominated by the Slavs tribes. The influence of Christianity was soon brought from the land of Moravia by prince Wenceslas who later became the patron saint of Bohemia. As an independent state and part of the Holy Roman empire, several Bohemian kings were crowned emperor of the Holy Roman empire as well, one of whom is Charles IV who established Bohemia to the peak of its power [4].

Charles' successor, though, was not able to carry his legacy and the turbulent era of reformers including the Hussite weakening rule of Bohemian kingdom until it was defeated by the catholic Habsburg empire

in mid-16th century. It was still an independent state but it was largely influenced by the Habsburg nobles' rule. Catholic rule over the Christian majority during this period created much tension within the area, especially in Prague [4].

The 17th century witnessed several dramatic events that shaped Bohemia, the first of which was the defenestration (out-windowing) in Prague in 1618 A.D. Two Habsburg-appointed catholic regents were forcibly thrown out of Hradcany fortified palace windows. This event triggered the events leading to Thirty Years' War between the Catholics and the Protestants in Central Europe. At the time, the catholic Bohemian king crowned by the Habsburg, Ferdinand II, imposed rigorous Catholicism of Counter-Reformation which was not welcomed by the population. In 1619, he became the Holy Roman Emperor but was dethroned in Bohemia when the protestant Frederik V was crowned Bohemian king by the local protestant party. However, Frederick was soon defeated at the battle of White Hill (1620) by the forces of Ferdinand II and his allied Bavarian army. The following Thirty Years' War (1618 – 1648) had a significant effect on Bohemia, exhausting the country's finances and wiping out much of its infrastructure [4].

The Broumov group of churches were built in the beginning of the 18th century as Bohemia started to recover from the damages inflicted by the war. These events from the 16th to early 18th century preceding the construction of these churches would have significant impact on the monument [5].

2.2 Baroque architecture in Bohemia

The defeat of reformist Bohemian nobles at the Battle of White Mountain (1620), the Thirty Years and emphatic re-Catholicization led to the emigration of leading advocates of Czech architecture and the influx of foreign nobles. The great wealth and political power of the church and the nobles resulted from confiscation of properties from the old ruling nobles enabled the new ruling power to reconstruct even the countryside churches and chapels to support their re-Catholicization campaign throughout Bohemia. This resulted in change in the landscape of Bohemian architecture that lasts up till now [6].

Baroque architecture in Bohemia comes to Bohemia together with the influx of foreign Catholic nobles and originates from Italy. Baroque architecture in Italy started in the early 17th century accompanying the Counter-Reformation that was intended to restore Catholic's popularity after issues it had faced due to Protestant Reformations. As the Roman Catholic Church looked for a way to manifest its influence and regain lost souls all over Europe, it turned its attention to church architecture. The new style of church architecture was intended to touch human emotion as compared to the previous styles which appeals more to human intellect. The very act of approaching and stepping into a church had to become more of an experience that entice believers into the grandeur of the church, but also strongly welcome them to a strong attachment to the church [7].

Baroque style architecture differs from the previous Renaissance style which was very strict with rules. It allows very dynamic designs, employing a mixture of repetition, breaking-up, and distortion of Renaissance classical motifs. Typically, Italian Baroque architecture makes much larger use of

abstracted or exaggerated elements to provide more dynamic interiors. The building interiors usually contains much decoration including frescoes, paintings and ornaments. These exaggerated features coupled with large gold statues of Christian figures imposes feeling of domination and protection [7].

While the early baroque period in Bohemia in the early 17th century was dominated by Italian architects, the high Baroque period later in that century saw emergence of architects of Bohemian or Moravian birth and architects from Bavaria. One of the most significant architects of the High Baroque period was Dientzenhofer family, who came to Bohemia from Bavaria and lived in Prague. Christoph and his son Kilian Ignaz Dientzenhofer are known for their style called "radical Baroque", which was inspired by examples from northern Italy, particularly by the works of Guarino Guarini, and which seeks to express movement. It is characterized by the curvature of walls and intersection of oval spaces. However, this was later adopted into a Czech version of the style by local architects. One of their most important work include the St. Nicholas Church in the Lesser Town of Prague which becomes one of the most important Baroque churches in Europe. It was with this style that the Broumov group of churches was constructed [6].

2.3 Broumov region

The region of Broumov is distinctive for its wild and poetic landscape and architecture. The landscape of this region is diverse with mountains, valleys and bizarre rock formations and also mosaics of forestland, meadows and grassland. Coupled with the Baroque buildings constructed mainly under the order of the Benedictine order, it creates a “genius loci” – spirit of this place – that makes Broumov an enchanting region. The construction of the most important historical buildings in this area was attributed to the history of this region being a very important cultural centre in the area from the 13th to the 19th century. These buildings include the two Benedictine monasteries in the towns of Broumov and Police nad Metuji, a group of twelve churches and chapels in surrounding villages, the oldest wooden church in the town of Broumov, brick farmhouses and typical German folk houses. Other than the monasteries and the oldest wooden church, most of these buildings have been neglected over the years and are in much need of repair [8].

The legacy of Broumov region goes back to the 13th century when it was colonized by the Benedictine order of Brevnov when the land was given to them by King Premysl Otakar I. The town of Police were occupied mostly by people of Bohemian origin, while the town of Broumov by people of German origin. Monasteries in Broumov and Police were later built as centres of Benedictine order in this region of Bohemia. After the completion of the monasteries, the monks carried out a planned colonization to anticipate the growing population. This results in the villages surrounding the towns and other functional buildings in the main towns, as what is present today [8].

Due to its location and diverse population, this region experienced many political and religious upheaval. This includes conflicts between Catholics and Protestant, Thirty Years’ wars and plagues. However, it has always managed to recover itself thanks to the good economic status and business activities of the

Benedictine abbacy. In the aftermath the Thirty Years' War in 18th century, this area saw major renovation of the monasteries and new constructions of new stone Baroque churches replacing old wooden churches by the order of the abbot. This development continued on to the 19th century when this area experienced great prosperity due to the development of the textile industry and the political freedom. This was manifested in the population boom and building of places of worship of architectural values in surrounding villages [8].

This prosperity would not last in the 20th century. After the Munich Agreement in 1933, the Broumov region was divided - Broumov and Teplice, whose inhabitants were mostly of German origin, became part of Hitler's Third Reich and Police was part of the Protectorate Bohemia - Moravia. German's defeat in the Second World Was undid this division and returned the area back to Czechoslovakia. The German inhabitants who would not swear allegiance to Czechoslovakia were evicted from the country. The population of this area would be reduced by about two third deeming many buildings unnecessary as the inhabitants were gone. This was made worse by the nationalization of many buildings due to the communist ideology leading to minimal or no maintenance of the buildings by the locals. This led to the current damaged state of the buildings currently [8].

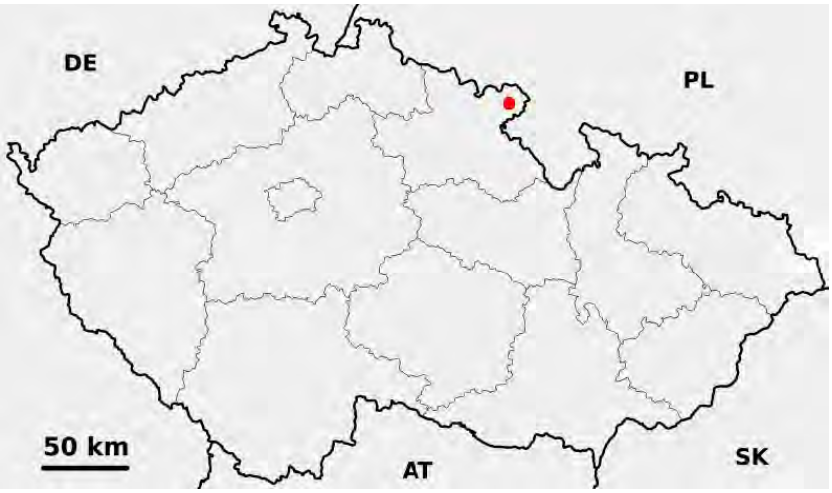

Figure 2.2. Location of Broumov within the Czech Republic [9].

2.4 Broumov group of churches

The term "Broumov group of churches" include numerous Baroque parish country churches in the villages of Broumov-Brevnov abbey. The important value of this group of churches also stems from the single client, the single family of builder and the short construction span. This gives a cultural identity of the whole complex of estate, geographically delimited area of plateau surrounded by ridges. This is further accentuated by the closeness of the Baroque shapes to the natural rocky formation surrounding the area [5].

Most of these churches were built in the beginning of 18th century under the order of abbot Otmar Zinke and builders Dientzenhofers. Charismatic Otmar Zinke replaced Sartorius as abbot in 1700 and in 1709 hired the Dientzenhofers as the architects and builders of his new churches. The Dientzenhofers began by constructing a new monastery and renewing the church in Police. Killian Ignaz Dientzenhofer worked under his father, Christoph Dientzenhofer, who later passed away in the middle of the construction of this group of church. Kilian took over the role as builder for churches in Vernéřovice, Ruprechtice and Otovice and completed them based on his father's previous designs in 1720, 1730 and 1726 respectively. In the years to follow, he built and designed churches in Hermakovice, Viznov, Bezdekov, Sonov and Bozanov. While Christoph's style revolves around centralized oval or octagon with embedded pillars, Killian took this further to incorporate more unconventional curves on the building plan [5].

This group of churches also has another similarity among them. They are country churches that had to meet very fundamental and practical requirements met in their designs. Due to the limited amount of funding available and the lower skill level of the local mason, design of these country churches had to be kept simple and economic while displaying its beauty. The typical design was a single nave structure with a bell tower without complicated structural details. All of the churches were built with false timber ceilings designed to imitate masonry vaults that significantly reduces horizontal thrust on the enclosure wall allowing thinner walls. Another distinguishing characteristic of these church is the steep hipped roof that rivals the bell towers in height and creates impressive silhouettes in the countryside. Other than for aesthetic reason, these roofs were designed to allow snow and rain to run off quickly. Originally the roofs were shingled in red painted wood but have been replaced by the more durable slate [5].

The main purpose of these churches was to present a dominating building at the main road or cross roads of a town along main trading routes. These extensive buildings were meant to showcase the prompt restoration of the area after the damages from the wars impressing travelling merchants with their wealth, ultimately resulting in larger trade and attention [5]. The Dientzenhofers were capable of meeting all the practical requirements of the churches while creating a unique Broumov Baroque architecture. Examples of their design are shown in Figure 2.4.2 and Figure 2.4.3.

Figure 2.3. Photo of St. Jacob the Greater's church in Ruprechtice, Czech Republic.

Figure 2.4. Photo of St. Ann's Church in Viznov, Czech Republic

2.5 All Saints' Church in Hermankovice

All Saints' Church in Hermankovice was built replacing the role of the wooden church constructed by abbot Thomas Sartorius in 1672 as the main worship place in this village. In the beginning of settlement of this village, there was a Gothic church in Hermankovice that was said to have already been there in the year of 1353. This was later replaced by the wooden chapel in 1672. Riding on the wave of stone church construction in the time of abbot Zinke, the current church was constructed in Hermankovice in

the first quarter of the 18th century. Preparation works for the construction of the current church started in 1720, the ground stone was laid in the following year and the church was finished and consecrated in 1723 by abbot Zinke. The design of the church was done by Killian Ignaz Dientzenhofer and the church was built by local master builder. Due to the lack of funding, the essential structural component was the main requirement of the initial construction. The decoration in the interior as well as the altar was brought into the church at a later time in the decade [5].

As mentioned in the previous section, the Broumov group of churches were built with an intention to flaunt the wealth of the region. This is reflected very well in the case of this All Saints' Church. The church is located on a hill in the middle of the village above a cross road of a track going to Ruprechtice. Furthermore, the church orientation, westward, is rather atypical. This was done to expose it more to traveller traveling to Broumov. View from the main road going to Broumov offers wide silhouette of the lateral façade [5].

The church is built on a ground plan with a distinctively prolonged central. The longitudinal axis is elongated with the inclusion of vestry behind the altar and the bell tower at the front façade location. The presence of the high bell tower and the high roof created a monumental effect of the building. The walls are accentuated with piedroits and cavities giving a more dynamic look to the church both from the outside and the inside. The building structural system itself is really simple with a single nave and columns embedded in the walls, but general shape of the church being an oval combined with the embedded rounded columns gives a continuous convex-concave curved internal wall. This church shows the mature work of Killian Ignaz Dientzenhofer in its exceptional scenic effect, dynamic size and impressive interior [5].

Figure 2.5. Walls accentuated with piedroits and cavities of All Saints' Church in Hermankovice, Czech Republic.

This page is left blank on purpose.

3. PRELIMINARY INVESTIGATION

3.1 Visual Inspection

Visual inspection was carried out to assess the current condition of the church in one visit on May 4th, 2017. The areas surveyed were the internal and external façade, the bell tower and the sacristy walls. The main objectives of the inspection were:

- Mapping of current damage and decay (including deformation, presence of moisture, material degradation, and biological activity) of the church with focus on the church wall.
- Categorization of cracks in terms of type, length, and width;
- Measurement of some critical dimensions of the wall

The inspection equipment included artificial light, measurement tools (measuring tape and ruler), and recording equipment (drawings, digital cameras).

The results from the investigations are elaborated in the following few sub-chapters.

3.1.1 Description of church geometry

The church is 44 metres long and 20 meters wide, including the bell tower and sacristy as can be seen in the floor plan in Figure 3.1. The masonry walls are on average 1.2 meters wide with exception of the sacristy wall which is 1.0 meters wide. The main nave is 27 metres by 17 metres.

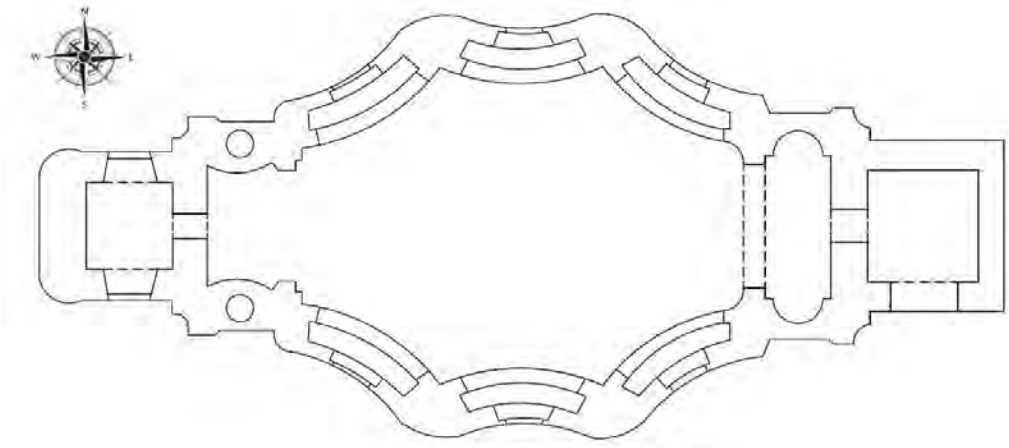

Figure 3.1. Floor plan of All Saints' Church in Hermankovice, Czech Republic.

3.1.2 Decay

3.1.2.1 Moisture

Moisture signs could be observed infiltrating the false stone that covers the bottom half meter of the external church enclosure wall [Figure 3.2]. Similar signs of moisture could be observed from the interior of the church [Figure 3.3].

3.1.2.2 Biological growth

Biological growth in the form of fungi, algae and moss could be observed at the bottom of the enclosure wall almost throughout the church. In the interior of the church, biological growth on the southern wall is limited to small patches of algae, but larger patches of fungi, algae and moss growth dominate the bottom of the northern wall [Figure 3.4]. At the exterior of the church, the same pattern is observed that the decay of the bottom of the wall is more extensive at the northern wall than it is on the southern wall. While there is microorganism growth on both façades, on the northern wall, it is more spread out and there is moss growth as well.

Other than at the bottom of the walls, algae and moss growths are concentrated at the kink where the enclosure wall joins with the wall of the sacristy [Figure 3.6].

3.1.2.3 Delamination of rendering and plaster

Throughout the church, the building plaster and rendering are observed to have deteriorated and at some parts the inner masonry are completely exposed due to decay of the rendering. In the interior of the church, this effect is limited to the bottom of the walls and the kink area where a new rainwater downpipe is observed at the exterior [Figure 3.7]. However, on the exterior, this effect is observed to be more extensive. Renders at the top of the wall as well as most of the renders at the convex part of the wall are observed to have been completely deteriorated exposing the inner masonry [Figure 3.7]. Furthermore, the condition on the northern wall is again observed to be worse than it is on the southern wall.

Figure 3.2. Moisture signs at the church exterior

Figure 3.3. Moisture signs in church interior

Figure 3.4. Biological growth on the southern wall (left) and on the northern wall (right) in the interior of the church

Figure 3.5. Biological growth on the southern wall (left) and on the northern wall (right) in the exterior of the church

Figure 3.6. Biological growth at the kink at the lateral façade where a water downpipe is located from the exterior (left) and the interior (right)

Figure 3.7. Render and plaster deterioration on the external southern wall (left) and northern wall (right)

3.1.3 Damage and cracks

3.1.3.1 Cracks on transverse arches of the church

Extensive series of cracks transverse arches bridging the northern and the southern façade were observed [Figure 3.8]. This series of cracks are found consistently throughout the church from the arch connecting the entrance hall and the main central area to the sacristy northern wall. The cracks could be categorized as small cracks at the bottom of the mid-arch, large cracks at the top left and right end of the arches.

Figure 3.8. Cracks on transverse arches bridging the northern and southern facade

3.1.3.2 Cracks at the sacristy vault

Cracks are also observed at the connection vault connecting the sacristy and the rest of the church. The cracks form a continuous line separating the sacristy and the rest of the church [Figure 3.9].

Figure 3.9. Continuous crack separating the sacristy vault to the main church wall

3.1.3.3 Cracks on the western façade behind the sacristy

As can be seen from Figure 3.11, there is a large crack running from the ground to the top of the western façade behind the sacristy. This crack is consistent with the other cracks in the transverse arches in the church.

3.1.3.4 Crack on the longitudinal façade near the kink of the church that is degraded due to faulty drainage system

Furthermore, there is a crack originating from the foundation to the window opening near the kink where faulty drainage system is observed []. This indicates potential movement of the church due to poorer soil condition in this area as compared to the other areas.

Figure 3.10. Crack on the longitudinal façade near the kink of the church

3.1.3.5 Minor typical cracks

Other minor typical cracks including the ones due to relieving arch above openings were observed as well, but they are of little concerns as they are rather small and limited. Hence, they will not be discussed here.

3.1.4 Signs of later reconstruction

Some signs of reconstruction could be observed on the walls from the presence of ill-located brick blocks that are covered with render recklessly at random location [Figure 3.12]. furthermore, the frames around the doors and windows are observed to be constructed with majorly regular brick masonry [Figure 3.13]. The same kind of stones that are randomly places in other parts of the walls are arranged in an organized manner at the sacristy walls. It could be inferred that these frames were reconstructed or added at a later time after the completion of the church.

Figure 3.11. Large crack on the western facade behind the sacristy

Figure 3.12. Ill-located brick blocks showing signs of reckless repair

Figure 3.13. Frame around sacristy door

3.2 Geotechnical Investigation

3.2.1 Subsoil in Hermakovice

The subsoil in the area where All Saints' church is sitting on is described as combination of feldspathic sandstone, volcanic breccia and conglomerate with layers of ryolitic tuff [Figure 3.14]. While sandstone, breccia and conglomerate are sedimentary stone, conglomerate is metamorphic stone and ryolite is igneous stone. The rock type is categorized as consolidated sediment and volcanic. The subsoil was a formation from continuous volcanic activities [10].

Ryolite is plutonic rock – rock that is formed by magma cooled rapidly at or near the earth's surface. This corresponds with the placement of ryolite at the bottom of the soil layers. Ryolite is a felsic extrusive rock with high silica content. Hence, it has high strength and hardness as compared to the other rocks [11].

Sandstone and breccia can be categorized as sedimentary stone. Sedimentary stones are formed either by build-up of sediments from rivers, sea, wind or precipitation. In the case of Hermankovice, it is likely the case that at the time when volcanic activity in this area became inactive, wind and rain erode sediment and build it up downstream creating layered sedimentary rocks. Due to its nature, elements constituting sedimentary stones are very diverse. Its durability and strength depends very much on the cementing material and the chemical constituents of the sediments. Furthermore, the thicker each bedding in sedimentary rock, the more resistant the rock is. This is due to low cohesion between each bedding as compared to cohesion between particles within each bedding [12].

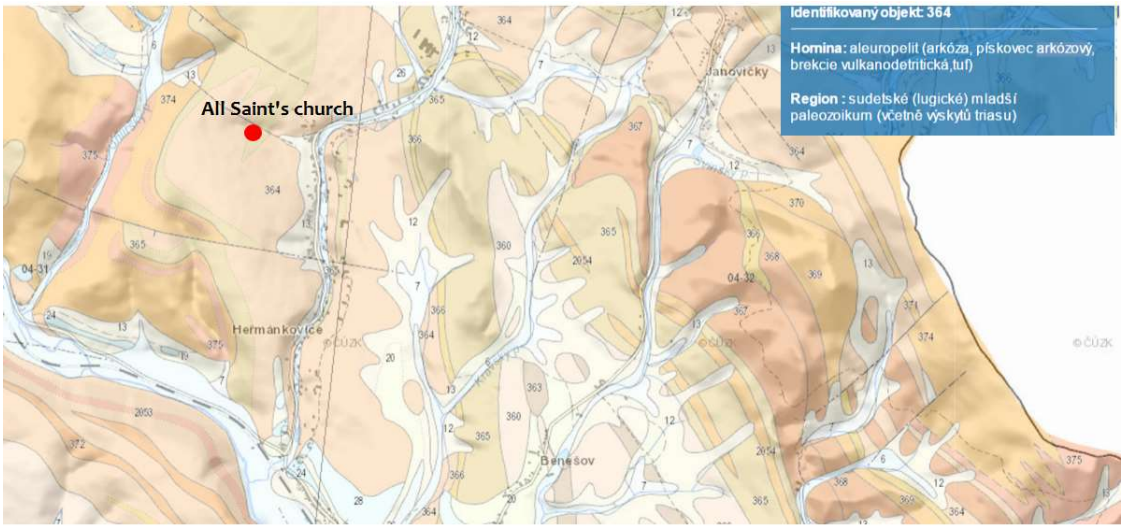

Figure 3.14. Soil map showing position of All Saints' church and its soil description

3.2.2 Subsoil description from boreholes next to church walls

Two boreholes were bored just outside the church wall. One borehole was installed next to the northern wall and another next to the southern wall. The bore log description and the photos of the extracted soil

and rock coring samples are shown in Table A.1 to Table A.3 and in Figure A.1 to Figure A.4 in Appendix A respectively.

In general, the soil extracted from the borehole next to the southern wall shows better characteristics rather than that from the borehole next to the northern wall. The soil extracted from the northern side shows more moist and weaker sandstone fragments, while that from the southern side shows drier and stronger sandstone fragments. However, below 6m, both sides show very good bedrock made of ryolite.

From the extracted soil samples from the southern wall, it could be observed that the soil of the first 1.65m is made up of larger and less degraded fragments as compared to the layer just beneath it. This could be an evidence showing that the former foundation of the church on the southern side was up to 1.65m. This distinct line of separation, however, is not present in the soil sample from the northern side of the wall. This indicates worse degradation of foundation under the northern wall.

As can be seen from the samples, the soil beneath the church consist mostly of weak rocks. Hence, Standard Penetration Test using N-number was not appropriate to be done to determine the soil properties. Furthermore, there is no soil extracted in between the rock fragments. This was because the soil is too loose. These components crumble as the tube is extracted leaving the rock fragments. Consequently, standard mechanical property tests were not able to be done on these samples. As a result, the only available information on the soil at the moment are the sample tubes and the descriptions.

3.3 Conclusion of preliminary investigation

3.3.1 Decay due to groundwater infiltration

As described in the previous chapter, much of the decay of mortar, stones and extensive biological growth could be found at the bottom of the wall. A plausible explanation is decay due to groundwater infiltration causing moist environment on the stones that is suitable living environment for moss, algae and fungi.

3.3.2 Deterioration due to rainwater splashing and drainage system failure

Furthermore, particularly appalling condition of a strip of wall at the kink on the enclosure wall near the sacristy was observed. Currently there is a rather new rainwater downpipe of to channel water from the gutter that is located surrounding the roof of the church. It could be plausible that this decay of this strip happened in the past due to broken water downpipe causing the wall being substitute channel for water to travel down. Alternatively, this could well be due to clogged water downpipe. The gutter at the top of the roof is an open channel. Leaves from nearby trees that are blown towards this channel would readily clog the pipe causing rainwater from the roof to gush down the wall instead.

3.3.3 Worse deterioration on the northern wall due to its orientation and terrain

The decay on the northern wall is observed to be more pervasive as compared to that on the southern wall. Since the decay is mostly due to presence of moisture on the wall, there are two likely explanations to this. Firstly, the northern facing wall is exposed to less sunlight. Moisture on these walls will evaporate at a slower rate due to less exposure to sunlight. Furthermore, the terrain on which the church is sitting on is sloping downwards with the northern lateral wall being on the higher ground as compared to the southern lateral wall. Rainwater that falls down from the roof and the adjacent higher ground will end up ponding this naturally made channel [Figure 3.15]. This ponding exposes both the wall and the subsoil underneath it to more moisture source.

3.3.4 Damage due to differential soil settlement

As described earlier, the soil below the northern façade is found to be poorer compared to that below the southern façade. This is likely to be connected to the higher exposure of moisture and less exposure of sunlight for the soil beneath the northern façade. Coupled with the series of cracks along the transverse arches and the transverse western wall, this could suggest differential settlement between the northern and southern façade resulting in stress build-up in these transverse elements.

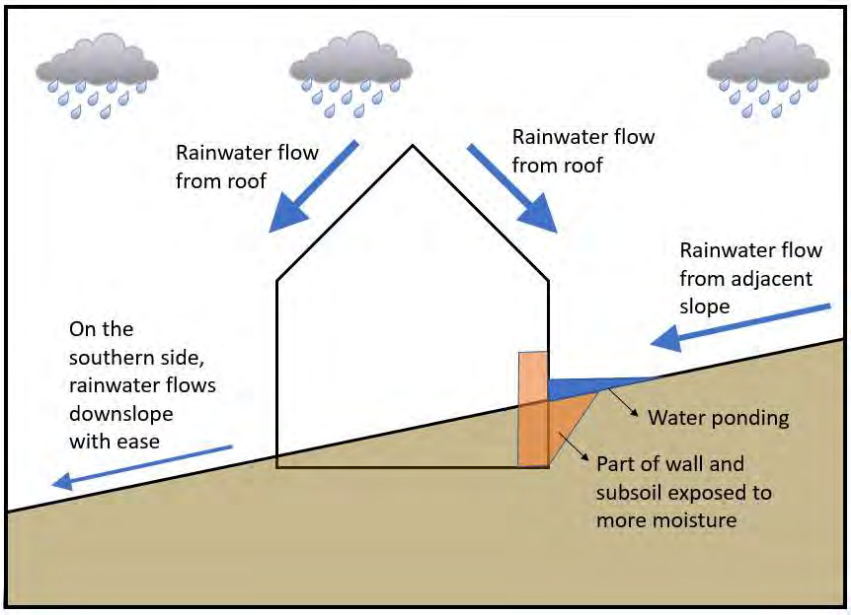

Figure 3.15. Diagram showing the higher exposure of moisture of the northern wall due to the church terrain

This page is left blank on purpose.

4. STUDY ON WALL BEARING CAPACITY

As can be seen from Figure 4.1, the church enclosure wall is made up of stone rubble masonry. The stones are of uneven sizes even if they are mostly of rectangular shape. There are at least three different types of stones that could be observed, along with some patches of bricks that were added in unsuitable manner. Furthermore, considering the thickness of the wall – up to 1.2 meters, it is very likely that the enclosure wall is made of at least three-leaf walls with inner infill material. This heterogenous nature of this enclosure wall makes estimation of wall bearing capacity using certain standards very much inappropriate and inaccurate. Hence, modelling representative parts of the wall to obtain its mechanical parameters would be necessary.

Figure 4.1. Enclosure wall masonry from the exterior shows non-uniform mixture of stones making up the outer leaf masonry layer

4.1 Description of models used for analysis

In this study, four different arrangements of cross-sectional cut of stone masonry from different parts of the enclosure wall and two arrangements of longitudinal cut of the wall will be analysed using ATENA 2D. It is a 2D Finite Element Software (Plane strain) for non-linear analysis of structures. The main advantage of this programme is that it automatically considers internal force redistribution due to cracking, which represent the real behaviour of the structure. Furthermore, it supports advanced

research in cementitious mat material as well. The portion of the structure modelled in this study is the lateral wall in the middle of the church that is subjected to the highest load due to the longest span [Figure 4.2].

In the sectional wall modelling, due to the limitation of the computer speed and the model size, 4m high walls with 1.2m thickness. Even though this is not the entire height of the wall, this model is deemed satisfactory in determining the bearing capacity of the wall. This is because the wall is not slender with its height to thickness ratio being less than 10. The wall is not very vulnerable to failure due to buckling and hence, model of the whole height of the wall is not so important. Furthermore, due to the simplicity of the structure with absence of masonry vault, the wall is subjected to very minimal horizontal load. Consequently, the failure mode could most probably be due to build-up of tension forces within the masonry between different layers of masonry due to the non-homogeneity of the masonry. In this respect, the size of wall modelled is sufficient to represent the behaviour of the masonry.

As for the modelling of the wall in longitudinal direction, 2m high walls with 4m width are modelled. In longitudinal direction, the likely failure modes include diagonal shear and crushing due to excessive compression after eliminating other failure modes that are related to large horizontal forces. In this respect, typically a wall with one-to-one height to width ratio would be a better representative. Originally, a 4m by 4m wall was envisioned to be analysed. This was thought to be optimal size as this is large enough such that the constituting stone blocks are small enough while small enough to represent a portion of the enclosure wall. however, due to limitation of the computer memory, the model was not able to be run in ATENA. A less ideal size of 2m height by 4m width wall with symmetry condition to its right and left was modelled instead.

The arrangement of the constituting blocks modelled are based on some on-site element measurement and observation from photographic documentation of walls with exposed masonry. The different arrangements and the corresponding locations from which these arrangements are derived from are shown in Appendix B.

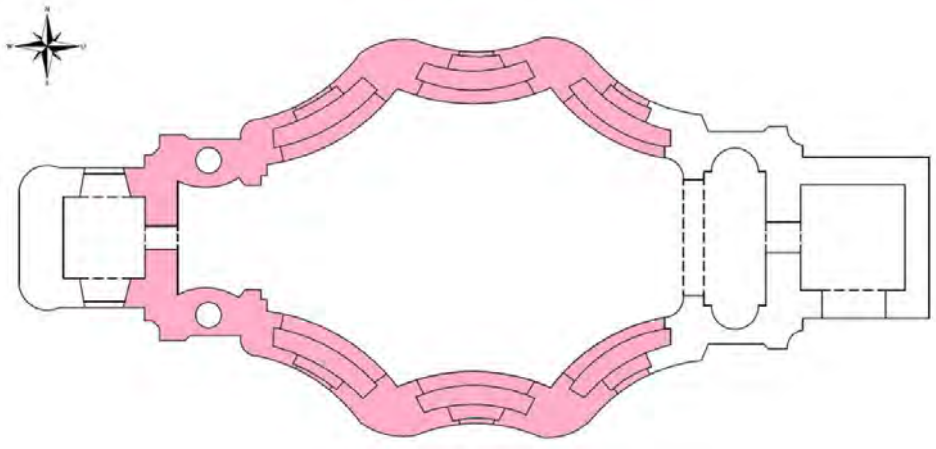

Figure 4.2. Analysed walls for its bearing capacity

4.1.1 Modelling assumptions

Material and geometrical non-linearity is considered in the finite element modelling in this report. Considering the limited tensile strength of masonry, material non-linearity has to be considered into this modelling. It is very likely that with the addition of load, the state of stress within the structure will be over its elastic limit and non-linearity in material is exhibited. Furthermore, as the intention of the modelling is to find the peak load that the wall can resist, it is to be expected that the structure will be subjected to significant displacement. Consequently, it will only be appropriate to use deformed shape of structure in modelling each step to reduce inaccuracy in modelling. Since the model assumes non-linearity in both material and geometrical, the modelling will be done in small increment of steps to capture this non-linearity, of 0.2 times of the currently applied load up to the currently applied load, and of 0.1 times of the currently applied load subsequently up to the peak load.

The interface between the elements are assumed to be rigid. This means that sliding of each element against adjacent elements assumed not to be possible. Even though this is not exactly true in the real life, this does not deviate too much from the real behaviour of masonry as the stones used in the construction of the church wall is not very smooth – this increases friction – and the stones are always connected to either mortar or rubble infill masonry that have rather low tension and shear strength capacity. Consequently, failure in the element rather than the interface is more likely. Hence, this simplification could be justified.

The load is assumed to be spread uniformly across the top surface of the modelled wall over a rigid steel plate top. Even though the surcharge exerted by the roof truss at the top of the wall resembles a point load more than a uniform load, the 1m ring beam that surrounds the top of the enclosure wall has enough depth to redistribute this point load to be uniform area load acting on the wall instead. To mimic this effect of rigid ring beam, a thin rigid steel plate is modelled on top of the wall analysed.

4.1.2 Material model

The material model used to model the different masonry elements including stone blocks, bricks, lime mortar layer and rubble masonry infill is Constitutive Model SBETA material. This material uses a smeared approach to model material properties in 2D plane stress model. This ensures continuity of strain between adjacent elements within the entire finite element model. The constitutive model is based on the stiffness and is described by the equation of equilibrium in a material point:

$$s = De, s = \{\sigma_x \quad \sigma_y \quad \gamma_{xy}\}^T, e = \{\varepsilon_x \quad \varepsilon_y \quad \tau_{xy}\}^T$$

where s, D and e are a stress vector, a material stiffness matrix and a strain vector, respectively. The stress and strain vectors are composed of the stress components of the plane stress state σ_x, σ_y, γ_{xy} and the strain components ε_x, ε_y, τ_{xy} [13].

This assumption of plane stress model works perfectly fine with the longitudinal wall as the actual width and height of the wall is much larger than the thickness of the wall. However, this assumption is not compatible with the sectional wall model as the sectional wall model has much larger dimension in the

direction perpendicular to the plan modelled. The sectional wall model fits a plane strain model better. In this case, certain transformation of the stiffness properties has to be performed to transform the model from plane stress to plane strain. A simple substitution of the right-hand side of both equations should provide the required results. The relations have been obtained from and mathematically expressed as:

$$v_{computer} = \frac{v_{wall}}{1 - v_{wall}}$$

$$E_{computer} = \frac{E_{wall}}{(1 - v_{wall})^{\frac{1}{2}}}$$

Where $v_{computer}$ and $E_{computer}$ are the Poisson ratio and Young's modulus to be modelled into the computer while v_{wall} and E_{wall} are the estimated actual Poisson ratio and Young's modulus of the modelled material [14].

The material model SBETA includes the following effects of material behaviour [13]:
- non-linear behaviour in compression including hardening and softening,
- fracture of material in tension based on the nonlinear fracture mechanics,
- biaxial strength failure criterion,
- reduction of compressive strength and shear stiffness after cracking,
- tension stiffening effect,

As mentioned in the previous section, the material matrix is derived using the nonlinear elastic approach. The elastic constants are derived from a stress-strain function called here the equivalent uniaxial law as shown in Figure 4.3. Dissipation of energy is assumed with the different loading and unloading curve as depicted in the same diagram. Another name for this approach is isotropic damage model [13].

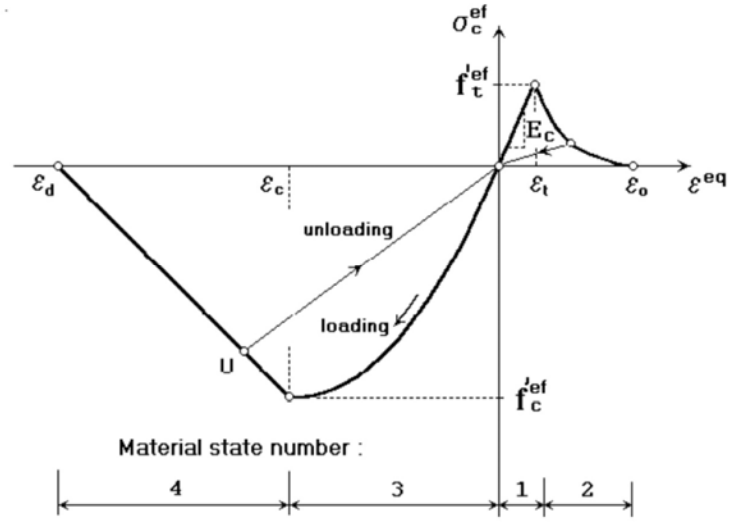

Figure 4.3. Equivalent uniaxial law considered for constitutive SBeta material [13]

Additionally, exponential crack law opening that represent the reduction of tensile strength of the material with presence of crack is adopted with the use of this constitutive model. The exponential factor adopted is shown in Figure 4.4.

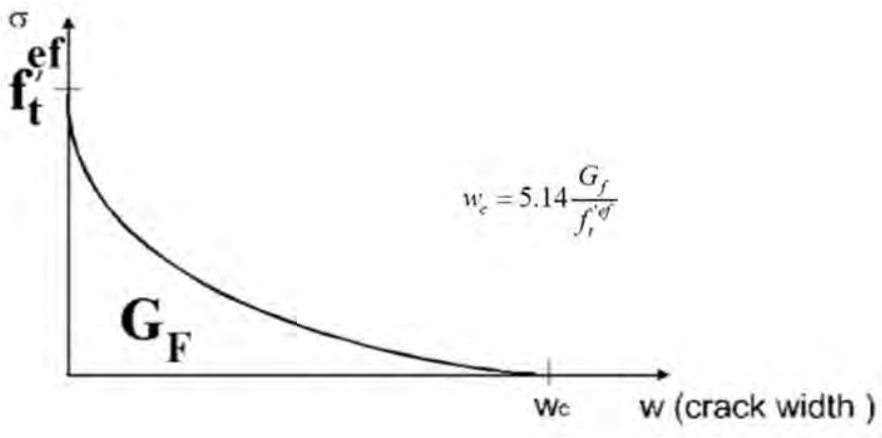

Figure 4.4. Exponential crack law opening adopted in SBeta material model [13]

4.2 Mechanical parameters of materials used in modelling

The wall is modelled as stacks of grey sandstone, red siltstone, bricks, mortar and rubble masonry infill. The first three elements are as observed from the site inspection while the rubble masonry infill is estimated to be in place due to the thickness of the wall. The relevant mechanical properties used for the modelling, as well as the transformed properties to simulate plane stress model for sectional model, are tabulated in Table 4.1 and Table 4.2 respectively. While the values of the mechanical properties used were derived from typical values of such stone, the lower bound of the range is used instead of the average values as the elements making up the masonry have been subjected to rather significant deterioration due to lack maintenance and moisture attack.

Furthermore, for modelling of the longitudinal wall section, reduced parameters are used to account for the effect of multi-leaves wall in the single leaf model. Only the outer leaf is modelled in this study. The reduction factor is obtained by modelling only the outer leaf sectional wall. Subjecting this wall to the same uniform loading, a load-displacement curve is obtained. The Young's modulus and the yield strengths of the stones and mortars in the model are modified such that a load displacement curve that is comparable to that of the three-leaves wall model is obtained. Ultimately, after rounds of iteration, reduction factors of 0.33 for the Young's modulus and 0.8 for the yield strength and the shear strength are used.

Table 4.1. Mechanical properties of elements constituting enclosure wall for modelling purposes

Material Name	Young's Modulus E	Poisson's ratio, v	Tensile strength	Compression strength	Fracture Energy in tension, Gf	Unit Weight
	GPa		MPa	MPa	N/m	kN/m3
Lime Mortar [15], [16] , [17]	2	0.375	0.58	-2.09	9.808	17.3
Red Siltstone [18]	10	0.275	0.35	-3.5	50	28.5
Grey Sandstone [19], [20], [17]	25	0.171	1	-10	150	28.5
Steel Plate for Rigid top	210	0.3	-	-	-	0
Brick [21]	4.2	0.2	1.85	-18.5	130	18.7
Rubble Masonry [22], [23]	0.5	0.3	0.07	-0.7	35	19

Table 4.2. Transformed parameter of mechanical properties of the elements for purposes to model in plane stress state

Material Name	Young's Modulus E	Poisson's ratio, v
	GPa	
Lime Mortar	2.53	0.60
Grey Sandstone	27.46	0.21
Red Siltstone	11.74	0.38
Steel Plate for Rigid top	251.00	0.43
Brick	4.70	0.25
Rubble Masonry	0.60	0.43

4.3 Finite Element Method

In ATENA, Updated Lagrange formulation is used to solve for equilibrium in structural analysis. In this case, behaviour of infinitesimal particles of volume dV is analysed. The change in volume of these particles determine the amount of deformation experienced by the structure. In Updated Lagrangian, the governing equation is written with respect to the deformation of the particles from its previous timestep [24].

Principle of virtual displacement is used to solve the equilibrium and from the solved displacements, the external energy applied to the particles is equated to the change in internal energy of the structure due to its change in shape and volume. In principle of virtual displacement, a load increment is applied at each timestep, Δt. Assuming that the response of the structure up to time t is known, the state of the structure at time $t+\Delta t$ is solved by solving the equilibrium equations using numerical methods [24].

Subsequently, incremental changes in virtual internal energy can be obtained by integrating the changes in strain to the internal stiffness for each infinitesimal particle. Correspondingly, the incremental external work done by external forces subjected to the deformation the particle experiences can be calculated by integrating the elements' body forces with respect to the volume of the structure and the surface forces to the surface with prescribed boundary forces [24].

The iteration method used to solve the equations numerically is Newton-Raphson method. The displacement error, residual error and absolute residual error specified for convergence is 0.01, while energy error tolerance is 0.0001.

4.4 Load Applied

In determining the magnitude of loading that the walls are subjected to, references to Eurocode was made. Although the current design code might not be very relevant in design of historical structures, it provides a base of the necessary load combination that could be modelled. The load combination assumed in the modelling is presented in Table 4.3. As can be seen, majorly, dead load, live load and snow load are considered. Since the analysis is done to determine the bearing capacity of the wall, only transient loading will be considered in the load applied.

Table 4.3. Loading combinations [25].

#	ULS Loading Combinations
1	1.35DL + 1.5LL + 1.5 (0.5SL + 0.2WL)
2	1.35DL + 1.5LL + 1.5 (0.6WL + 0.2SL)
3	1.35DL + 1.5WL + 1.5 (0.6SL)
4	1.35DL + 1.5SL + 1.5 (0.5WL)

Where DL is dead load of the elements, LL is live load of the roof spaces, WL is wind load and SL is snow load.

The self-weight of the wall elements modelled were incorporated into the finite element model by ATENA. The additional load due to portion of wall above the element, ring beam surrounding the roof, and wooden roof trusses were estimated based on actual wall and beam dimension, typical unit weight of historical masonry and typical area load of wooden roof. The snow load calculation includes exposure, thermal and shape coefficients in the standard calculation. Using equation specified by the Eurocode 1 as shown below, a snow load value, s_L, of 0.62 kPa was found and employed in the normally loaded model [26].

$$s_L = \mu_1 C_e C_t s_k$$

The live load assumed to act on the roof spaces that are not accessible except for normal maintenance and repair is recommended to be 0.4 kPa by Eurocode 1. This value will be used as the roof of All Saints' church is not accessible except for workers maintaining the roof truss condition [26]. Live load on the roof will not be considered as the roof is too steep for any access. In addition, even if there is little load

to be considered from rare access, it will be much smaller than the snow load that is assumed to be acting on the roof as well. The wind load is assumed to be 0.79 kPa as presented in the previous work on St Ann's church in neighbouring village in Broumov area [9].

Since the loads acting on the walls considered are all static loading, instead of inputting the different load cases, a lumped maximum load combination is keyed in as input to the ATENA analysis model. Table 4.4 shows the tabulation of the actions applied on the wall.

Table 4.4. Actions applied on the top of wall modelled [26]

Type	Load (kN/m^2)
Dead load due to pointed roof plank and wooden beam/bracing	2
Dead load due to ceiling plank and wooden beam	2
Dead load due to roof spaces platform and wooden beam	2
Masonry self-weight of wall and ring beam	20 kN/m^3

Complete tabulation of derivation of the actual load to be acting on the wall in the analysed model is shown in Appendix C.

4.5 Results

4.5.1 Sectional wall model

In general, the failure in the three-leaves wall modelled happens at the rubble masonry infill which has lower strengths in tension and shear as compared to the outer wall leaf. The crack patterns observed in the wall at failure are shown in Figure 4.5. The outer wall leaves are much stiffer as compared to the rubble masonry infill in the model. In this respect, bulk of the load is transferred through the outer leaves than the inner leaves. However, the two outer leaves are subjected to different stiffness due to the different masonry configuration. The difference in stresses between the leaves causes lateral tension to be built up in between the two outer masonry leaves [Figure 4.6]. This lateral tension causes the inner infill which is the weakest part among the masonry leaves to start cracking and cause failure.

Figure 4.7 shows the typical load-displacement diagram measured from the top of the wall that is subjected to the highest deformation. The graph shows a slightly non-linear behaviour that ends at a peak stress. The graph is discontinued at the peak stress because the external force is applied as incremental load. Thus, the program tries to increase the load at each new interval. However, after the peak stress, the stress decreases with increase in displacement. Hence, the program is not able to find a solution for higher load and stopped because of divergence issue. While this problem could be overcome by imposing prescribed displacement instead of vertical load, imposing vertical load is a more direct representative of the problem. Additionally, since the post-peak behaviour is of an interest in this analysis, this problem is ignored and vertical load is used to be imposed on the model instead.

The complete load-displacement diagrams for each wall arrangement with and without the connecting tie stones are presented in Appendix D.

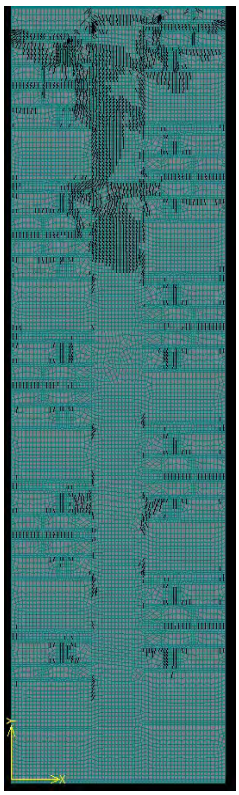

Figure 4.5. Crack pattern for sectional wall analysis with connecting stones of wall configuration 1

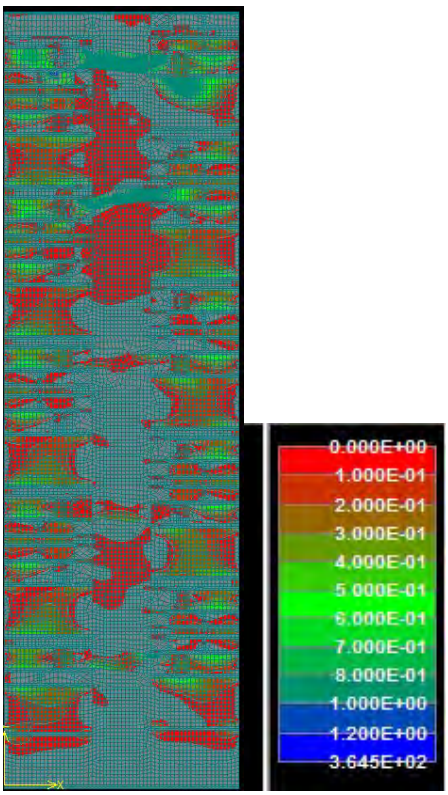

Figure 4.6. Horizontal tensile stress distribution for sectional wall analysis with connecting stone of wall configuration 1

Table 4.5 tabulates the peak stresses and displacement of different wall arrangements with and without tie stones connecting the leaves. It can be seen that the peak stress before failure for all of the wall is more than 1MPa, which is about two times the current working load of 0.5MPa. This means that the walls have more than sufficient strength to withstand the loading it is currently subjected to. From this, one could derive that the damages that is experienced by the church is not likely to be caused by the failure in the sectional capacity of the wall.

In the same table, equivalent compressive stress of the masonry is shown. This value is derived from the lowest peak stress from the different wall arrangements. The values from masonry without connecting tie stones are always used in this case. Furthermore, the tensile strength is assumed to be 1/10 of its compressive strength [27]. A value of strain at the elastic portion of the graph is calculated by dividing total wall deformation to the total height of wall modelled. Engineering strain is assumed here as it is assumed that the lateral enlargement of the masonry could be ignored. Lastly, the Young's modulus is easily calculated by dividing the corresponding stress to strain obtained earlier.

Another observation from the tabulation is that the peak stress experienced by the wall before failure is higher for walls with tie stones connecting the two outer leaves as compared to the ones without. The presence of the stiffer tie stones in the masonry infill alleviate some of the lateral tension from the

masonry infill as the stiffer tie stones attract more load. This in turn increases the compressive load that the masonry is able to withstand.

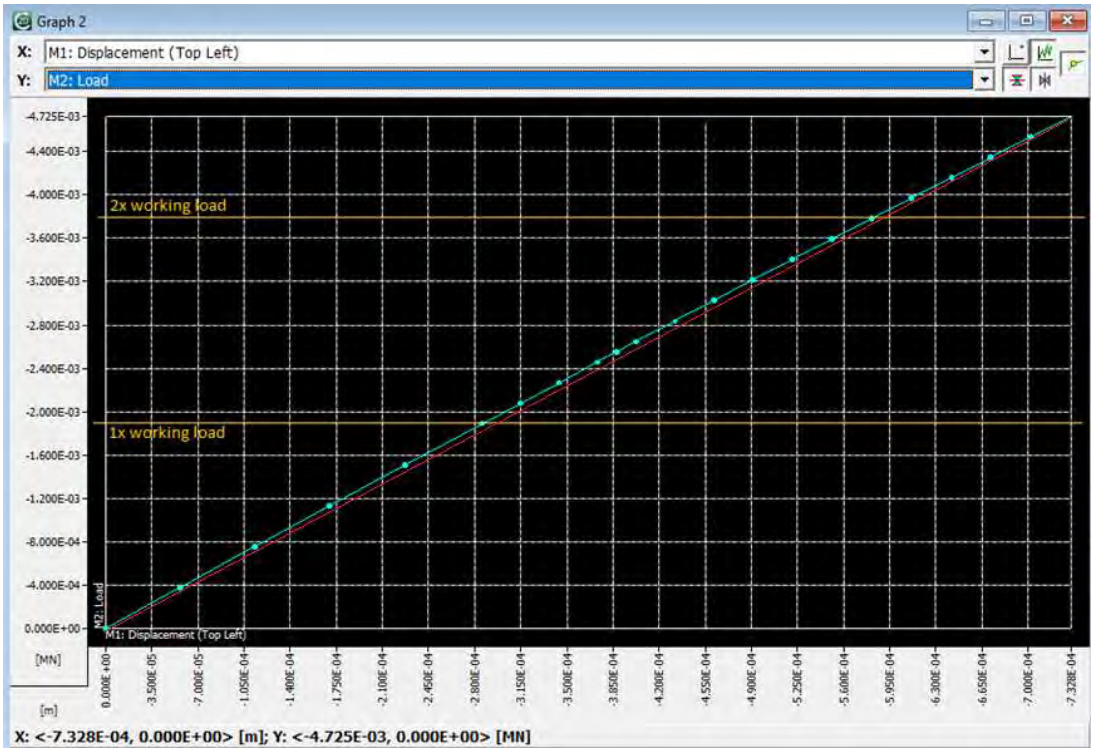

Figure 4.7. Load-displacement curve for sectional wall of configuration 1 with connecting stones between the walls leaves (blue line showing the wall behaviour while red line showing linear line drawn by connecting the peak and initial points

Table 4.5. Tabulation of peak stress and corresponding displacement with compressive strength and Young's modulus derived from these values

Arrangement No.	Peak stress 1 (kPa)	Peak stress 2 (kPa)	Compressive strength (MPa)	Estimated Tensile Strength	Corresponding displacement (10^{-4}m)	Corresponding strain (10^{-4})	Young's modulus (Gpa)
1	1161.86	1114.44	1.11	0.11	6.87	1.73	6.43
2	1344.22	1246.46	1.25	0.12	8.40	1.84	6.77
3	1621.23	1597.03	1.60	0.16	8.90	2.04	7.82
4	1198.94	1174.96	1.17	0.12	9.68	2.31	5.08
Note: Peak stress 1 is for walls with connecting tie stones connecting the outer leaves while Peak stress 2 is the ones without.							

4.5.2 Longitudinal wall model

Different from the sectional model, in this sectional model, the failure is observed to appear on the mortar joint. However, the same load pattern is observed in load-displacement curve obtained from the longitudinal wall model. A linear curve that is followed by non-linear section to the point the curve stops as it reaches the peak stress. Load displacement curve for longitudinal wall models are shown in Figure 4.8 and Figure 4.9 below.

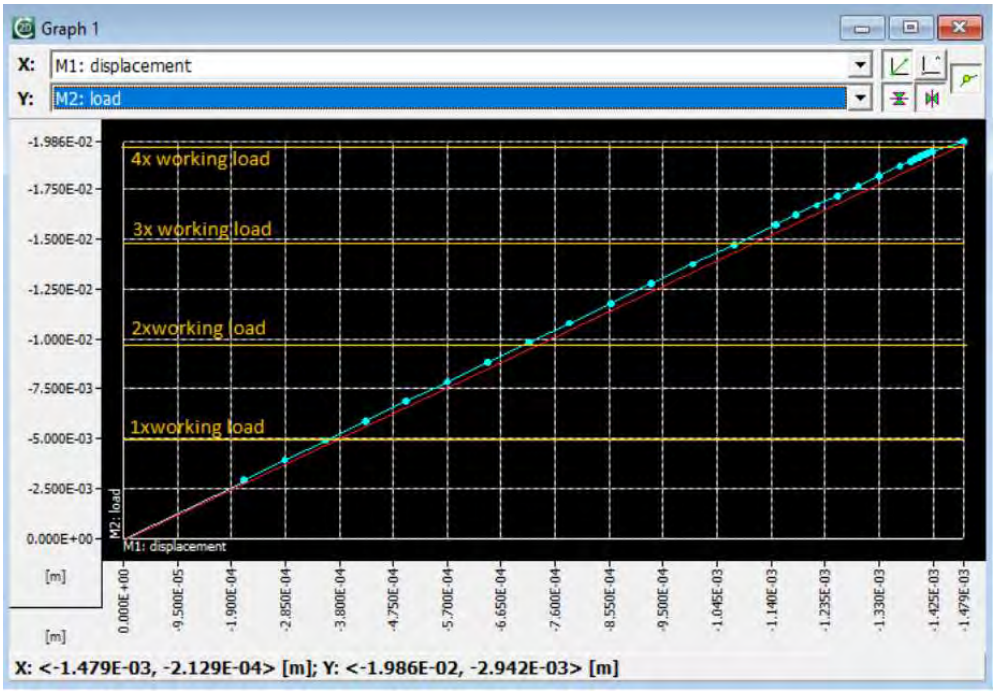

Figure 4.8. Load-displacement curve for longitudinal wall of configuration 1 (blue line showing the wall behaviour while red line showing linear line drawn by connecting the peak and initial points

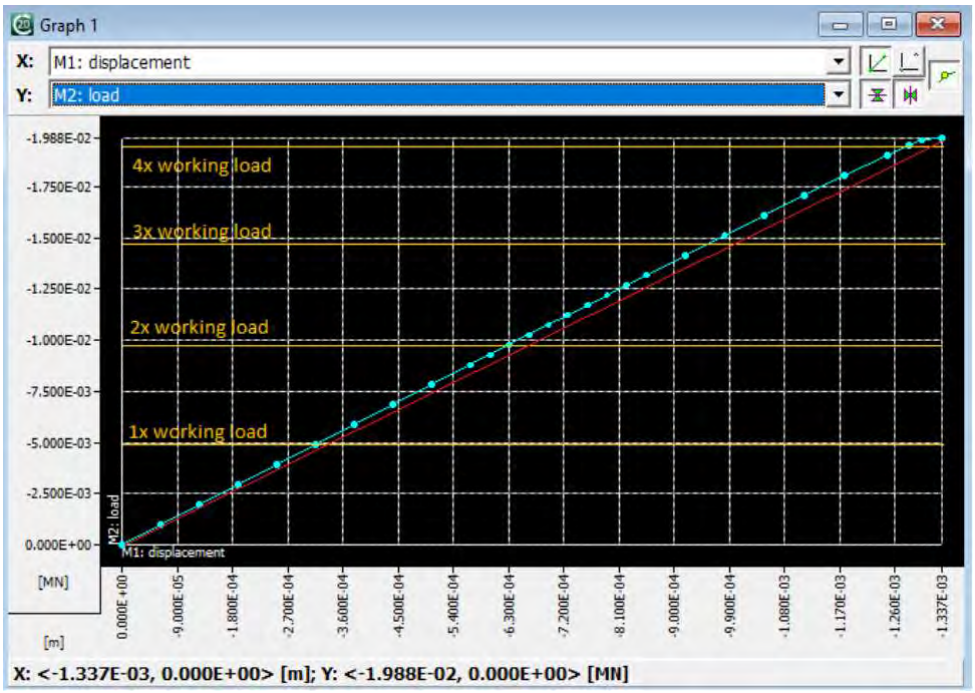

Figure 4.9. Load-displacement curve for longitudinal wall of configuration 2 (blue line showing the wall behaviour while red line showing linear line drawn by connecting the peak and initial points

As compared to the sectional model, the failure load is observed to be much higher. This might be because only a small area of the wall is modelled and the lateral tension does not build up sufficiently in this small area. Furthermore, the absence of the poorer inner infill causes a more even stress distribution throughout the wall resulting in higher failure load.

The peak stresses and displacement of different longitudinal wall arrangements are tabulated in Table 4.6.

Table 4.6. Tabulation of peak stress and corresponding displacement with compressive strength and Young's modulus derived from these values

Arrangement No.	Peak stress (kPa)	Compressive strength (MPa)	Estimated Tensile Strength	Corresponding displacement (10^{-4}m)	Corresponding strain (10^{-4})	Young's modulus (Gpa)
1	2205.82	2.21	0.22	5.70	2.49	8.86
2	2210.14	2.21	0.22	6.30	3.06	7.23

4.5.3 Mechanical properties to be adopted for 3D wall analysis

Looking at Table 4.5 and Table 4.6, the masonry strengths and the young's modulus for the 3D analysis will be based on the sectional wall model from wall configuration 1 and 3 respectively. The lowest compressive strength of 1.11 MPa is adopted while the highest Young's modulus of 7.82 GPa is used. This is to ensure conservative approach to the problem due to the high uncertainty of the material. Since the 3D model analysis is assessing the stress distribution in the walls due to differential settlement, adoption of higher Young's modulus generates higher stresses in the walls, which is conservative for this analysis.

5. STUDY ON SOIL STRUCTURE INTERACTION AND EFFECT OF DIFFERENTIAL SETTLEMENT ON WALL STRUCTURE

To study the soil structure interaction and the effect of differential settlement on wall structure, a series of 2D model and a 3D model modelling the enclosure wall with properties obtained from the previous chapters resting on different subsoil parameters are analysed. The first part of this chapter will explain the theory on soil structure interaction followed by explanation and results of 2D and 3D models in this order.

5.1 Soil Structure Interaction

The modelling of foundation in structural engineering is often simplified to be pin supports on selected areas, lines and/or points. While this is relevant for modern structures where deep and stiff foundations are normally utilized, this assumption is not usually relevant for historical buildings that usually have shallow and less stiff foundation [28]. In the case of the church in our study, this is more so because of the suspected different subsoil condition below the foundation.

To model the soil structure interaction, there are two methods that can be used, one is modelling structure as a beam element on elastic subsoil layer and the other is continuum approach using numerical analysis method. Using these methods, deformation of subsoil and structure which finally determines settlement are analysed. The resulting stresses on the structure and soil could subsequently be studied or analysed. The first method is simpler as it requires only two input parameter which include modulus of subgrade reaction and shear modulus of shear layer. However, there are a lot of estimations involved to obtain these parameters [29]. In this study, the first method will be used to simulate the supports for the 3D FEM modelling and the second method will be used for the 2D modelling in Geo5 geotechnical software.

The first method could be done using two model of subsoil idealization. The first one being Winkler foundation model and the other one is an improvement of the previous model, Winkler-Parsenak foundation model [29]. These two models and the continuum approach will be explained in the following sub-chapters.

5.1.1 Winkler Method

This idea of Winkler method idealize subsoil to be an elastic layer that could be represented as a series of vertical independent springs supporting a beam element as shown in Figure 5.1 [29]. The mathematical expression representing Winkler method is as presented below

$$EI\frac{d^4w_s}{dx^4} + kw_s = q$$

The settlement is dependent on the flexural stiffness of beam element, EI, surcharge, q, and idealised deformation modulus of soil, k. With the first two parameter being readily available in design, this leaves this method with one variable, ‘k’.

This ‘k’ value is determined by finding the ratio of the pressure acting on soil by the settlement it causes (k=p/w). The settlement can be determined by different methods including Koppejan formula, Terzaghi formula or commercial software. Since settlement is not only dependent on the type of soil but also the load distribution as well as pre-consolidation and duration of loading, this parameter not only depends on the nature of the soil, but also on the dimensions of the load area and the type of loading. Consequently, this ‘k’ value is a floating value that changes with time, space and load state even for a single slab. Assuming this ‘k’ value as a single constant inherently ignores these variations. However, many a time, this is a good estimation for a preliminary study or when these variation is not too large. After all, this model offers simplicity and convenience of use [29].

Another disadvantage of this model is the independent behaviour of each spring. In actual case, when a volume of soil is compressed vertically, it expands exerting pressure on adjacent volumes. This phenomenon shows that each subsoil columns do interact. This model again overlooks this effect [29].

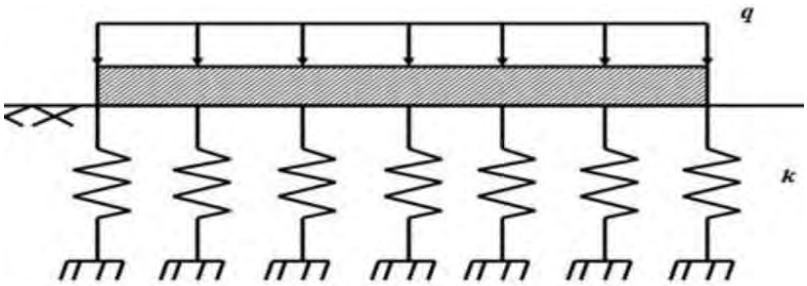

Figure 5.1. Winkler foundation method

5.1.2 Pasternak Model

To overcome the previous model’s shortcoming that overlooks interaction between each spring, Pasternak formulated a new model as shown in Figure 5.2. As can be seen in Figure 5.2, a horizontal layer connecting the vertical springs at the top of the spring just below ground surfaces is added into the model. This horizontal layer is modelled as a thin elastic membrane connecting the springs subjecting them to constant horizontal tension [29].

This horizontal interaction between the vertical springs is often represented by the shear modulus of shear layer, G_p parameter. With this extra parameter, the displacement of the model can be more realistic compared to the previous model. This new parameter is related to the shear modulus (G) even if they are not identical. G_p can be calculated as product of shear modulus and an effective depth over which the soil is shearing [29]. However, due to the difficulty in obtaining this G_p parameter, another expression for Winkler Pasternak as shown in equation below is commonly used [30].

$$c_1.w_s + c_2.\Delta w_s = f_z$$

Where c_1, c_2 are constants representing compressive and shear deformability respectively, w_s represents displacement in the vertical direction and f_z represents vertical load acting on a layer.

In Geo5 software, these two constants are calculated from the condition of equal compliance matrices of infinitely stiff infinite strip footing [13]. Using the same concept, Program Depth generates equivalent constants for a single elastic layer of soil for a given width and load [31]. The constants from this program will be used later in this report.

In this study, this approach will be used to estimate a spring constant for 3D modelling of the church to simulate the different soil condition at different parts of the church.

$$Pasternak - EI\frac{d^4w_s}{dx^4} + kw_s - G_p\frac{d^2w_s}{dx^2} = q$$

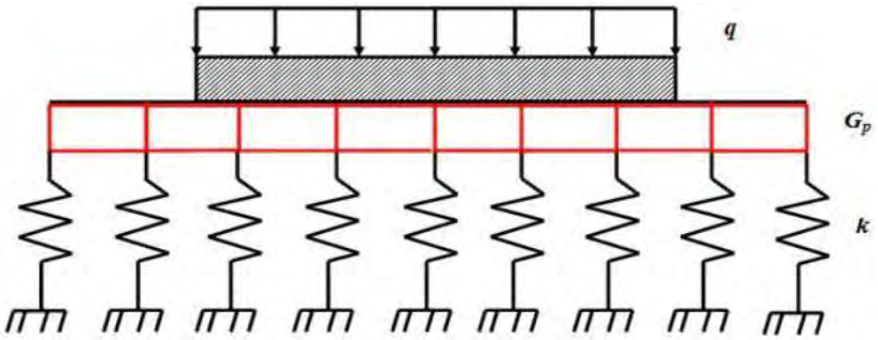

Figure 5.2. Winkler-Pasternak foundation model

5.1.3 Continuum Approach

In continuum approach, the subsoil layers are modelled as continuous distributed matter through the space. Various constitutive model can be used to represent the soil properties. The simplest one being linear elastic isotropic material. A continuum model can approximately be analysed with numerical methods which include Finite Element Method (FEM) and Boundary Element Method (BEM). FEM is a preferred to solve model with non-linear soil properties, while BEM is more compatible with semi-infinite linear elastic analysis [32]. Since modelling of shallow foundation is not a problem of semi-infinite structure, FEM is more relevant in the course of this study and hence will be discussed in more detail.

Several analytical solutions for this continuum approach have been developed. One of the most well-known approach is Boussinesq theorem. In his theorem, the sub-soil is assumed as a semi-infinite, homogenous, isotropic, linear elastic matter. The analysis was carried out for point loads and infinite strip loads regardless of Poisson's ratio. The self-weight of the soil is disregarded in this approach [32]. The mathematical representation of this theorem is shown in the equation below:

$$\sigma_z = \frac{3Q}{2\pi z^2}\frac{1}{\left(1+\left(\frac{r}{z}\right)^2\right)^{\frac{5}{2}}} = \frac{Q}{z^2}I_B$$

Where r represents the horizontal distance of the point in study to the point load application, z is the depth of the point from the load application and I_B is the Boussinesq coefficient.

From the above equation, it could be observed that the maximum stress is obtained when r value equals to zero. This corresponds to a point directly beneath the point of application, and this yields I_B value of 0.48 [33].

Another proposed method of estimating the vertical stress is Westergaard's analysis. Westergaard's analysis assumes that subsoil is reinforced by thin, horizontal sheets of negligible thickness. Westergaard's formula is especially useful to model subsoil with alternating layers of stiff and soft material. Vertical stress increases below a stiff soil stratum calculated using this method had been shown to be less than that of Boussinesq's method. In this paper, however, since the subsoil is not consisted of layers of very different soil, Boussinesq's method will be sufficient to perform calibration of the results obtained from the other program [33].

5.1.4 Depth of Influence Zone

Influence zone is critical in investigation of geotechnical deformation of subsoil due to applied surface load. Only this portion of subsoil under the ground is contributing to the total deformation of the subsoil and hence, the soil settlement. Typically, the strains in the soil are negligible when the stresses at that point are 10 to 15% the applied surface load. Terzaghi proposed a higher stress state of 20% the applied surface load [34].

In this analysis, the depth of influence zone was calculated using Program Depth which uses Winkler Pasternak and the Theory of Structural Strength as a basis for its calculation. It also provides the values of the constants c_1 and c_2.This program is based on the assumption that the only deformation that occurs is deformation of virgin soil. It is assumed that the soil is incompressible until it experiences stress that is higher than the initial stress state it had previously experience. This is represented as excavation depth. The subsoil is assumed to perfectly retain the original stress state the excavated soil previously exerts on it [31].

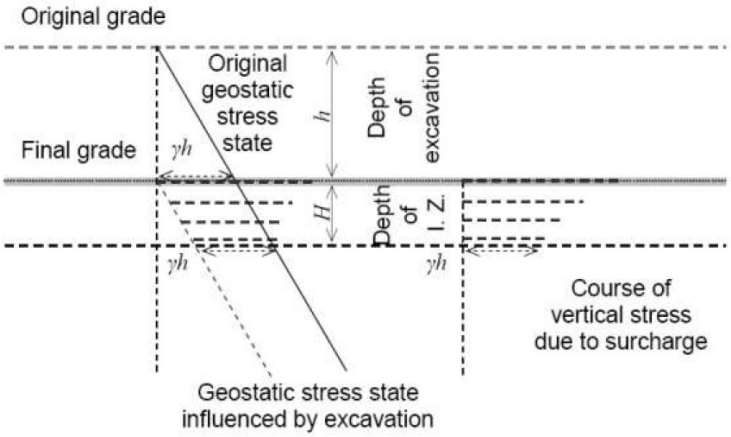

Figure 5.3. Depth of influence zone as calculated by Program Depth [31]

This program estimates the depth of influence zone based on the deformation of an elastic subsoil layer. Furthermore, it assumes no horizontal displacement as in Westergaard assumption. The mathematical representation of the estimation of the depth of influence zone (H) due to line load with a width of 2a is presented below.

$$H = \frac{\pi a}{2}\left(\frac{2-2v}{1-2v}\right)^{\frac{1}{2}}\left(\frac{1}{\ln(\sin\left(\frac{\pi\gamma h}{2f_z}\right) - \ln\left(\cos\left(\frac{\pi\gamma h}{2f_z}\right)\right))}\right)$$

It could be observed that the depth of influence zone is not related to Young's modulus but only to Poisson's ratio in this formulation [31].

Geo5 makes use of theory of structural The Theory of Structural Strength which is similar to the previously explained method. The influence zone is defined as the depth at which the increment in vertical stress is used as a standard to equate with the original structural strength of soil multiplied by the coefficient (m) and the settlement is expressed as a function of these parameters. The value of m is dependent on the fundamental type of soil, consolidation and deformation modulus [13].

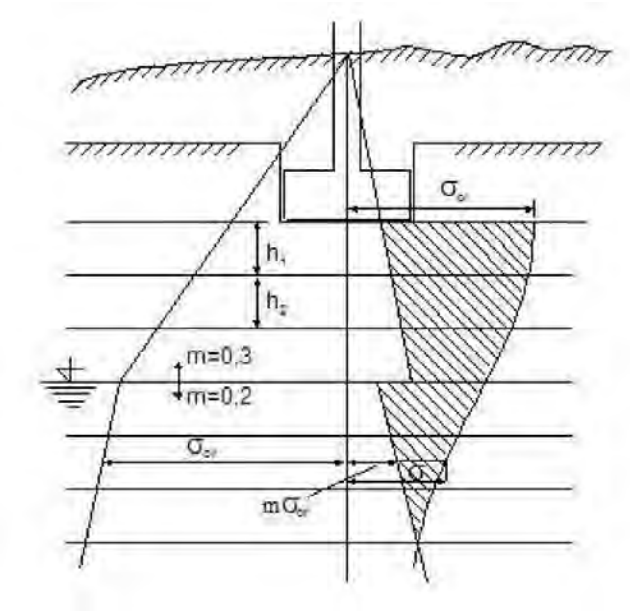

Figure 5.4. Depth of influence zone based on Theory of structural strength

In a previous work by Meera Ramesh, these two methods had been calibrated to show that the settlement obtained from FEM model of a shallow foundation model is in accordance to the Winkler Parsenak theorem. Additionally, influence depth estimated by Boussinesq analysis differs much from that obtained by Winkler Parsenak theorem using Program depth. Hence, for the rest of the paper, influence depth will be determined using Program depth and soil up to this depth will be modelled into FEM model and the settlement will be assessed using FEM Model [14].

5.2 2D Model

This study will be conducted using Finite Element Analysis (FEM) module in software FINE Geo 5. Geo5 is a 2D Finite Element software that is able to analyse behaviour of soil with surcharge using continuum soil approach [13]. Even if the 2D model does not represent completely the behaviour of the church's 3D problem due to soil settlement, this serves a preliminary model and a comparison to the 3D model that is also modelled.

5.2.1 Modelling assumptions

The church enclosure walls are idealised to be of rectangular arrangement in this 2D modelling. One side of the rectangle would be 44m as is the length of the church and the other side of the rectangle, 20m as is the width of the church with 11m in height. Three wall strips will be modelled - one to represent differential settlement between the northern and the southern façade, one to model the behaviour of northern with weaker soil at the kink of the church near the water downpipe location and the last one to model the same longitudinal wall section but on the southern part of the church. In these modelling, the door and window openings will be modelled accordingly.

The first model to represent differential settlement between the northern and southern façade will be done in two stages. Cutting a transversal church cross section through the middle of the church, these walls are not rigidly connected. The only connections between them are the wooden roof truss, which is significantly less stiff as compared to the walls, and the ground floor which typically do not have rigid connection to the walls. As a result, these two walls will deform independent of each other. The first stage of modelling will model this effect of two independent walls 20m apart from each other, exerting surcharge on two different types of soil [Figure 5.5]. Two stages of this model were run, first using the southern soil throughout the entire terrain, the second using the current soil type. The respective deformation caused by each wall will be noted. The second stage of the modelling involves imposing the differential deformation obtained from the previous models to the front and back façade [Figure 5.6]. This is done by applying additional load on one end of the wall. The stresses experienced by the western and the eastern façade are then analysed.

The last two models to study the effect of poorer soil condition under the kink of the church will be done by modelling a 44m wall sitting on subsoil representing each side's soil condition with a 2m strip of poorer soil located approximately at the presumed poorer soil location [Figure 5.7]. The tensile and shear forces that the wall experience as a result will then be assessed.

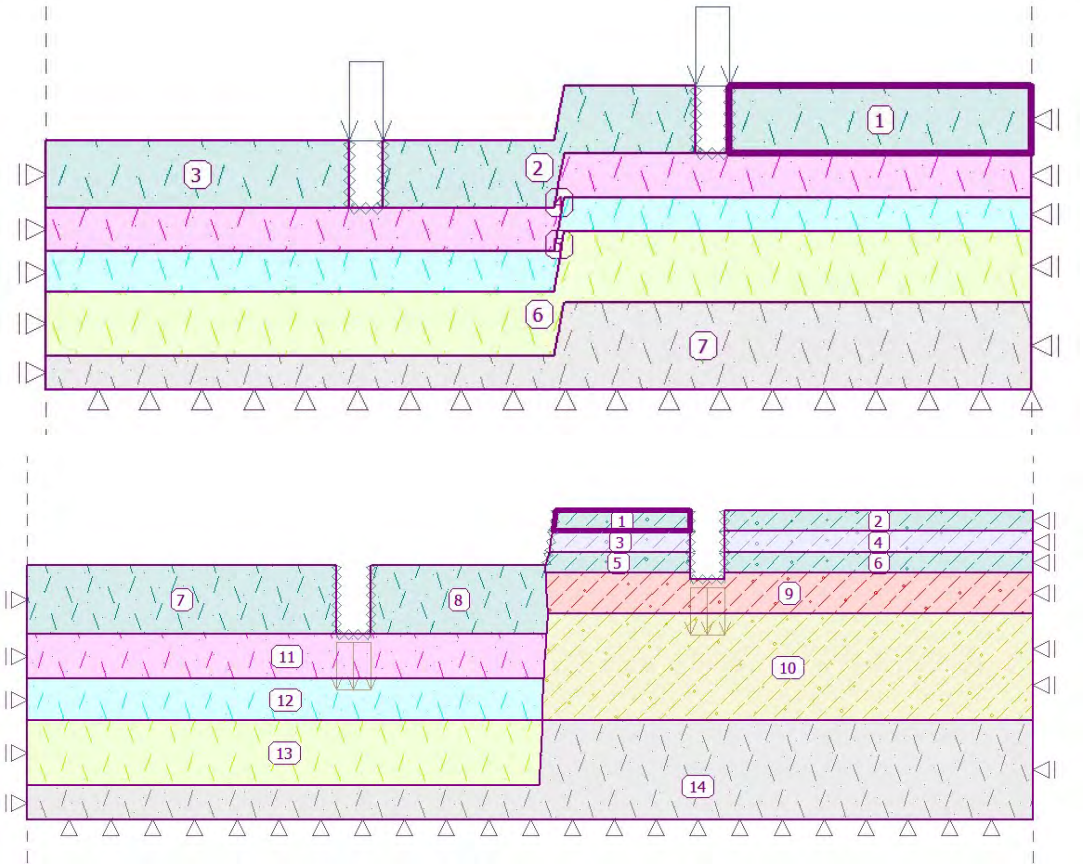

Figure 5.5. Modelling the differential settlement cause on the soil due to different soil type (top – stage 1, bottom – stage 2)

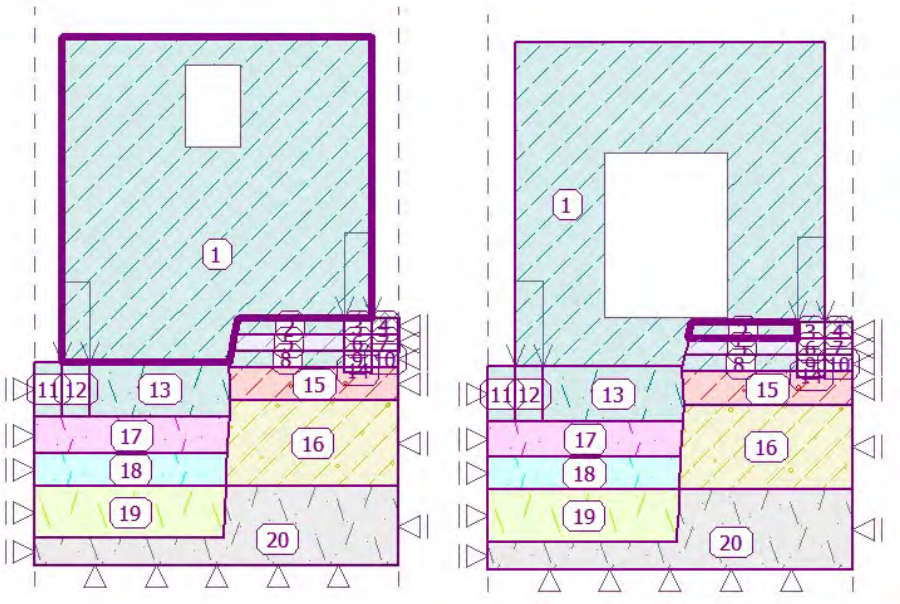

Figure 5.6. Modelling eastern (left) and western (right) transverse facade to analyse the stresses due to differential settlement

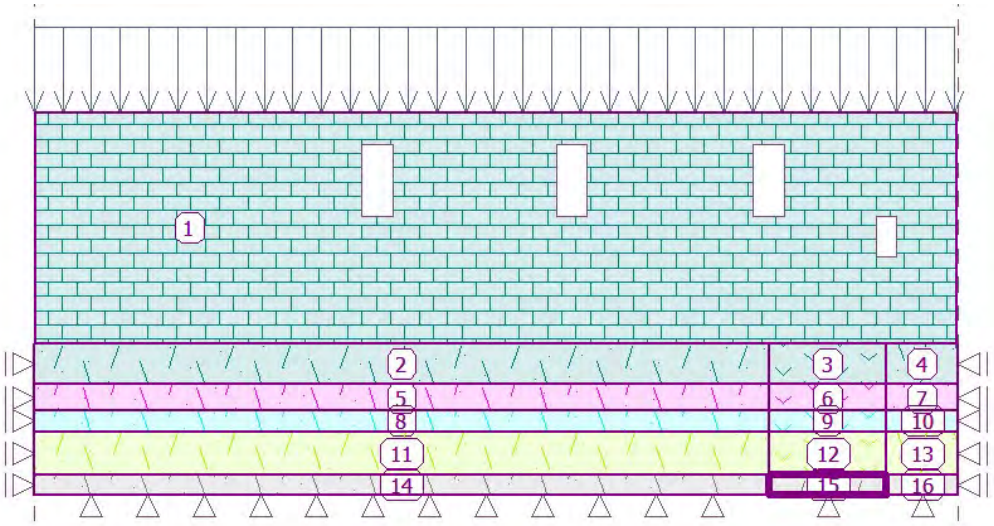

Figure 5.7. Modelling northern and southern longitudinal wall stresses due to differential settlement

5.2.2 Material Model

A few frameworks of material model are available. In general, they can be categorized into linear and non-linear modelling. In Geo5, two models are available for linear material model including elastic and modified elastic model. The former assumes a secant Young's modulus during loading, unloading and reloading. The modified version introduces another parameter, unloading/reloading Young's modulus denoted as E_{ur}, to differentiate loading of over-consolidated and virgin soil [Figure 5.8]. This modified version is especially useful for modelling of series of loading and unloading of surface load.

The non-linear material models include Mohr Coulomb failure criterion and critical state of soil. The Mohr Coulomb Failure Criteria is capable of capturing the change of stiffness of soil at each stress state [Figure 5.9]. Employing this material model involves acquiring information on angle of friction, cohesion and dilatation angle of the soil. The first two parameters determine the start of plastic phase while the last one determine the extent of plasticity. The other non-linear model is based on the assumptions that the soil is isotropic, elasto-plastic and deform as continua, unaffected by creep. Different from Mohr Coulomb method, the yield surfaces using this method is of an ellipse shape.

In this analysis however, the material model employed for soil was the simplest linear model, linear elastic model. As limited information is known about the soil, it would not be appropriate to estimate more advanced soil properties as the ones that are required for modelling the non-linear soil model. Furthermore, as can be seen by comparing the linear and non-linear stress-strain curve depicted in

Figure 5.8 and Figure 5.9 respectively, linear stress-strain curve provides a more conservative estimation in terms of soil settlement that it causes to the soil which the main focus in this study. Hence,

the use of this method is not inappropriate as a preliminary approach in this study with the limited information available.

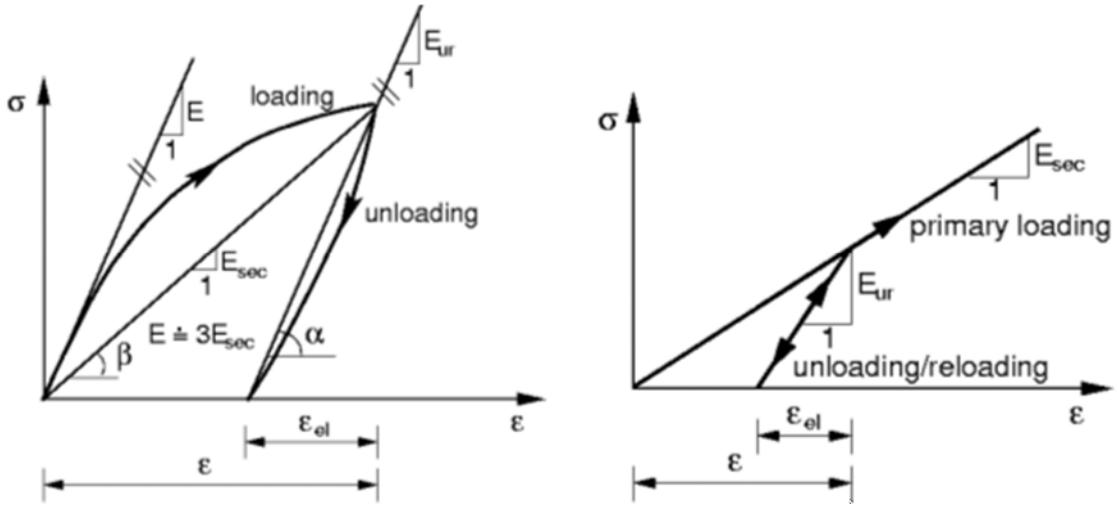

Figure 5.8. Stress-strain curve of modified elastic material model in Geo5

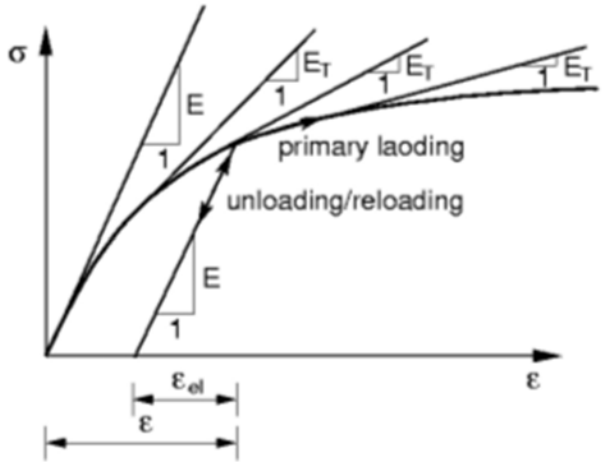

Figure 5.9. Stress-strain curve of non-linear soil models

5.2.2.1 Conversion of Parameters to Plane Stress Analysis

Geo5 software analyses soil and structure using plane strain state assumption. This is compatible for soil modelling as the soil could be considered to be bounded in other direction by adjacent soil. However, this is not compatible in modelling the wall since the wall has a finite depth as contrast to the soil. The wall studied fits a plane stress assumption. Hence, a conversion of mechanical parameters including Young's modulus and Poisson's ratio has to be performed before modelling.

This conversion is as explained in chapter 4.1.2 earlier. However, instead of converting from plane strain to plane stress, the conversion is the other way around. The relations can be mathematically expressed as [14]:

$$v_{computer} = \frac{v_{wall}}{1 + v_{wall}}$$

$$E_{computer} = E_{wall}\left[1 - \left(\frac{v_{wall}}{1 + v_{wall}}\right)^{\frac{1}{2}}\right]$$

5.2.3 Mechanical properties of soil and structure used in modelling

As mentioned earlier, the subsoil is modelled as layers of elastic compressible soil layer. This assumption is applicable to the wall structure as well. Categorization of soil layers in the bore log description into different soil model is tabulated in Table A.1 to Table A.3 in Appendix A.

Typical values of mechanical parameters for sandstone and compact sand are used to estimate mechanical properties in a layer of soil. Based on the proportion of rock and void shown from the bore log, a simple conversion is performed using the following equations.

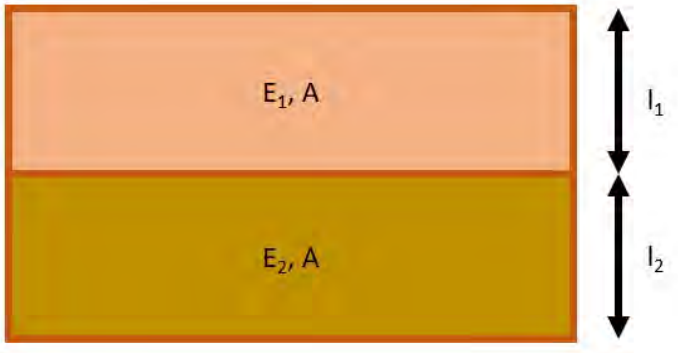

Figure 5.10. Depiction of a few layers of soil

Consider two layers of soil with different Young's modulus, different thickness and same cross-sectional area as shown in Figure 5.10. Assuming that the total depth of all the soil layers are not so large, the force acting on the soils could be assumed to the same and equals to the average force acting in the middle of the total depth, F. Correspondingly, the strain acting on each layer of soil could be represented as:

$$\varepsilon_1 = \frac{\sigma_1}{E_1} = \frac{F}{A \cdot E_1}, \varepsilon_2 = \frac{\sigma_2}{E_2} = \frac{F}{A \cdot E_2}$$

As strain is the ratio of reduction in length, X, to the initial length of an element, l, the reduction in length for each soil layer is:

$$X_1 = \frac{F \cdot l_1}{A \cdot E_1}, X_2 = \frac{F \cdot l_2}{A \cdot E_2}$$

The equivalent Young's modulus of the entire depth of soil as shown in Figure 5.10 is

$$E = \frac{\sigma}{\varepsilon} = \frac{F.l}{A \cdot X} = \frac{F(l_1 + l_2)}{A(X_1 + X_2)}$$

By substituting the definition of reduction of length into above equation of equivalent Young's modulus, the equivalent Young's modulus could be reduced to be:

$$E = \frac{F}{A}\left(\frac{l_1 + l_2}{\frac{F \cdot l_1}{A \cdot E_1} + \frac{F \cdot l_2}{A \cdot E_2}}\right) = \frac{l_1 + l_2}{\frac{l_1}{E_1} + \frac{l_2}{E_2}} = \frac{E_1 \cdot E_2\,(l_1 + l_2)}{E_2 \cdot l_1 + E_1 \cdot l_2}$$

As for the equivalent values of unit weight and Poisson's ratio, a weighted average based on the depth of each component in a soil layer has been assumed.

The rock and compact sand mechanical properties had been used to do the abovementioned estimation is shown in Table 5.1. Higher Young's modulus is used for subsoil under the southern part as they are observed to be less deteriorated as compared to the northern subsoil. Furthermore, the lower soil layers are assumed to have be less compressible, i.e. having higher modulus, since it has been subjected to higher surcharge in the form of soil overburden.

Table 5.1. Table showing rock and compact sand mechanical properties used to estimated mechanical properties of each soil layer

Material Name	Location	Poisson's ratio, v	Unit weight	Young's Modulus E	Typical values
			kN/m3	GPa	GPa
Sandstone [35]	North (0-3m)	0.25	26.50	1.00	3 to 14
	North (3-6m)	0.17	28.50	3.00	
	South (0-3m)	0.17	26.50	3.00	
	South (3-6m)	0.17	28.50	5.00	
Sandy silt [36]	North (0-3m)	0.30	18	0.01	0.007 to 0.05
	North (3-6m)		20	0.02	
	South (0-3m)		18	0.02	
	South (3-6m)		20	0.05	

Using the values shown in Table 5.1, the following mechanical properties of each soil layer as shown in Table 5.2 in the next page is obtained.

Table 5.2. Mechanical parameter of each soil layer in North and South part of the church based on the bore log visual investigation

Location	Layer description by coordinate location (m)		Young's modulus	Unit Weight	Poisson Ratio
	Top	Bottom	GPa	kN/m^3	
North	0	0.6	10.00	18.00	0.30
	0.6	1.2	14.22	20.55	0.29
	1.2	1.8	10.00	18.00	0.30
	1.8	3	15.30	20.98	0.25
	3	6.1	39.74	24.25	0.24
	6.1	9.04	1000.00	28.50	0.10
South	0	2	78.43	24.38	0.20
	2	3.3	97.40	24.80	0.20
	3.3	4.5	458.72	27.65	0.18
	4.5	6.4	240.38	26.80	0.20
	6.4	8.077	1000.00	28.50	0.10

5.2.4 Load Applied

The load cases and load combination assumed in this study is assumed to be the same as that explained in the previous chapter.

For the first model, since the wall and the foundation are not modelled, but applied on the soil as a surcharge, the load applied is equal to the load applied to the sectional model but with addition of foundation load. The additional load due to foundation equals to the following:

$$\begin{aligned} &Additional\ load\ due\ to\ foundation\ and\ wall\ self\ weght \\ &= Area \times Unit\ Weight \times Safety\ Factor \\ &= 2 \cdot 1 \cdot 20 \cdot 1.35 + 4 \cdot 1.2 \cdot 20 \cdot 1.35 = 183\ kN/m \end{aligned}$$

For the rest of the models, since the wall and the foundation are modelled accordingly, the applied surcharge consists of only load from the roof area. The tabulation of total applied load in this load combination is tabulated in Table E.1 and Table E.2 in Appendix E.

5.3 3D Model

ATENA-Gid 3D is a 3D finite element software to analyse non-linear behaviour of a structure. As mentioned in the previous section, this software has an advantage of being able to study the stresses based on the deformed shape of the structure and represent the non-linearity accurately.

5.3.1 Modelling assumptions

The church enclosure wall is modelled as 3D solid structure of 11m high wall with different thicknesses surrounding the church. Due to the size of this model, introducing mesh smaller than 0.35m in size is not practical as the running time for analysis of this model becomes too long. Consequently, there are only 2-3 mesh element within the wall thickness. There is no problem with convergence in the model due to this, but the out-of-plane wall bending might not be assessed through this model. Considering that the problem assessed here is problem of soil settlement of subsoil along the wall length, the out-of-plane wall bending could be neglected in this study. Hence, the model is sufficiently meshed.

The material model used is the same as the one used in estimating the bearing capacity of the wall [refer to section 4.1.2]. However, macro-modelling of masonry is used in this analysis instead of the micro-modelling used in analysing the sectional wall bearing capacity in Section 4. The mechanical property of masonry used in this section was estimated by taking the highest Young's modulus as depicted from the load-displacement curves obtained in Section 4.

$$E = \frac{\sigma}{\varepsilon} = \frac{\sigma}{d/H_w} = 7.82\ GPa$$

Where E is the Young's modulus of masonry, σ is the pressure applied on top of the wall, d is the deformation of the wall due to the applied load, and H_w is the total height of the wall modelled.

Since it is not possible to model the layers of subsoil in ATENA-Gid, the different soil condition at relevant locations will be modelled as different spring supports. The conversion of subsoil layers estimated in the previous section to spring constant will be discussed in the next sub-chapter.

5.3.2 Conversion of subsoil layers properties into spring constants

The deformation modulus, k, of the subsoil is obtained by first transforming the soil into the two Winkler Pasternak constant, c_1 and c_2. This transformation is done using Program Depth as explained earlier. The limitation of this program is that it is only able to do the transformation for a single layer of subsoil [31]. To overcome this limitation, an equivalent value of Young's modulus, Poisson's ratio and unit weight of the subsoil is obtained for the north and south borehole respectively. This equivalency is done for subsoil within the influence depth of the surcharge assumed. Similarly, the influence depth is obtained from the same Program Depth. Hence, an iteration of process has to be performed such that an influence depth value that gives an equivalent value of unit weight and Poisson's ratio that in turn generates the same influence depth for the specified surcharge value is obtained.

Using this method of iteration, the influence depth obtained equals to 9.93 m and 8.89 m for the north side and south side of the church respectively.

In contrast with the previous equivalent value estimation, since the soil is of deeper depth, the force acting on each soil layer could not be assumed to be equal. A simple triangular force attenuation is assumed [Figure 5.11]. Due to this, transforming the equations to obtain an expression to represent the equivalent value of Young's modulus is not practical. Instead, deformation caused by a force, F, of 1kN

is assumed to act at the ground level. The sum of deformation caused by each layer is computed and the equivalent Young's modulus is calculated by dividing the pressure to the ratio of the sum of deformation to the total depth of soil considered. Using this method and the influence depth obtained earlier, the equivalent Young's modulus, Poisson's ratio and unit weight for soil at northern and southern side of the church for the given load are tabulated in Table 5.3.

Table 5.3 also shows the mechanical parameters assumed for the degraded soils under the kink area with higher moisture and biological growth that is possibly degraded due to broken drainage system. A reduction of 80% of the Young's modulus of each soil layer is assumed for both the northern and the southern side in this estimation.

Table 5.3. Parameters of the idealised single elastic subsoil layer on the south and north side of the church respectively

Location	Influence Depth	Load Applied	Equivalent E	Equivalent v	Equivalent γ	C_{1w}	C_{2w}
	m	kN	GPa		kN/m³	MN/m³	MN/m
South	8.892	561	222.18	0.23	26.55	17.501	17.742
South (Degraded)			48.59	0.23	26.55	2.911	2.948
North	9.931		39.73	0.20	23.02	2.828	3.351
North (Degraded)			7.96	0.20	23.02	0.577	0.682

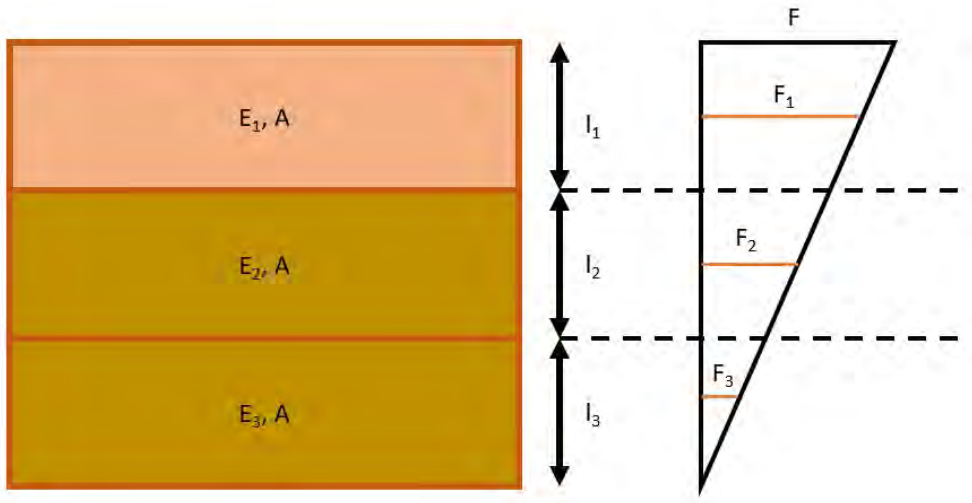

Figure 5.11. Attenuation of force experienced by soil layer with increasing depth that is assumed

Analytical solution to the equation presented in chapter 5.1.2 that expressed the stress experienced by subsoil as a function of c_1 constant, c_2 constant, displacement, w_s, and change in displacement, Δw_s, could be expressed in equation below [30]:

$$f_z = w_s\left(2\sqrt{c_{1w} \cdot c_{2w}} + c_{1w}b\right)$$

Where f_z (kN/m) represent the total load acting on subsoil, c_{1w} and c_{2w} are Winkler Pasternak constants, b (m) is the width of the foundation modelled.

Considering that the deformation modulus, k, of subsoil is defined as the settlement, w, that a load, f_z, causes. This modulus of deformation, k, could be represented as [30]:

$$k = 2\sqrt{c_{1w} \cdot c_{2w}} + c_{1w}b$$

Based on the abovementioned equation, the modulus of deformation that would be used as spring constants for the 3D modelling is tabulated below.

Table 5.4. Spring constants to be used at different part of the wall

k values (MPa)		
Wall thickness	1.2m	0.6m
South	77.24	56.24
South (Degraded)	12.84	9.35
North	12.94	9.55
North (Degraded)	2.64	1.94

5.4 Results

5.4.1 2D Models

In the 2D transverse wall modelling, the resulting maximum deformation due to the church loads in the original soil is 3.3mm, while it is 20.3mm in the current soil condition. It can be deduced that the northern part the church has a differential settlement of 17mm. This amount of deformation is then simulated in the model of the transverse wall. The pictorial deformation results from the 2D models could be seen in Figure F.1 to Figure F.4 in Appendix F.

The resulting stresses in the transverse wall due to differential settlement imposed are shown in Figure 5.12. In general, since the northern (right) side of the church is deforming more than the southern (left) side of the church, the right part of the transverse walls is undergoing compressive shear stress while the left side tensile shear stress. The stresses could be seen to be the maximum in the middle of the wall and at the bottom right corner of the church. The stresses at the bottom right corner of the church will not be taken into account in this part as this is due to incompatibility of the corners.

As such, the maximum shear stress is shown to be acting on the western transverse walls and is of 0.2 MPa in value. As can be seen from the diagram, this is mainly due to the large opening in the façade that opens to the sacristy. As the sacristy is built later and due to the large crack separating the main church and the sacristy, the sacristy wall is not modelled in this case. This shear stress is rather high considering the wall is deduced to have about 0.1 MPa tensile strength, which are usually not much lower compared to the shear stress. This is, then, a cause of concern.

One limitation of this model, however, is that it does not take into account the bracing provided by the longitudinal walls of the church. Hence, another 3D model to simulate the whole church behaviour was analysed and the results will be presented in the next section.

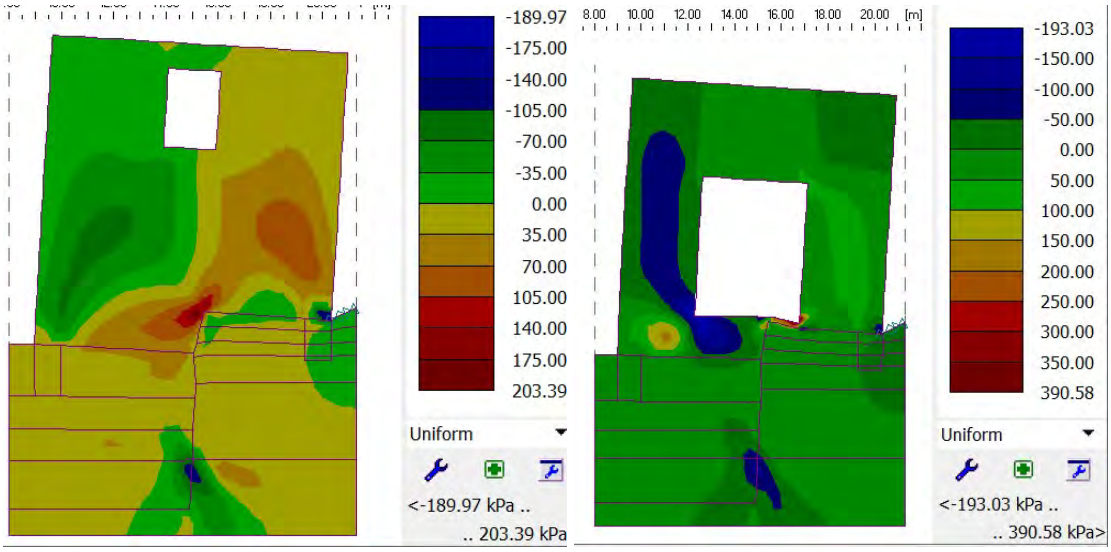

Figure 5.12. Shear stresses in the eastern (left) and western (right) transverse walls of the church due to imposed soil settlement

In the longitudinal wall modelling, the maximum deformation for the southern and northern is 13.8mm and 72.6mm respectively. This is higher as compared to the values of deformation obtained by the sectional modelling of the walls. This is because of the stretch of poorer soil at the kink of the church due to faulty drainage system. While the value looks outrageously high, this value is not too far off the ratio suggested by Eurocode for normal usage of concrete building, which is L/250 [37]. Since the width of the building at this edge is around 13m, the allowable deformation according to Eurocode for concrete structure would be 52mm. Hence, the current differential settlement between the longitudinal walls could be considered acceptable as masonry has generally more ductility as compared to concrete and should be able to sustain higher deformation. The figure showing deformation of each part of the longitudinal wall can be found in Figure F.5 to Figure F.6 in Appendix F.

Figure 5.13 and Figure 5.14 shows the horizontal stress attributed in the wall due to the different soil stiffness. It could be seen that the tensile stresses are concentrated at the top and bottom of the window openings, as well as above the poorer subsoil section. This is because both the window openings and the poorer subsoil is not able to transfer vertical load down as effectively as the adjacent elements. Hence, the vertical load is transferred diagonally. This diagonal force is resolved to be vertical force and horizontal force directed from the middle of the opening away from it. This horizontal force causes tensile force above these openings [Figure 5.15].

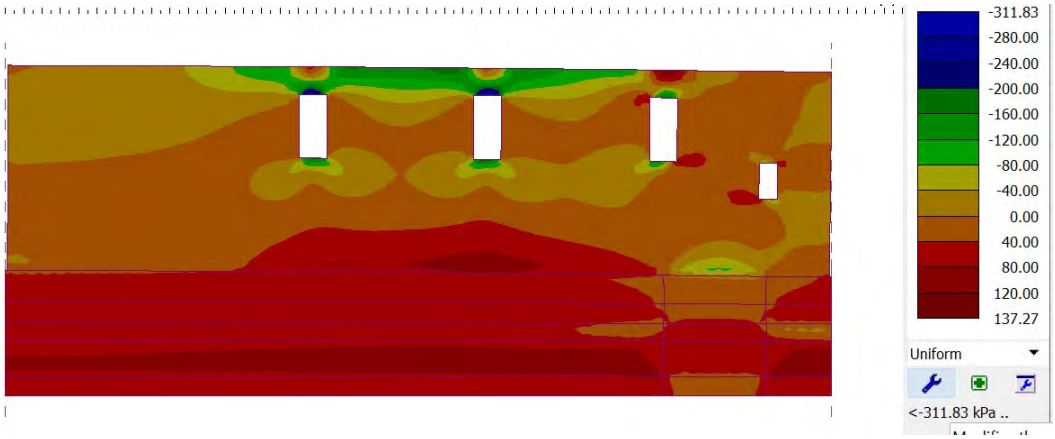

Figure 5.13. Horizontal stress distribution of southern longitudinal walls

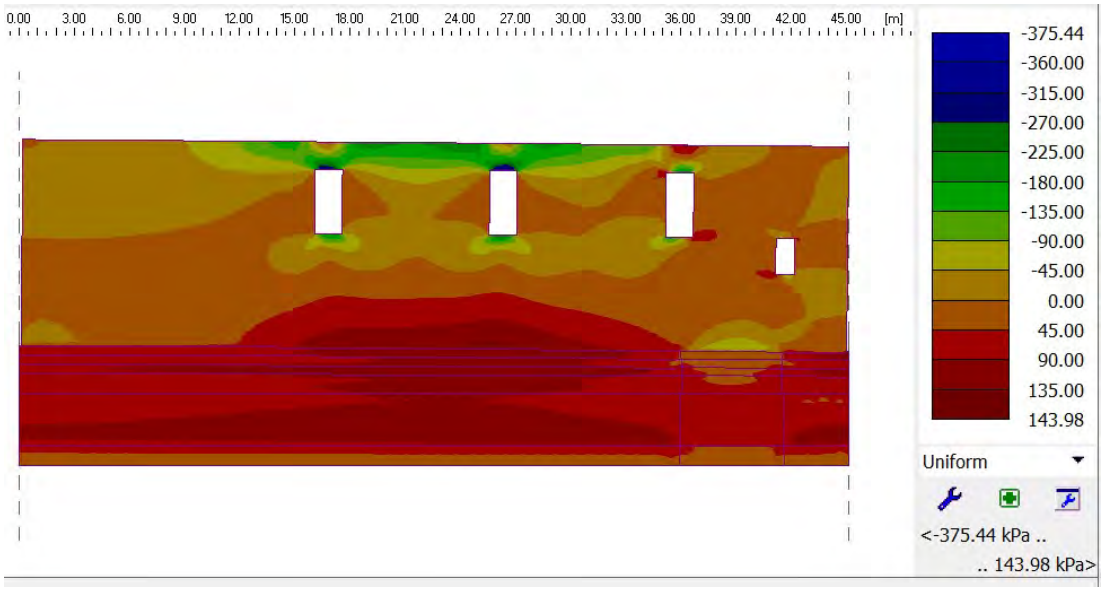

Figure 5.14. Horizontal stress distribution of northern longitudinal walls

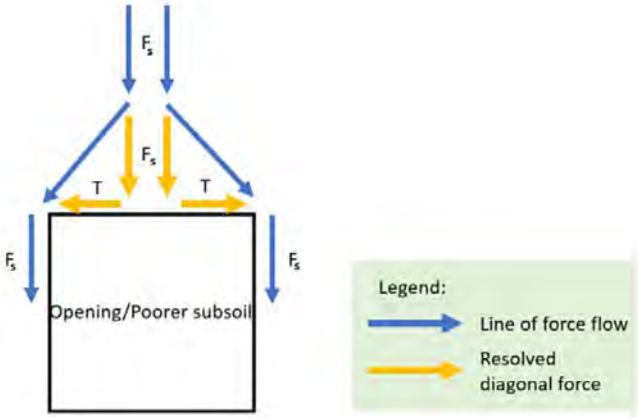

Figure 5.15. Schematic diagram of tensile force build-up above opening and poorer subsoil

In this study, the part above the window openings could be ignored at this time due to the presence of stiff ring beam across the top of the wall that is able to transfer this force more effectively. With that in mind, the maximum tensile stress that the wall is subjected to is about 0.135 MPa. This is rather significant as this is slightly more than 10% of the compressive strength of the wall obtained from earlier analysis. Further study should be conducted to ascertain the tensile capacity of the wall to ascertain if remedial action to strengthen the foundation or the window wall should be considered.

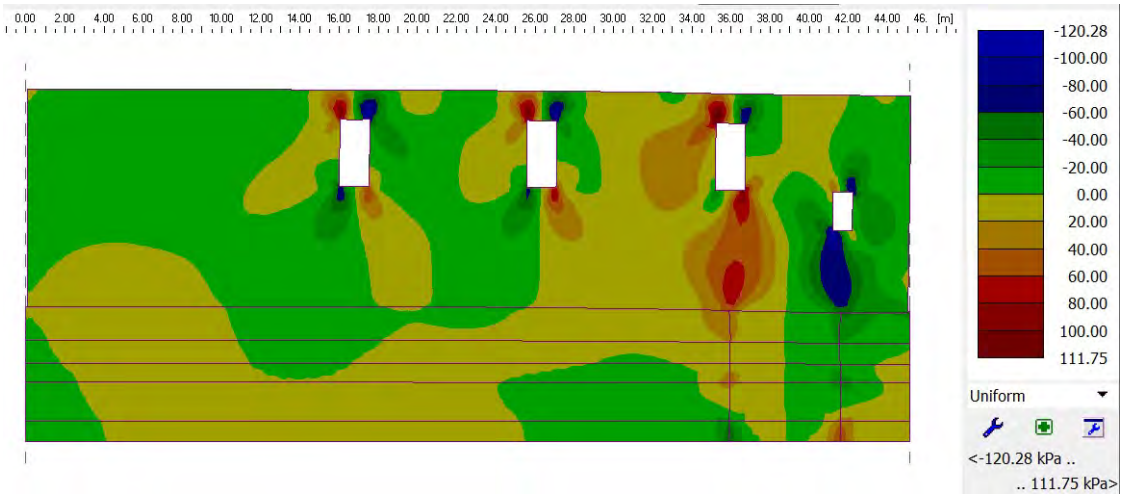

Figure 5.16. Shear stress distribution of northern longitudinal walls

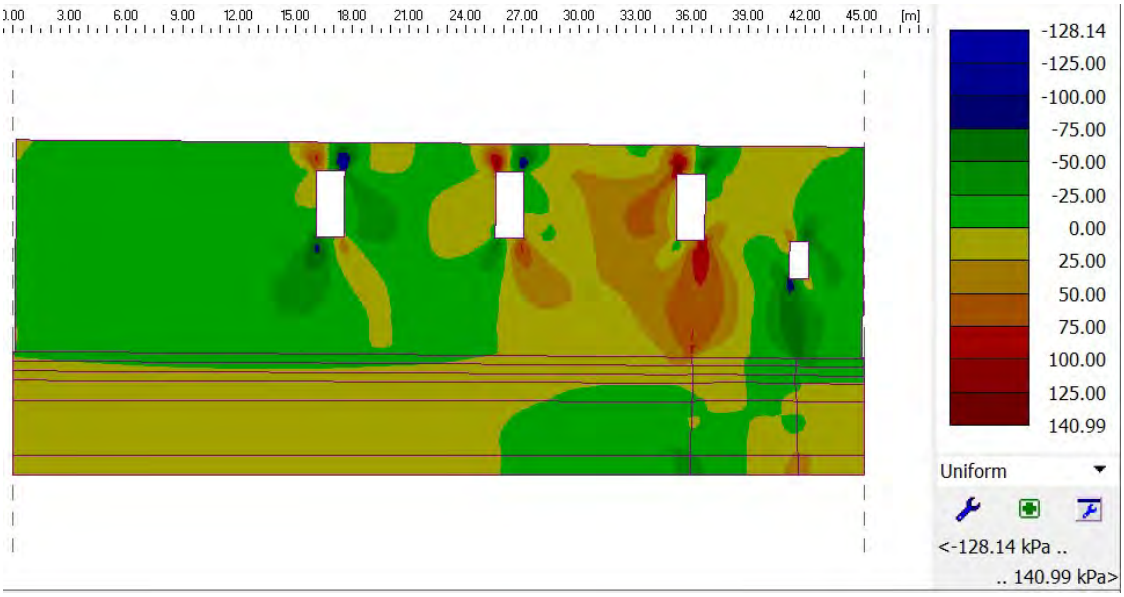

Figure 5.17. Shear stress distribution of northern longitudinal walls

Figure 5.16 and Figure 5.17 shows the shear stress attributed in the wall due to the load and the different soil type it is subjected to. Similarly, it can be seen from these two diagrams that the stresses are concentrated near the openings and the poorer subsoil border. The maximum values of the shear stress are found to be about 0.12 MPa, which is again rather significant for the masonry of the church in study.

Hence, this effect should be studied in more detail with parameters from further tests to ascertain the safety of the church.

In addition, it could be noted that the highest portion of the shear stress occur across the wall from the bottom of the rightmost window on the northern wall façade. This coincides with the crack on this part of the wall as shown in Figure 3.10 shown in the previous section.

5.4.2 3D Models

The results obtained from the analysis of the 3D models shows similar stress patterns as the ones obtained from the 2D models, but with lower magnitudes.

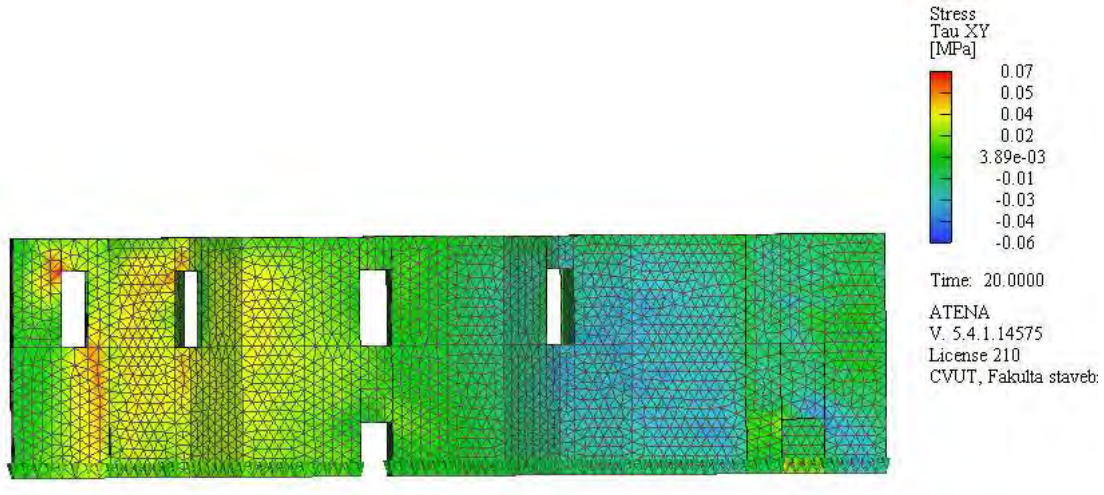

Figure 5.18. Shear stress distribution on the southern facade

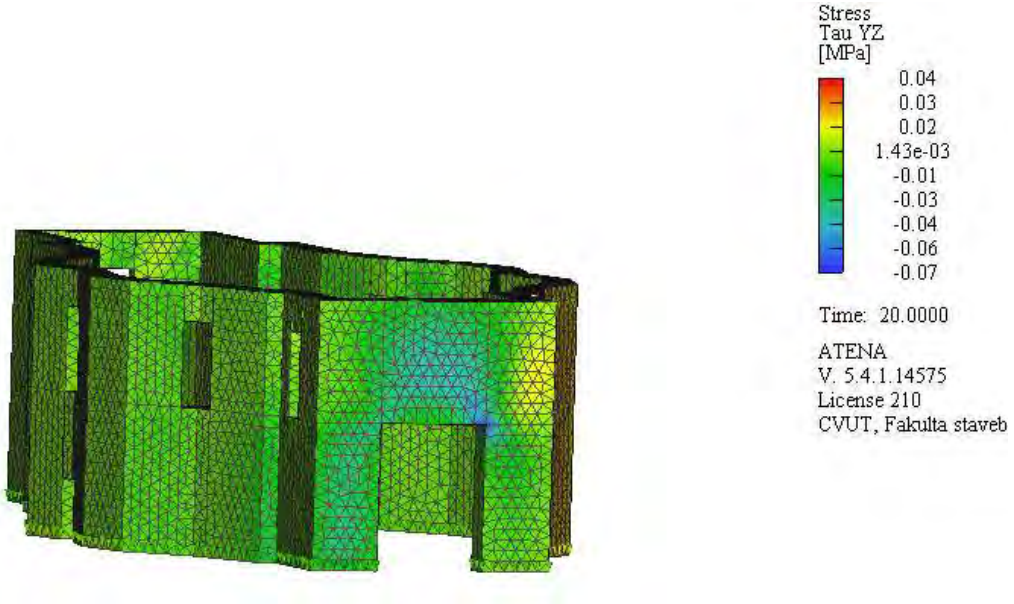

Figure 5.19. Shear stress distribution western façade

Figure 5.18 and Figure 5.19 shows the shear stress distribution on the lateral and transversal façade of the church respectively. On the lateral façade, it could be seen that the shear stresses in general have different direction on the left and the right side. Furthermore, stress concentrations could be observed around openings. Maximum stress is seen near the kink where the soil condition is worse near the western side of the church. However, the magnitude of the maximum stress is lower than that in the 2D models, it is 0.07 MPa, which is slightly lower than the estimated tensile strength of the material, which is about 0.1 MPa. While this shows that currently the church might not be in danger, this value is really close to the tensile capacity. Deterioration of the subsoil and the building stones should be monitored and controlled so that these stresses do not increase to be beyond the limiting values.

Regarding the horizontal stress distribution, the highest horizontal stress is observed on the western façade where there is a large opening to the sacristy. And this is observed at the top left and right of the façade. Considering the large opening on this façade, this is expected because the stress due to differential settlement on the northern and southern part of the church would pass through the stiffer part of the church, hence, from the solid top of the façade, the stresses would pass through the corners of the façade to the southern and northern façade. As for the magnitude, the maximum tensile stress is about 0.10-0.14MPa. Again, this is about the estimated tensile stress. It is rather alarming and as mentioned earlier, further tests and monitoring to ascertain the damage should be done.

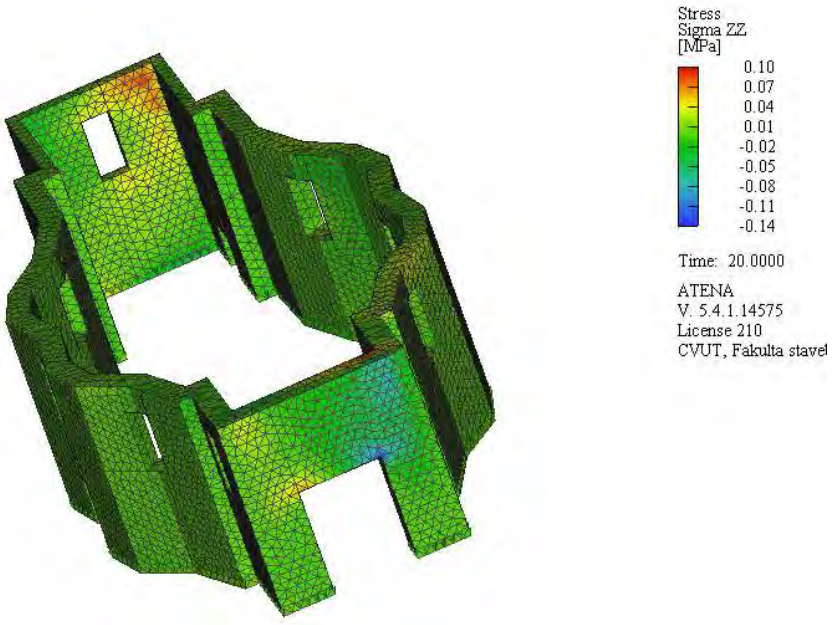

Figure 5.20. Horizontal stress distribution showing the front of the western facade and the back of the eastern façade

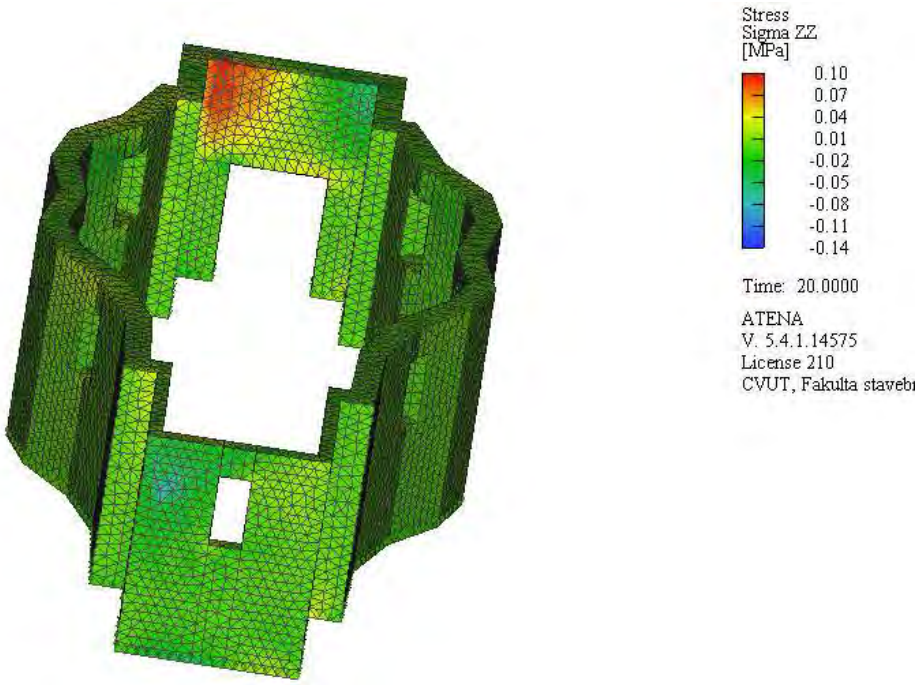

Figure 5.21. Horizontal stress distribution showing the front of the eastern facade and the back of the western facade

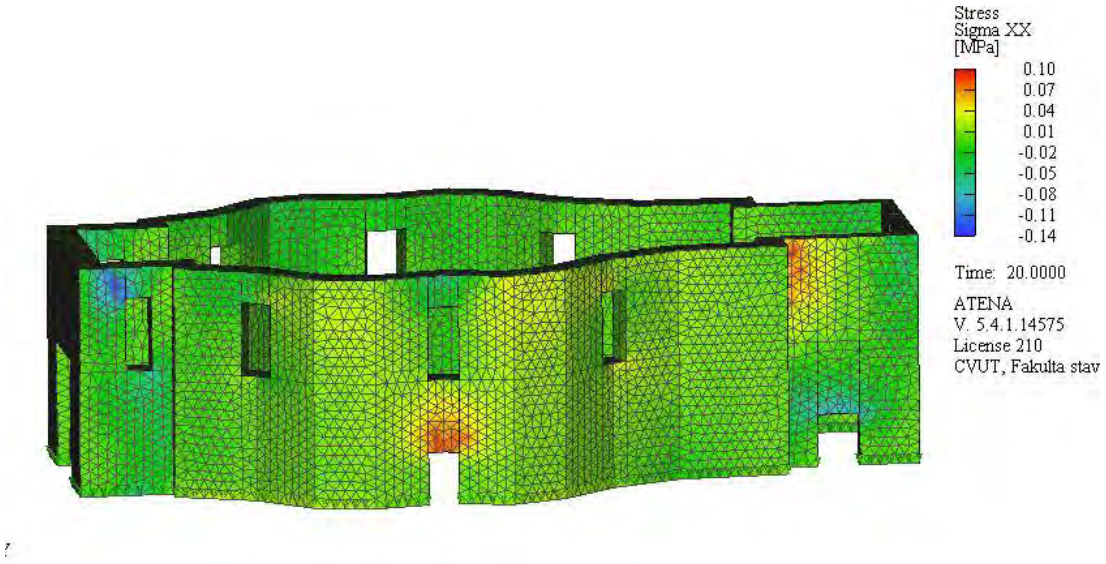

Figure 5.22. Horizontal stress distribution on the southern facade

This page is left blank on purpose.

6. CONCLUSION

The main threat to All Saints church in Hermankovice is the attack due to moisture from faulty drainage system, water ponding and groundwater infiltration. These problems lead to deterioration in the structure material capacity as well as deterioration in the subsoil properties. While deterioration in the subsoil properties might not be harmful to the structure if it happens uniformly across the building, in this case, the positioning of the church on an uneven terrain makes it worse by pronouncing the deterioration effect on one side of the church and lessening the effect on the other side. Differential settlement that occurs as a result has been shown, through series of 2D and 3D modelling, to potentially be causing significant damage to the structure.

From the analyses, conclusions regarding the original structure's capacity could be derived. Even with the currently deteriorated building blocks properties assumed, the wall structural capacity in terms of compression capacity is at least 100% higher compared to the load it is subjected too. As are other historical structures that were built without much knowledge about building statics, structures tend to be overdesigned. However, this is also the reason why these structures are able to be to sustain such deterioration over the years.

The results of the 2D analysis of the wall bearing capacity on the Young's modulus are very close to those recommended in the Italian circular for three leaves wall with regular brick masonry while the estimated value of strength of the masonry is similar to that of poor irregular stone masonry [22]. Furthermore, EC6 suggest a ratio of 1:1000 between compressive strength and Young's modulus of masonry [38]. This should yield a Young's modulus of 1GPa, as compared to the value of 7GPa adopted. This might suggest that the Young's modulus is overestimated while the strength values are underestimated leading to a conservative approach of higher stress and lower capacity adopted. However, in the case of this study, due to limited information, this more conservative values are still adopted.

Furthermore, the low bound values for mechanical parameter of the constituting stone blocks, mortar and infill material had been adopted in the analysis. This might further lower the capacity of the masonry analysed. Again, due to limited information, this assumption cannot be changed. Hence, further tests and monitoring should be carried out before a major restoration is done to the structure. Having said that, minor restoration and maintenance that prevent the situation from progressing further should be adopted immediately. Some of them are mentioned in the subsequent chapter.

This page is left blank on purpose.

7. RECOMMENDATION

7.1 Further studies

7.1.1 Tests

7.1.1.1 Double flat jack testing to obtain the Young's modulus

Since it is suspected that the Young's modulus might be overestimated for the masonry wall and a larger stress is obtained in the FEM analysis, one test that could be done is double flat jack test. In this test, two pressurizing tubes are installed horizontally parallel to each other. Strain gages are installed between the strain tubes to measure the deformation resulted from the pressure applied from the tubes. By plotting a stress-strain curve, the Young's modulus at different stresses could be obtained [39].

This instrument should be located carefully at heavily loaded part of the wall so as not to create uplift in the structure. In this case, it should be located on either side of the lateral wall at the bottom of the wall [Figure 7.1]. Furthermore, since the wall should not be loaded more than its original surcharge, the expected deformation should be around about 3.5cm, hence, strain gage with suitable sensitivity should be used.

7.1.1.2 Hole drilling with endoscopy test to ascertain the infill material

Furthermore, from the 2D analysis of the wall bearing capacity, the cracks are mostly located at the infill material. Since these are the weakest part of the masonry that ultimately cause failure, it may be worthwhile to ascertain the strength of these materials so that the FEM model could yield a more accurate results.

The first method that could be used to check the infill material is by visual inspection using endoscopy. Endoscopy is very useful in inspecting the interior of a structural element. It is done by introducing a borescope into a small hole, either newly drilled or existing ones. Borescope is a tube with a light source and an eye piece. Using this method, images of the interior of structural elements could be obtained [40].

This minor destructive method not only leaves very minor damage to the wall but gives a very important insight to how thick the outer leave wall actually is and images of the inner infill that would enable very much more accurate estimation of the infill properties [40]. Depending on the amount of void observed in the images, the strength of the infill material could be better apprehended.

Due to the minor impact of the test on the building, several numbers of this test could be performed. One should be done at each side lateral and transverse wall, away from areas with high stress concentration (i.e. away from openings and supports) [Figure 7.1].

7.1.1.3 Removal of infill material for lab testing to obtain the material properties

Another method that could be used to determine the infill material properties causes more damage to the structure, but it is more precise. This method involves creating a small opening on the wall exposing the infill material. The infill materials could then be removed and tested in the lab for its mechanical properties.

Due to the destructiveness of this method, this method should be limited to thicker wall. This test is proposed to be done on the southern side of the lateral wall from the inner side [Figure 7.1]. As was noted for the previous test, this test should be located away from areas with stress concentration.

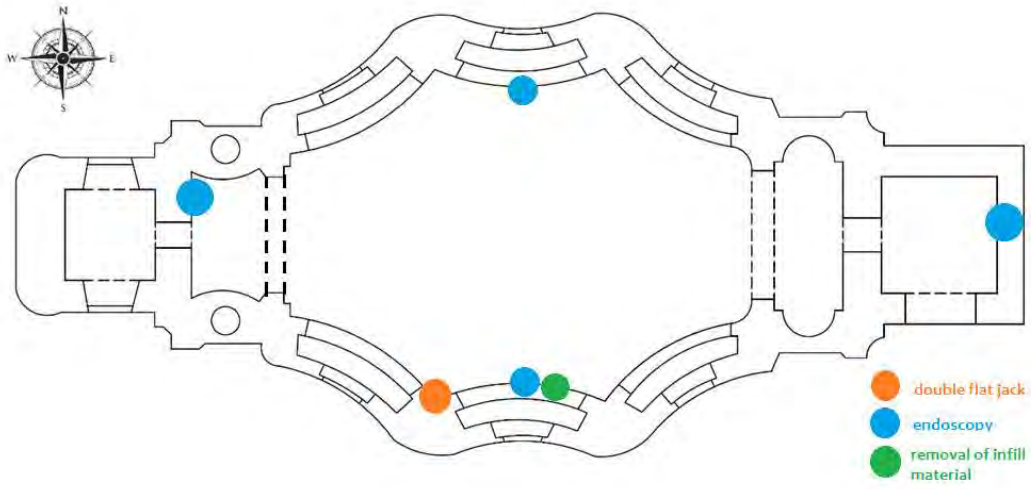

Figure 7.1. Proposed location of additional tests

7.1.2 Monitoring

The most prominent damage observed in the church is the pattern of cracks along the church transverse arches. And from this study, it was concluded that there is a possibility that this is related to differential soil settlement of the church. Since restoration of historical buildings should be kept at minimum to preserve its historical value and well as to reduce resources spent, damages should be proven as active damage before a major restoration plan is conducted.

The two major variables to be monitored in this church include structural damage (crack) monitoring and settlement monitoring. Since there has already been a settlement monitoring to monitor the settlement of the building in either side of the church, only crack monitoring will be proposed in this work.

One way to ascertain active damage is by placing a set of sensors to monitor if the crack is opening or whether the opening has stabilized over the years. In the case of All Saints Church, one number of LVDT fitted with temperature sensor is proposed to be placed to monitor the largest cracks on each transverse arch. furthermore, one should be placed outside the sacristy where a large crack through the

transverse sacristy wall could be observed. Hence, this would total up to 3 numbers of LVDT sensors [Figure 7.2].

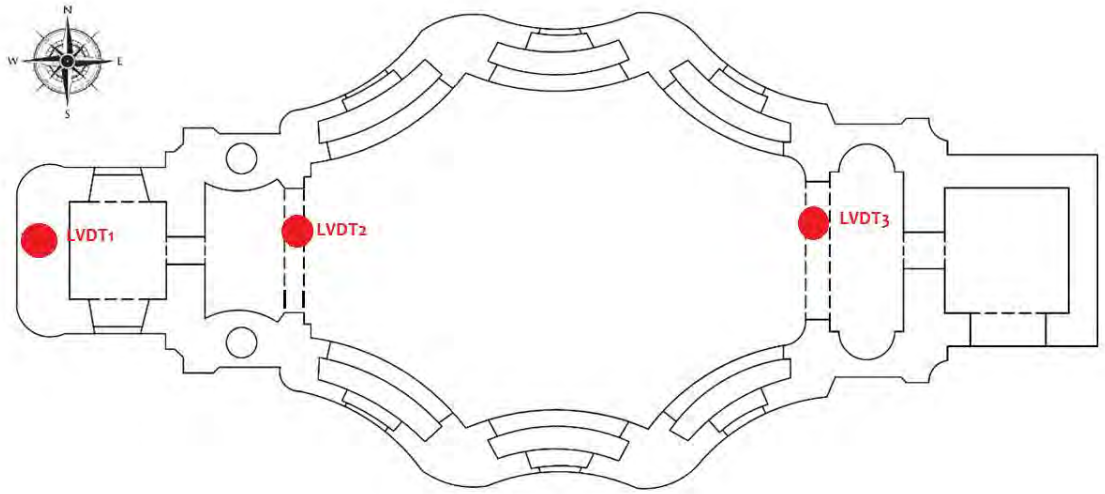

Figure 7.2. Proposed placement of crack monitoring LVDT fitted with temperature sensor

7.2 Recommendation for remedial work to be done

In this sub-chapters, a few recommendations for remedial work will be elaborated. Some are to be done immediately as the repair technique requires no changes to the structural component and is easily removable. Furthermore, these repairs aim to fix cases that are obviously causing harm to the structure. Other major interventions are categorized as future repair that should only be carried out upon further confirmation of problem and if no other more minor interventions are available.

7.2.1 Immediate repair

7.2.1.1 Replacement of drainage system from the roof with slanted protective steel net cover and larger rainwater downpipes to prevent clogged drainage

The first immediate repair proposed is to replace the drainage system of gutters channelling water down through a rainwater down pipe by the side of the wall. Even though the pipes channelling the water down to the ground looks rather new, drops of water were observed to be dripping near these pipes. This could mean clogging of these pipes causing water to overflow from the rooftop gutters to the ground or to seep through the wall. Considering proximity of the church to large trees, the clogging could potentially be due to the leaves from the trees that were blown onto the gutters.

A proposal is to create a special gutter system that is placed little lower than the roof with slanted grating cover to prevent the leaves to accumulate in the gutter and thus allowing smooth water flow in times of rain or snow melting. Furthermore, the grating cover is envisioned to be slanted so that leaves would not be accumulated on the cover at all times. Lastly, the rainwater downpipe is proposed to be enlarged

to a size of 25-30cm to reduce the possibility of clogging. Figure 7.3 shows a simple illustration of the proposed improvement of the rooftop gutter system.

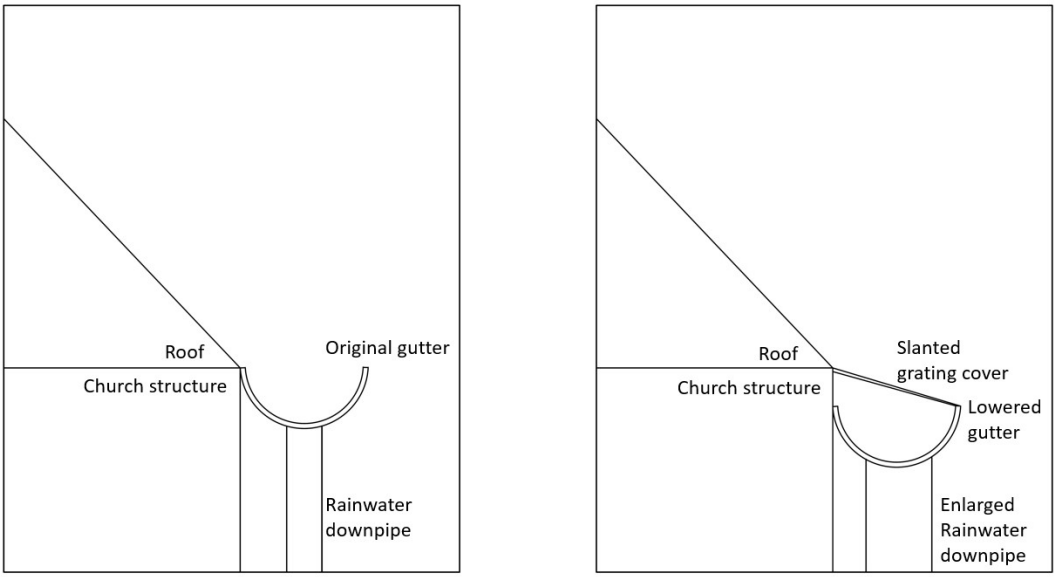

Figure 7.3. Proposed improvement to the rooftop gutter system to avoid clogging (current condition (left) and proposed improvements (right)

7.2.1.2 Repair of drainage channels on the ground to be larger and more resistant with open covers to allow water to penetrate quick enough as to not allow water ponding

The second immediate repair proposed is the drains on the ground level. As mentioned in the earlier chapters, due to the terrain of the location on which the church is sitting on, the northern part of the church is prone to water ponding and higher exposure of water flow. To minimize this effect, proper water channelling system should be constructed such that water flowing from adjacent slope will be directed towards this drain instead of to the church wall or absorbed by the subsoil under the church. To ensure this, the drain should be large enough and the top of the drain should be covered with porous grating instead of solid concrete cover that is used currently allowing smooth water flow into the drain.in order to reduce the aesthetical impact on the church surrounding, instead finishing the drain with steel grating, a 10cm deep large gravels topping is proposed. Large gravels with low thickness is proposed to allow water porosity.

Furthermore, the repair should also ensure minimal water seepage from the subsoil to the wall since substantial evidence of groundwater infiltrations had been observed. This could be done by moving the drain away from the side of church, but creating an empty space allowing air circulation after rain or wet event to encourage evaporation and quick drying of the walls.

The proposed system is illustrated in diagram shown in Figure 7.4.

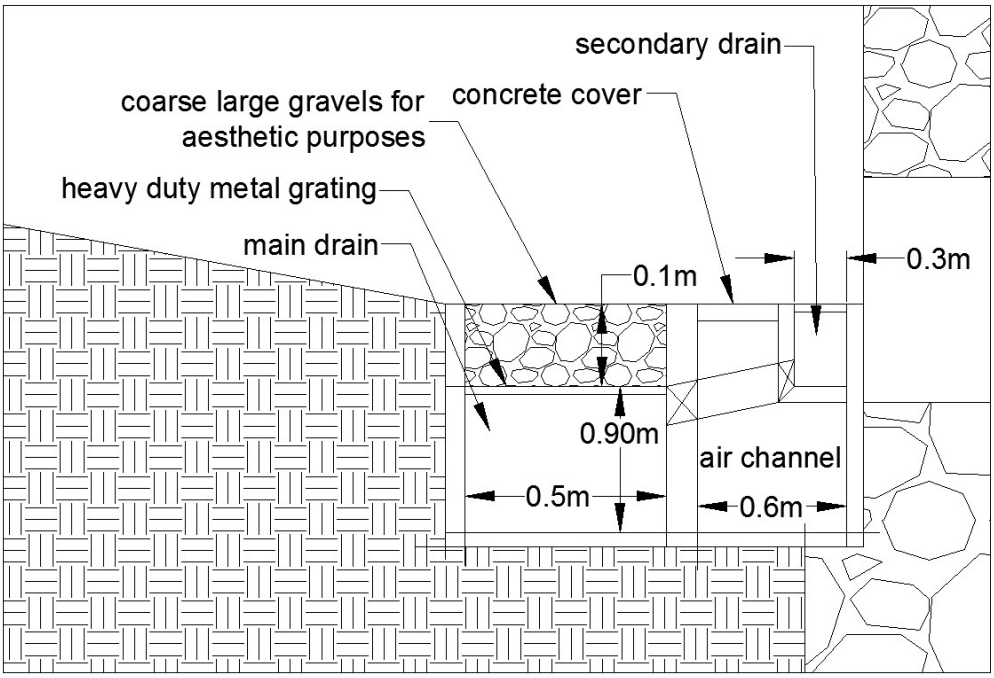

Figure 7.4. Illustration of the proposed drainage and air channel system along the norhtern facade

7.2.1.3 Reduce effect of water infiltration by means of providing covered air channels surrounding the foundation of the church

Figure 7.4 also shows an air channel to be constructed beside the main drain with a shallow secondary drain of about 100mm to 150mm deep to channel any rainwater that might accumulate near the church. The purpose of providing this air channel is to keep the church foundation and structure dry and reduce the potential groundwater infiltration to the structure. Furthermore, this brings moisture away from the subsoil under the church as well leaving the subsoil drier and reduce the rate of degradation of the subsoil, thereby stopping further possible differential settlement problem.

7.2.2 Potential repair to be done in the future

The abovementioned immediate solutions are meant to prevent further degradation of the church structures, foundation and subsoil. However, they do not restore the church to its original condition. While this might be sufficient in the short run, the actual extent of differential soil settlement problem on the safety of the church should be assessed in greater detail and if it is necessary, strengthening should be done to improve the soil condition near the kink location and on the northern side of the church. Alternatively, the church structure could be strengthened by addition of ties.

Various methods could be implemented to strengthen the foundation of a structure sitting on a settling ground. Two most commonly used methods include lime injection to the subsoil and change of foundation system to piling system. Lime injection is proposed in this study instead of addition of micropiles. From the borehole boring done previously, it was could be seen that pieces of rock exist in

the subsoil from depth of 2m onwards. Furthermore, from 6m onwards, the subsoil is made of very hard ryolite. Since micropiles have normally more than 6m of depth, it is not very suitable to be implemented in All Saints' church's subsoil.

Lime injection is suitable in this case because the subsoil seems to consist of very hard rock pieces with voids in between filled with sandy silt. Since the sandy silt is rather dense, the lime injection should be of low viscosity and is able to penetrate small voids. The lime injection will be done by placing steel tubes with openings into a few small holes drilled in the poorer subsoil areas.

REFERENCES

[1] Embassy of the Czech Republic in Stockholm, “History of the Czech Republic,” 2015. [Online]. Available: http://www.mzv.cz/stockholm/en/information_about_the_czech_republic/history/index.html. [Accessed 15 May 2017].

[2] P. Hajek and J. Tywoniak, “Towards Sustainable Building in the Czech Republic,” in *World Sustainable Building Conference*, Melbourne, 2008.

[3] Euratlas, “Bohemia-Hungary in 1500,” 2012. [Online]. Available: http://www.euratlas.net/history/europe/1500/entity_35.html. [Accessed 10 May 2017].

[4] B. Gascoigne, “History of Bohemia,” From 2001, ongoing. [Online]. Available: http://www.historyworld.net/wrldhis/PlainTextHistories.asp?groupid=2617&HistoryID=ac40&gtrack=pthc. [Accessed June 2017].

[5] B. Prokop, J. T. Kotalik and P. Suva, Broumov Group of Churches - Guide to Czech Baroque in the Landscape of Sandstone Rocks, Vernerovice: Modry Andel, 2007.

[6] J. Kotalík, Architektura barokní, Praha: Správa Paržského hradu, 2001.

[7] D. Gerson, “Baroque Architecture - A Stroll through the Epochs - 16th - 18th Century,” 18 March 2015. [Online]. Available: https://www.gentlemansgazette.com/baroque-architecture-guide-explained/. [Accessed 10 May 2017].

[8] Mesto Broumov, “The Region of Broumov,” 2003. [Online]. Available: http://arch.broumov-mesto.cz/verze/b_gb_region.html. [Accessed 10 June 2017].

[9] P. Duinker, “First and second order analysis of St. Ann’s church timber roof in Vižňov, CZR,” Czech Technical University in Prague, Prague, 2009.

[10] Ceska Geologicka Sluzba, “Geologicka mapa,” [Online]. Available: http://mapy.geology.cz/geocr_50/. [Accessed 20 June 2017].

[11] The University of Auckland, “Rhyolite,” The University of Auckland, 2005. [Online]. Available: https://flexiblelearning.auckland.ac.nz/rocks_minerals/rocks/rhyolite.html. [Accessed 27 June 2017].

[12] E. M. Winkler, Stone in Architecture - Properties and Durability, Berlin: Springer-Verlag, 1994.

[13] M. Sejnoha, *GEO FEM - Theoretical manual,* Prague: Fine, Ltd, 2009.

[14] M. Ramesh, *Analysis of Lusitanian Timber Framed Walls with Shallow Foundations,* Prague: Czech Technical University, 2016.

[15] V. B. Bosiljkov, “The use of industrial and traditional limes for lime mortars,” *Historical Constructions,* pp. 343-352, 2001.

[16] L. A. Palmer and D. A. Parsons, “A Study of the Properties of Mortars and Bricks and their Relation to Bond,” *Bureau of Standards Journal of Research,* vol. 12, pp. 610-643, 1934.

[17] M. R. A. Vliet and J. G. M. Mier, “Size effect of concrete and sandstone,” *HERON,* vol. 42, no. 2, pp. 97-108, 2000.

[18] Engineering ToolBox, “Compression and Tension Strength of some common Materials,” 2015. [Online]. Available: http://www.engineeringtoolbox.com/compression-tension-strength-d_1352.html. [Accessed June 2017].

[19] P. Sammonds, “Earth Materials,” 2015. [Online]. Available: http://www.ucl.ac.uk/EarthSci/people/sammonds/13%20Earth%20Materials.pdf. [Accessed June 2017].

[20] X. Yu, C. D. da Gama, Y. Na, Q. Wang and Q. Xie, “Deformation behaviour of rocks under compression and direct tension,” *The Journal of The South African Institute of Mining and Metallurgy,* pp. 55-62, 2006.

[21] F. M. Fernandes, P. B. Lourenco and F. Castro, “Chapter 3: Ancient Clay Bricks: Manufacture and Properties,” in *Materials, Technologies and Practice in Historical Heritage Structures*, Dordrecht, Springer Science+Business Media B. V., 2010, pp. 29-48.

[22] IMIT, *Circ. 02.02.2009, n. 617: Istruzioni per l'applicazione delle Nuove Norme Tecniche per le Costruzioni di cui al decreto ministeriale 14 gennaio 2008,* Rome: Italian Ministry of Infrastructures and Transportation, 2009.

[23] J. Milosevic, R. Bento, A. S. Gago and M. Lopes, "Seismic Vulnerability of Old Masonry Buildings - SEVERE Projects," Department of Civil Engineering and Architecture (DECivil), Instituto Superior Tecnico, Lisbon, 2011.

[24] V. Cervenka, L. Jendele and J. Cervenka, *ATENA Program Documentation Part 1 : Theory,* Prague: Cervenka Consulting, 2016.

[25] EN1990, *Eurocode: Basis of structural design,* CEN European Committee for Standardization, 2005.

[26] EN1991-1, Eurocode 1: Actions on structures, CEN - European Committe for Standardization, 2003.

[27] C. Modena, P. B. Lourenco and P. Roca, Structural analysis of historical construction, Leiden (Netherlands): A. A. Balkema Publishers, 2005.

[28] J. P. Wolf, Dynamic Soil-Structure Interaction, Englewood Cliffs, New Jersey: Prentice-Hall, Inc, 1985.

[29] B. J. S. Breeveld, *Modelling the Interaction between Structure and Soil for Shallow Foundations,* Delft: TU Delft.

[30] P. Kuklik, M. Kopackova and M. Broucek, "Elastic layer Theory and Geomechanics," *CTU Reports,* vol. 13, no. 1, 2009.

[31] P. Kuklik and M. Broucek, "Stavarina.cz," 2010. [Online]. Available: http://www.stavarina.cz/depth/depth.htm. [Accessed June 2017].

[32] A. Caselunghe and J. Eriksson, "Structural Element Approaches for Soil-Structure Interaction," Chalmers University of Technology, Göteborg, Sweden, 2012.

[33] V. N. S. Murthy, "Chapter 6: Stress Distribution in Soils due to Surface Loads," in *Geotechnical Engineering - Principles and Practices of Soil Mechanics and Foundation Engineering*, New York, Marcel Dekker, 2005, pp. 173-203.

[34] Bracken Engineering Inc., "Establishing and Investigating Foundation Zones of Influence," 2014. [Online]. Available: http://www.structuraldamage4.com/pdf/Bracken-Engineering-Establishing-and-Investigating-Foundation-Zones-of-Influence.pdf. [Accessed June 2017].

[35] A. Graham, "Young's Modulus," 1997. [Online]. Available: http://community.dur.ac.uk/~des0www4/cal/dams/geol/mod.htm. [Accessed June 2017].

[36] Geotechdata.info, "Soil elastic Young's modulus," 2013. [Online]. Available: http://www.geotechdata.info/parameter/soil-young's-modulus.html. [Accessed June 2017].

[37] EN1992-1-1, *Eurocode 2 Part 1-1: Design of concrete structures - General rules, and rules for buildings,* CEN European Committee for Standardization, 2004.

[38] EN 1996-1-1, *Eurocode 6: Design of masonry strructures - Part 1-1: General rules for reinforced and unreinforced masonry structures,* CEN European Committee for Standardization, 2005.

[39] NCREP - Consultoria em Reabilitação do Edificado e Património, "Flat-jack tests (simple and double)," 2017. [Online]. Available: http://www.ncrep.pt/view.php?id=14388. [Accessed 1 June 2017].

[40] I. Lombillo, L. Villegas and J. Elices, Non (minor) destructive methodologies applied to the study and diagnosis of masonry structures of the building heritage: a state of the art, 2009.

A. APPENDIX A – BORELOG DETAILS

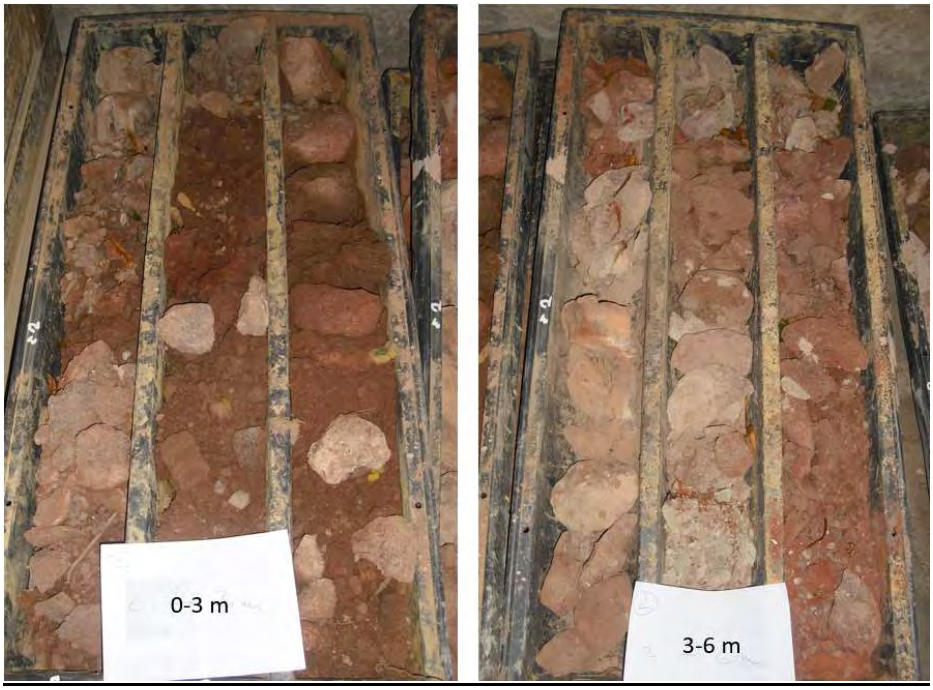

Figure A.1. Extracted soil tube from borehole beside the northern wall at depth 0-3m (left) and 3-6m (right)

Figure A.2. Extracted soil tube from borehole beside the northern wall at depth 6-9m (left) and 9-12m (right)

Figure A.3. Extracted soil tube from borehole beside the southern wall at depth 0-3m (left) and 3-6m (right)

Figure A.4. Extracted soil tube from borehole beside the southern wall at depth 6-9m (left) and 9-12m (right)

Table A.1. Bore log description of extracted soil sample from borehole close to northern wall

Depth (m)	Description	Categorization for modelling purposes
0,00 - 0,30	bigger pieces of strongly weathered sandstone, max. size 10 cm, from fine-grained to medium-graiened, sometimes so weathered positions, that they look like soil; light coloured sandstone	sandy silt
0,30 - 0,60	fine masonry fragments from strongly weathered sandstones - both light coloured fine-grained, as well as red Permian sandstones, which are harder; light coloured sandstones are falling into pieces in hand; average size 4 cm; significant amount of brownish-red slimy soil	
0,60 - 1,20	bigger peices of weathered coarse-grained sandstone, both dark as well as light coloured, in some places smaller pieces of almost sandy siltstone (weathered), high amount of fine masonry fragments of almost soil character	weathered sandstone
1,20 - 1,55	strongly weathered ferruginous sandstone, mostly already incoherent creating "soil"	sandy silt
1,55 - 1,65	"harder" light coloured sandstone, lightly weathered	
1,65 - 1,80	strongly disintegrating "sandsotne" almost to sandy soil of brownish-red colour	
1,80 - 2,00	compact piece of ferruginous sandstone	weathered sandstone
2,00 - 2,30	quartz porphyre, compact big pieces, beige-red colour	
2,30 - 2,40	"hard" sandstone (almost of greywacke character)	
2,40 - 2,50	weathered sandstone (fragments), see upper lines, together with "soil"	
2,50 - 2,60	ignimbrite, hard	
2,60 -3,00	strongly weathered basement (probably originally brownish-red Permian sandstones) with bigger pieces of quartz porphyre and brown-black sandstone	
3,00 - 3,10	brownish-red sandstone, weathered	weathered sandstone
3,10 - 3,80	sandstone to arcose sandstone, firstly with brownish-red colouring, at the end brown-black (greywacke character), in some places strogly silicified (cement, compacted grains), relativ hard	
3,80 - 3,85	position of greenish siltstone to silty marlite	
3,85 - 4,00	brown-black sandstone, fine- to medium-grained, high portion of feldspars	
4,00 - 4,20	very fine-grained sandstone to silty sandstone, thinly laminated, soft, weathered	
4,20 - 4,60	pinkish to brownish-red sandstone, very coarse-grained, hard	
4,60 - 4,90	silty sandstone to siltstone, in some places brown laminas, at the end strongly weathered with the position of slimy soil	
4,90 - 5,00	fine-grained brownish-red sandstone, relativ hard	
5,00 - 5,25	silty sandstone to siltstone, in some places brown laminas, at the end strongly weathered with the position of slimy soil	
5,25 - 6,10	brownish-red coarse-grained sandstone, at the end strongly weathered, completely crumbling, pieces without coherent core	
6,10 - 6,50	smaller compact pieces of quartz porphyre (paleryolite)	weathered ryolite
6,50 - 7,00	compact drill cores of quartz porphyre, feldspars kaolinizated	
7,00 - 7,40	bigger pieces of quartz porphyre of beige-brown colour, partly weathered, coherent (disintegrates after hammer hit)	
7,40 - 7,60	light beige to grey quartz porphyre (paleoryolite), partly weathered, feldspars ochre (kaolin.)	
7,60 - 8,00	strongly weathered sandstones to fine-grained conglomerates, dominance of powdery material, without compact core pieces	
8,00 - 9,00	strongly weathered coarse-grained sandstone to conglomerate	
9,00 - 9,50	quartz porphyre (paleoryolite), hard, with positions of clay soil	
9,50 - 9,70	quartz porphyre (paleoryolite), hard, pieces	
9,70 - 10,9	pyroclastic sediment (?), changing of soily clay positions with vulcanic stones fragments (q. porphyre), completely falling into pieces after light hit	
10,9 - 12,00	compact pieces of drill core made by quartz porphyre, in some places soil-clay insertion	

Table A.2. Bore log description of extracted soil sample from borehole close to southern wall from 0-6.36m

Depth (m)	Description	Categorization for modelling purposes
0,00 - 0,30	soil, loess-sandy soil	weathered sandstone
0,30 - 0,59	faine-grained to coarse-grained brownish-red sandstones, slightly weathred (faine-grained are harder). Smaller pieces strongly weathered (easy to break up, coarse-grained easy to crumble by hand)	
0,59 - 0,77	smaller pieces of sandstones with soil (with the presence of calcitic component)	
0,77 - 1,00	bigger pieces of stones with soil, mostly faine-grained ferruginous sandstone (relatively hard); light gray fine-grained sandstone (very soft, easy to break up by hand, but does not crumble)' brown faine- to medium-grained sandstone (partly weathered, possible to break up, very soft)	
1,00 - 1,65	bigger compact pieces of stone material of a round shape (as a consequence of drilling) with the height 1,5 to 10 cm; very softly weathered sandstones (medium-coarse, gray-wine-coloured); conglomerate; ignibrite; conglomerate with ferruginous cement; coarse-grained ferruginous sandstones to conglomerates (very soft, easy to break up by hammer)	
1,65 - 2,00	brown-redish sandy soil	
2,00 - 2,44	dark brown-redish sandstone, smaller pieces extremely weathered (extremely soft, are crumbling in hand, big pieces compact)	very weathered sandstone
2,44 - 2,76	extremely weathered ferruginous sandstone to sand (coherent), wet	
2,76 - 3,30	very weathered ferruginous sandstone with the admixture of calcite, easy to be falling into pieces, wet, extremely soft	
3,30 - 3,90	compact sandstone, brown-redish with parts of lighter coloured sandstones, close to 4 m sandstone changes colour to gray-black; medium- to coarse-grained	weathered sandstone
3,90 - 4,05	silty-clay sediment, thin insertion, ochre colour	
4,05 - 4,50	brown-redish disintegrated sandstones, non-compact pieces, weathered, coarse-grained	
4,50 - 4,70	brown-black coarse-grained sandstone to conglomerate, strongly weathered (very soft, easy to crumble by fingers, but compact pieces)	very weathered sandstone
4,70 - 4,90	fine-grained light gray sandstone with greenish positions (Cu compound), extremely soft	
4,90 - 5,00	gray-beige medium-coarsed sandstone, not crumbling in hand, but easy to break up by hammer, very soft	
5,00 - 5,62	gray-beige medium-coarsed sandstone, not crumbling in hand, but easy to break up by hammer, in some places coarse-grained, very soft	
5,62 - 5,77	strongly disintegrated sandstone to coarse-grained sand with sandstone pieces, brown-redish col., in some places grey-beige, extremely to very soft	
5,77 - 5,90	coarse-grained sandstone to conglomerate, brown-redish, compact pieces, strongly weathered	
5,90 - 6,00	black-brown crushed sandstone with the portion of fine-grained gray-greenish siltstone (to marlite), soft	
6,00 - 6,12	gray-green fine-grained clastic sediment (siltstone to fine-grained sandstone) - gradually changes to coarse-grained parts	
6,12 - 6,20	strongly weathered sandstone to conglomerate, is crumbling in hand, wet, brown, extremely soft	
6,20 - 6,36	light coloured gray-green, fine-grained clastic sediment to marlite, soft, but compact	

Table A.3. Bore log description of extracted soil sample from borehole close to southern wall from 6.36-12m

6,36 - 6,60	light gray ryolite (quartz porphyre) with predominant fine-grained matrix, compact pieces, easy to break up by hammer, moderately hard	weathered ryolite
6,60 - 6,70	compact drill core made by the same light coloured stone, clay-soily waste around	
6,70 - 7,00	fragments of light coloured stones, mixed clay-soily waste with clods	
7,00 - 7,30	extremely soft, crumbling in hands, fragments of light coloured stone	
7,30 - 7,67	big compact pieces, cores to 10 cm height, hard, quartz porphyre (paleryolite), very hard	
7,67 - 8,00	smaller fragments of the same stone, very hard	
8,00 - 8,60	fragments of the same stone (max 10 cm)	
8,60 - 8,70	fragments of the same stone, in some places strongly disintegrating to white fine dust	
8,70 - 8,80	the same stone, at the beginning hard - changes to strongly disintegrating, wet, crumbling in hand, preserved compact cores, very soft	
8,80 - 8,90	completely disintegrated stone to soily matter	
8,90 - 9,00	hard stone (see upper line)	
9,00 - 9,30	weathered light coloured stone with brown-beige parts; cores seems to be compact, but pieces stay in hand	
9,30 - 9,70	the same stone (see upper line), but hard	
9,70 - 9,90	compact piece of gray stone, in the middle rusty-coloured clay-soily dolls, which is slimy in hands	
9,90 -10,00	light coloured crushed stone, breaking up in fingers to smaller pieces	
10,00 - 10,30	smaller pieces of the same stone with rusty-brown positions	
10,30 - 10,40	completely weathered, clay-silty sedimenty, strongly disintegrating	
10,40 - 10,45	light gray to light brown strongly disintegrating stone	
10,45 - 10,60	same, in some places strongly partially weathered	
10,60 - 11,00	strongly partially weathered, see upper line, in some places compact cores	
11,00 - 12,00	weathered magmatic stone (quartz porphyre, paleoryolite), in some places harder positions	

This page is left blank on purpose.

B. APPENDIX B – WALL MODEL ARRANGEMENTS

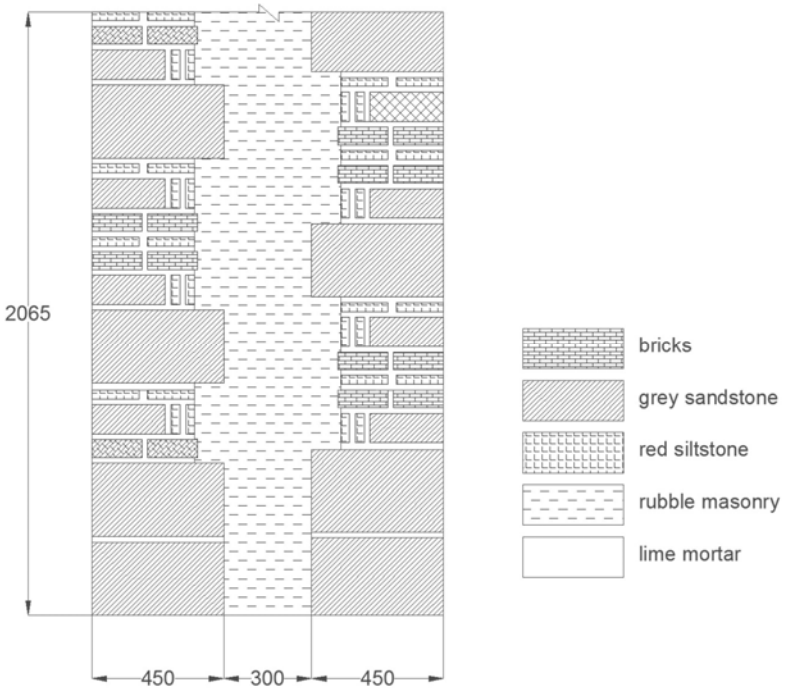

Figure B.1. Sectional wall configuration 1 with legend

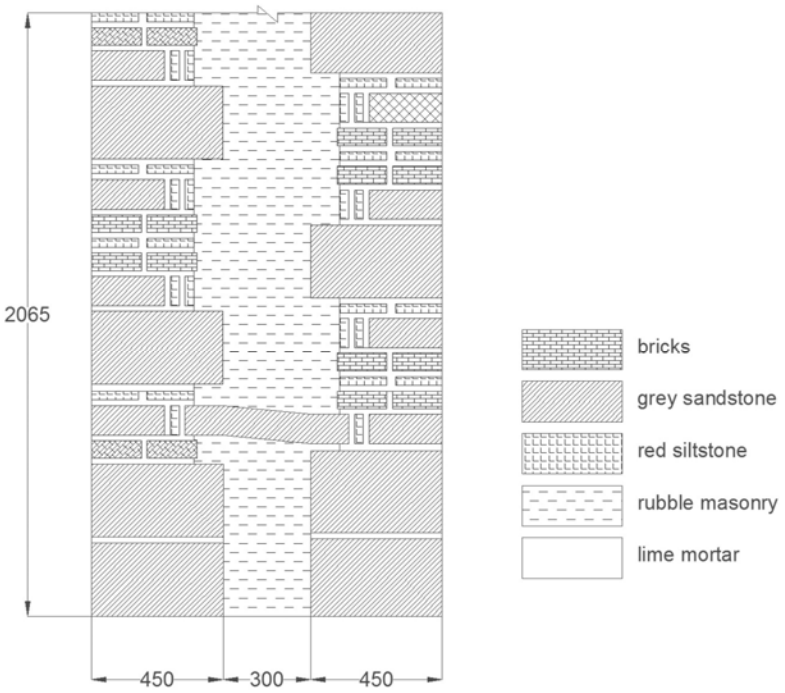

Figure B.2. Sectional wall configuration 2 with connecting stones and legend

Figure B.3. Derivation of sectional wall configuration 2

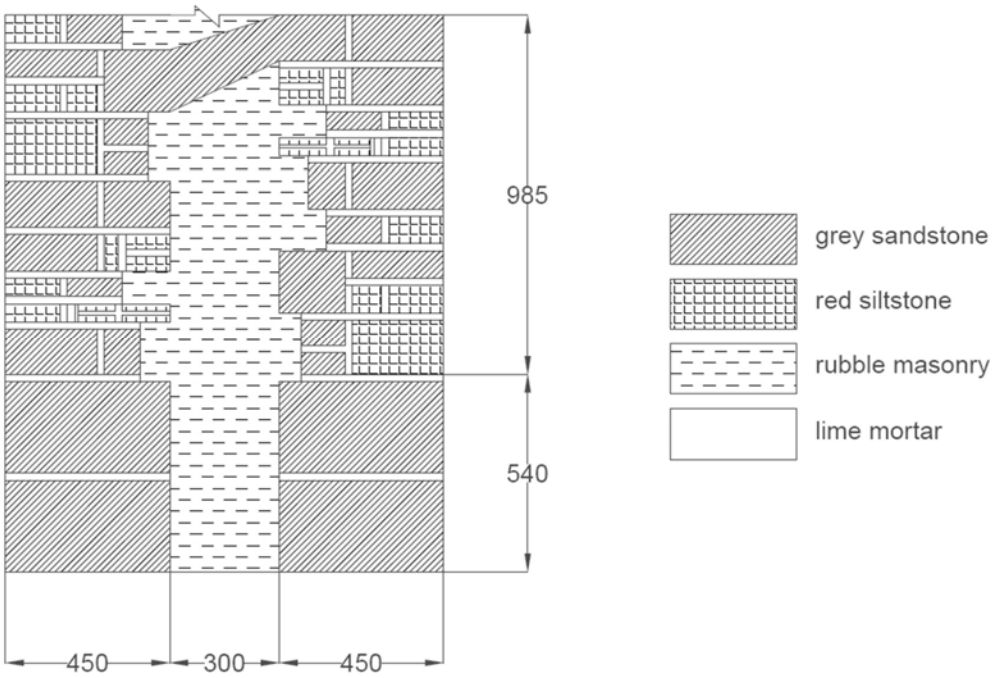

Figure B.4. Sectional wall configuration 2 with connecting stones and legend

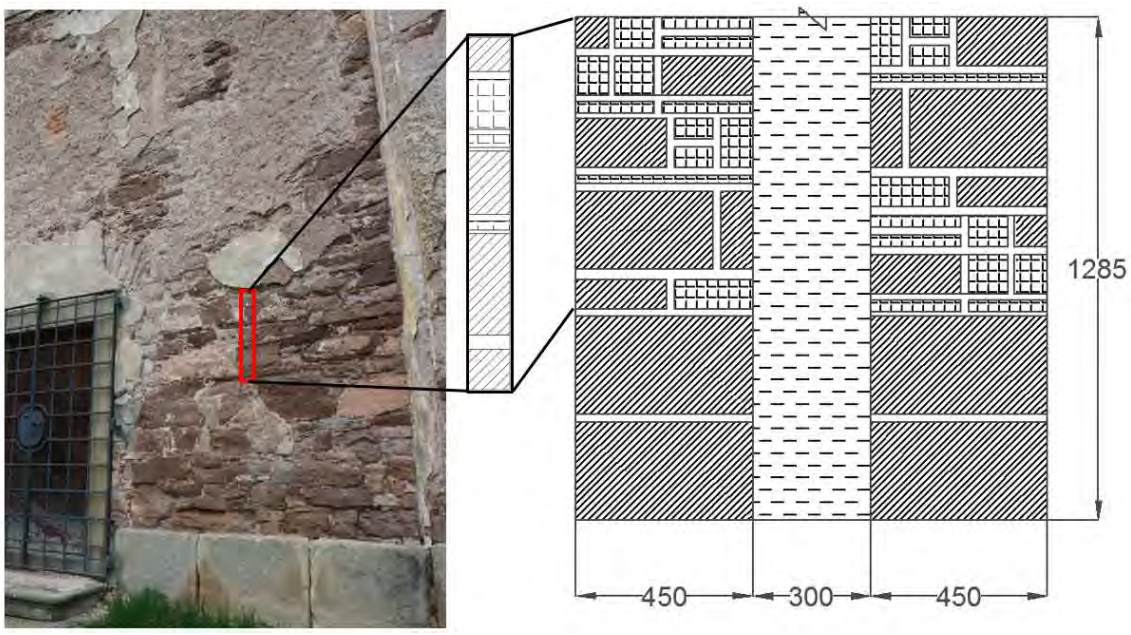

Figure B.5. Derivation of sectional wall configuration 3

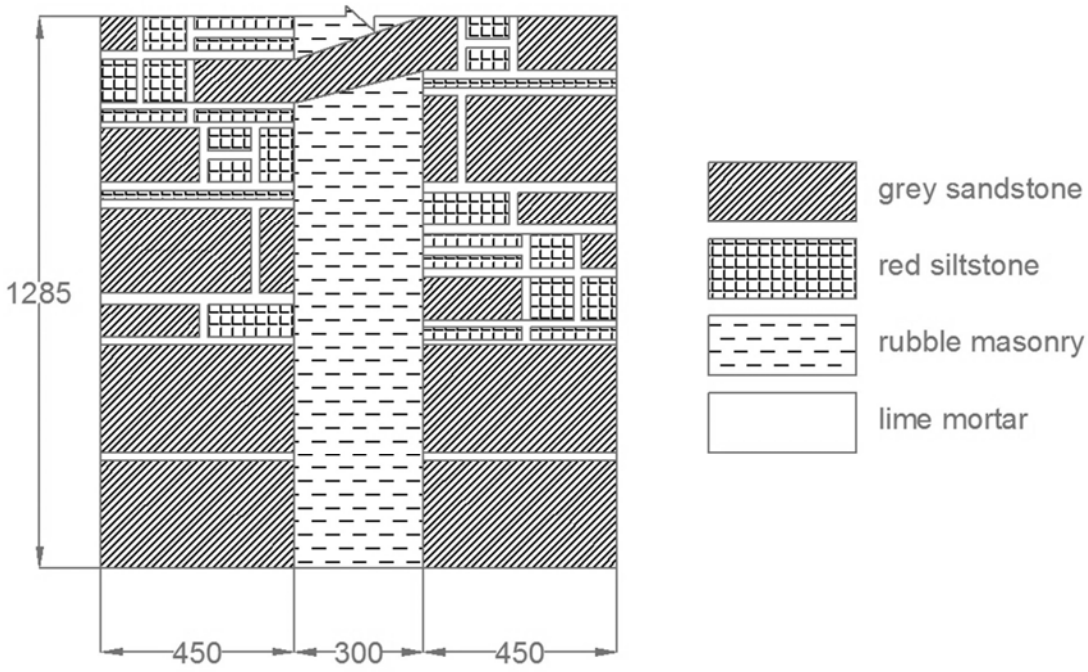

Figure B.6. Sectional wall configuration 3 with connecting stones and legend

Figure B.7. Derivation of sectional wall configuration 4

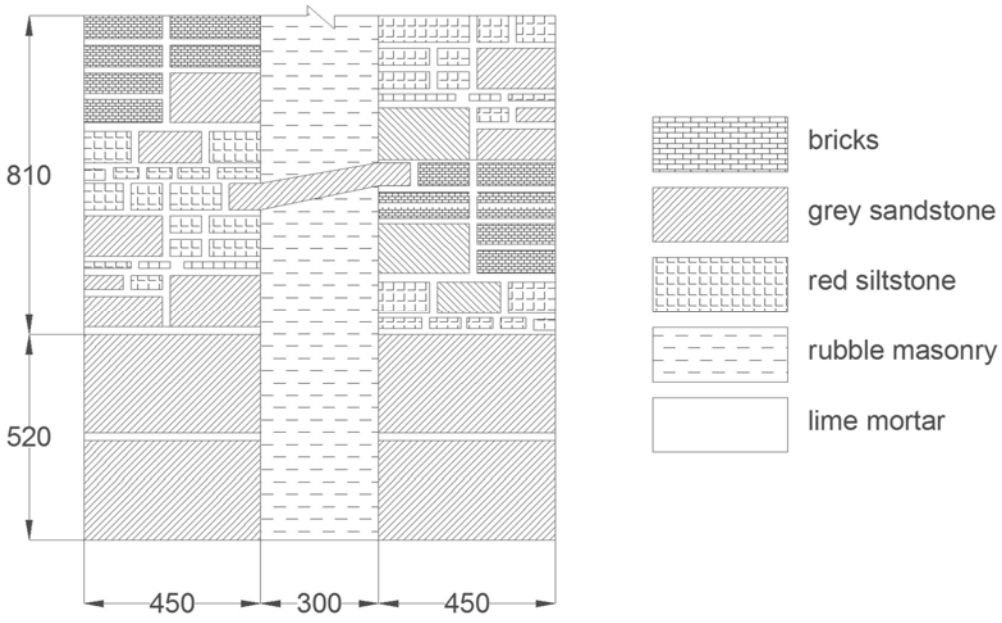

Figure B.8. Sectional wall configuration 4 with connecting stones and legend

Figure B.9. Location longitudinal wall configuration 1 is derived from

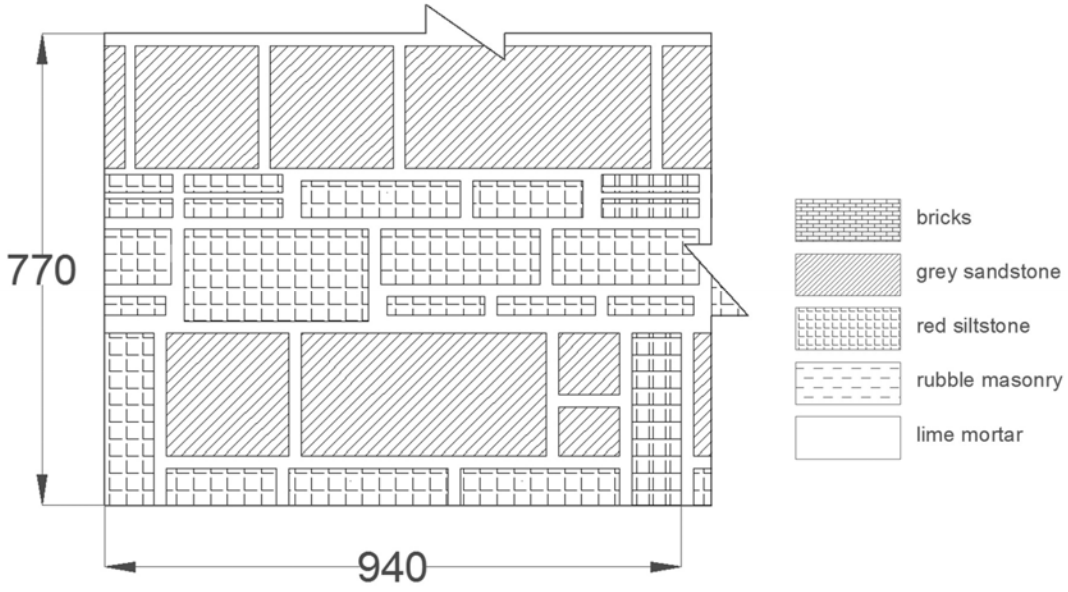

Figure B.10. Longitudinal wall configuration 1 and legend

Figure B.11. Location longitudinal wall configuration 2 is derived from

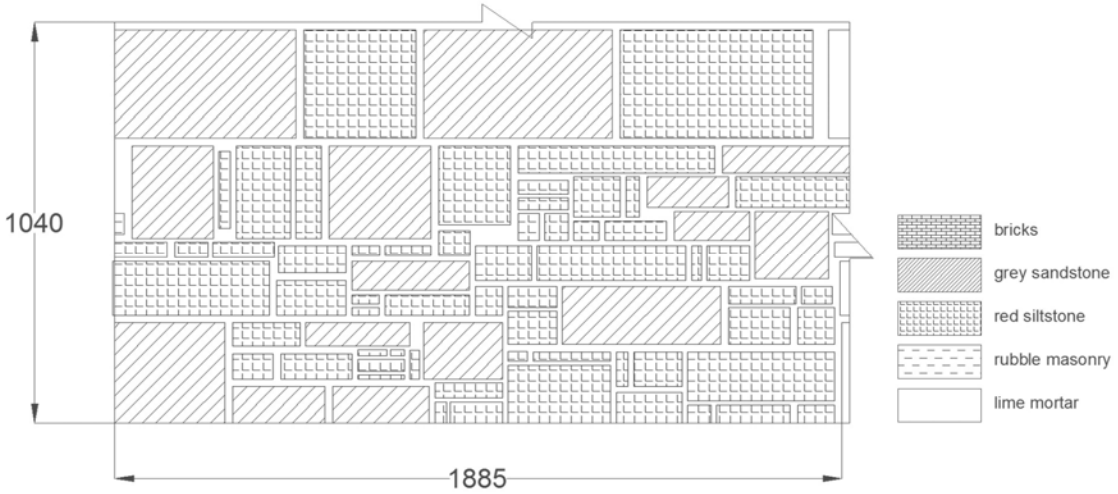

Figure B.12. Longitudinal wall configuration 2 and legend

C. APPENDIX C – APPLIED LOAD IN ATENA 2D BREAKDOWNS

Table C.1. Breakdown of loads acting per meter span of the sectional model of the enclosure wall excluding self-weight of the wall modelled

Element	Description	Load span (m)	Load area (m^2)	Unit Load (kN/m^2)	Unit Load (kN/m^3)	Total load (kN/m)	
Dead Load							
Roof	Pointed roof beam, bracing, cover and cladding	14.1		3		42.3	
Roof space	Access platform and beam supporting platform	10		2.5		25	
	Wooden ceiling and beam supporting it	10		2.5		25	
Wall	Ring beam		1.5		20	30	
	Wall above the wall modelled		7		20	140	
						Total Dead Load	**262.3**
Live Load							
Roof space	Live load on roof space	10		0.4		4	
						Total Live Load	**4**
Snow Load							
Roof	Snow load above pointed roof	14.1		0.62		8.742	
						Total Snow Load	**8.742**
Wind Load							
Roof	Wind pressure acting on the roof	14.1		0.79		11.139	
						Total Wind Load	**11.139**

Table C.2. Load combinations assumed in modelling and the maximum ultimate load for sectional wall modelling

No	Load Combination	Total Load (kN/m)
1	1.35DL + 1.5LL + 1.5 (0.5SL + 0.2WL)	370.0032
2	1.35DL + 1.5LL + 1.5 (0.6WL + 0.2SL)	372.7527
3	1.35DL + 1.5WL + 1.5 (0.6SL)	378.6813
4	1.35DL + 1.5SL + 1.5 (0.5WL)	375.57225
	Maximum ULS Load	**378.6813**

Table C.3. Breakdown of loads acting per meter span of the longitudinal model of the enclosure wall excluding self-weight of the wall modelled

Element	Description	Load span (m)	Load area (m^2)	Unit Load (kN/m^2)	Unit Load (kN/m^3)	Total load (kN/m)	
Dead Load							
Roof	Pointed roof beam, bracing, cover and cladding	14.1		3		42.3	
Roof space	Access platform and beam supporting platform	10		2.5		25	
	Wooden ceiling and beam supporting it	10		2.5		25	
Wall	Ring beam		1.8		20	36	
	Wall above the wall modelled		10.8		20	216	
						Total Dead Load	**344.3**
Live Load							
Roof space	Live load on roof space	10		0.4		4	
						Total Live Load	**4**
Snow Load							
Roof	Snow load above pointed roof	14.1		0.62		8.742	
						Total Snow Load	**8.742**
Wind Load							
Roof	Wind pressure acting on the roof	14.1		0.79		11.139	
						Total Wind Load	**11.139**

Table C.4. Load combinations assumed in modelling and the maximum ultimate load for longitudinal wall modelling

No	Load Combination	Total Load (kN/m)
1	1.35DL + 1.5LL + 1.5 (0.5SL + 0.2WL)	480.7032
2	1.35DL + 1.5LL + 1.5 (0.6WL + 0.2SL)	483.4527
3	1.35DL + 1.5WL + 1.5 (0.6SL)	489.3813
4	1.35DL + 1.5SL + 1.5 (0.5WL)	486.27225
	Maximum ULS Load	**489.3813**

D. APPENDIX D – ATENA LOAD DISPLACEMENT CURVES

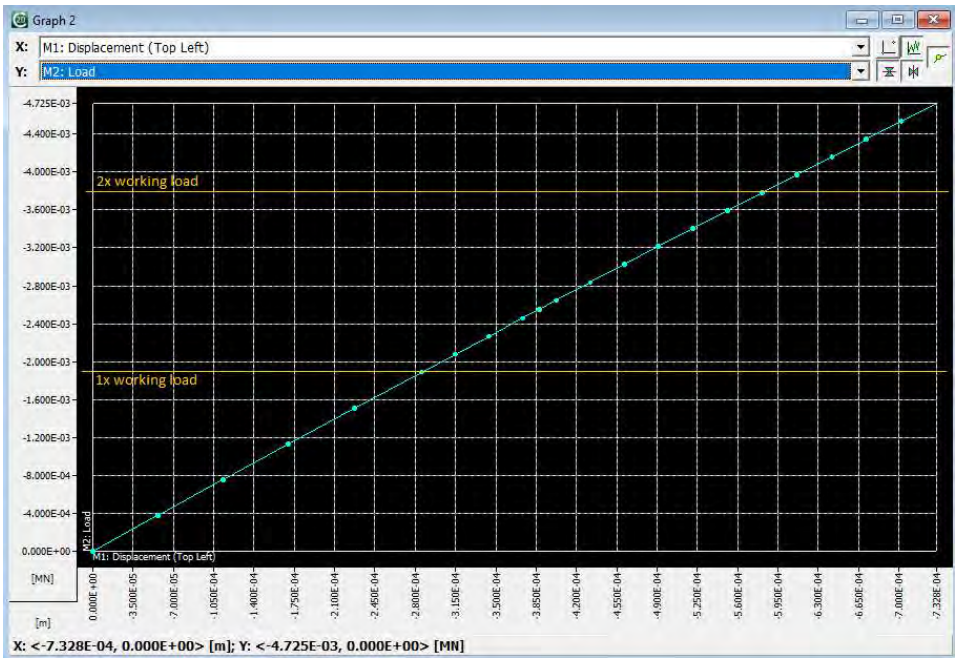

Figure D.1. Load-displacement curve of sectional wall of wall configuration 1 with connecting tie stones

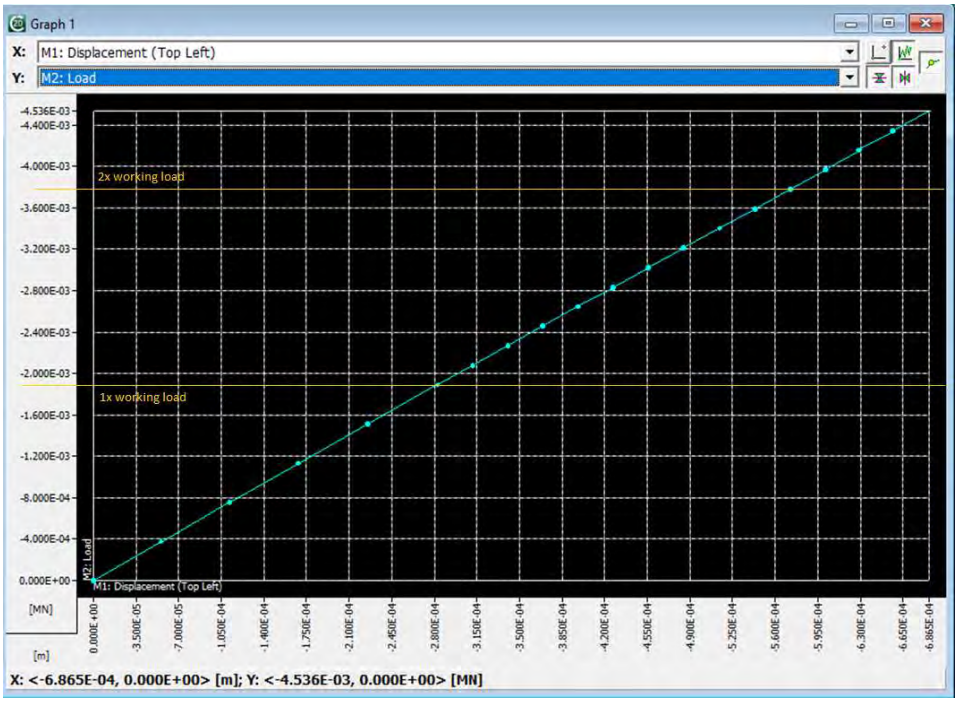

Figure D.2. Load-displacement curve of sectional wall of wall configuration 1 without connecting tie stones

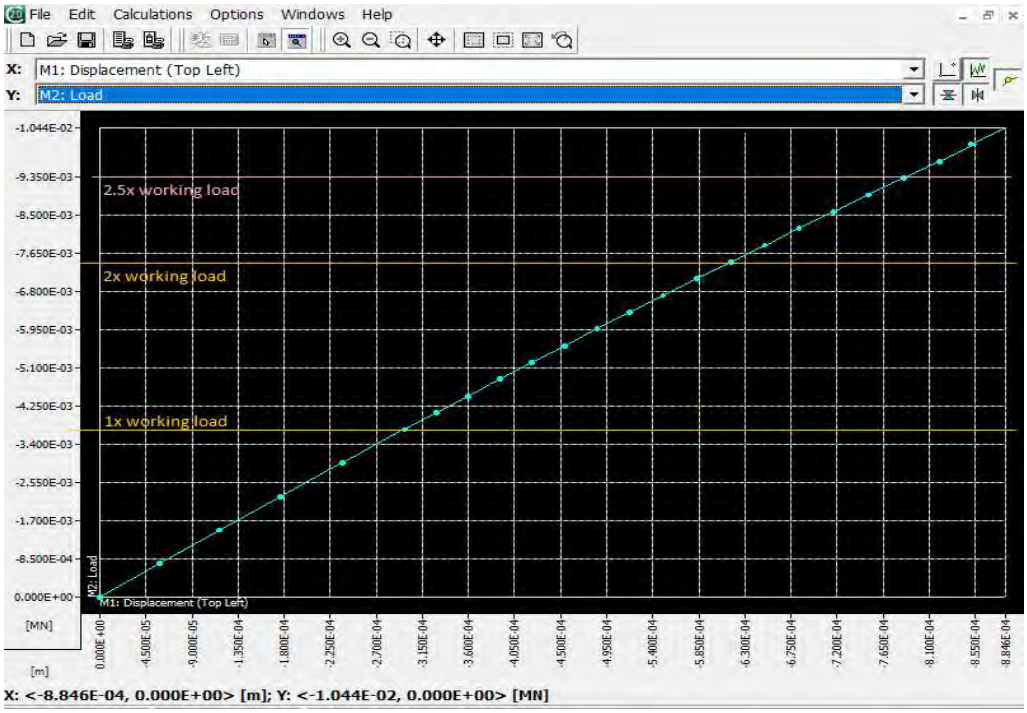

Figure D.3. Load-displacement curve of sectional wall of wall configuration 2 with connecting tie stones

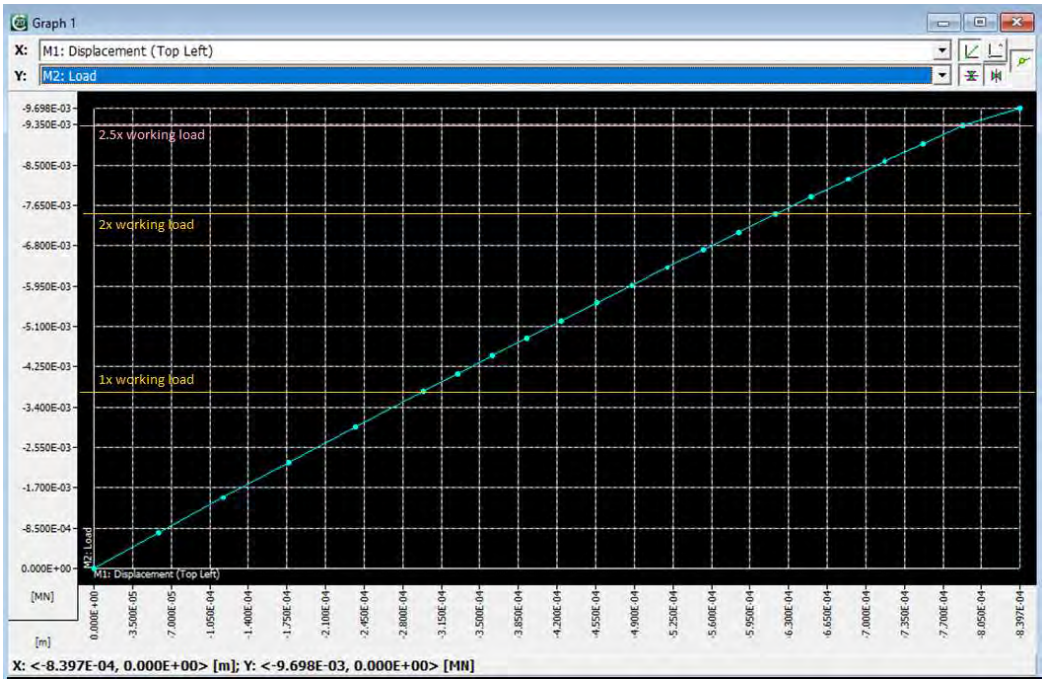

Figure D.4. Load-displacement curve of sectional wall of wall configuration 2 without connecting tie stones

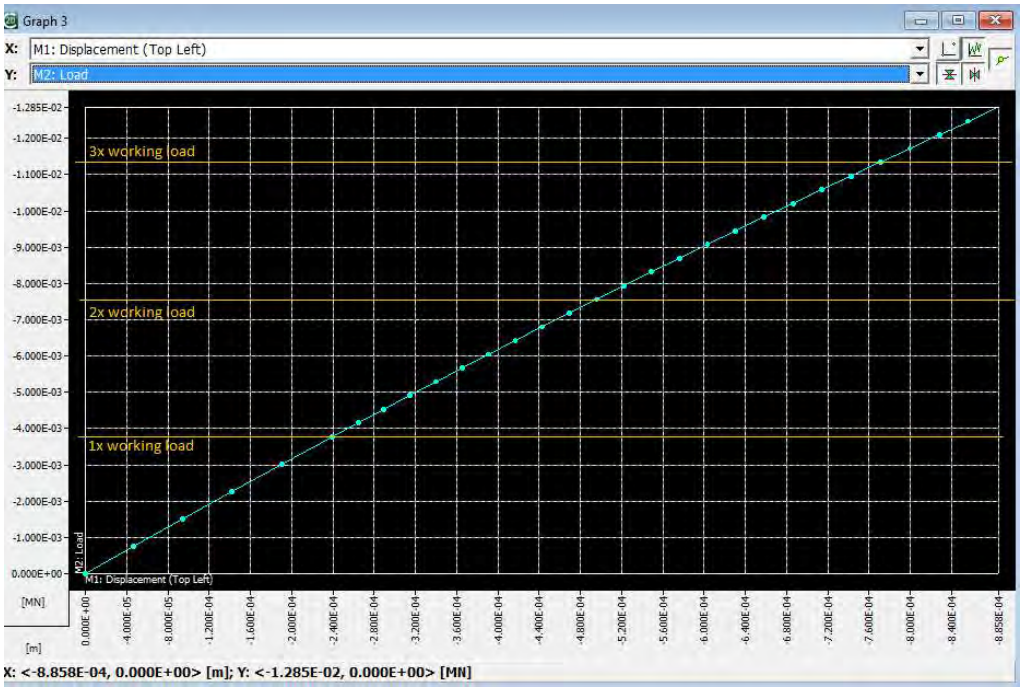

Figure D.5. Load-displacement curve of sectional wall of wall configuration 3 with connecting tie stones

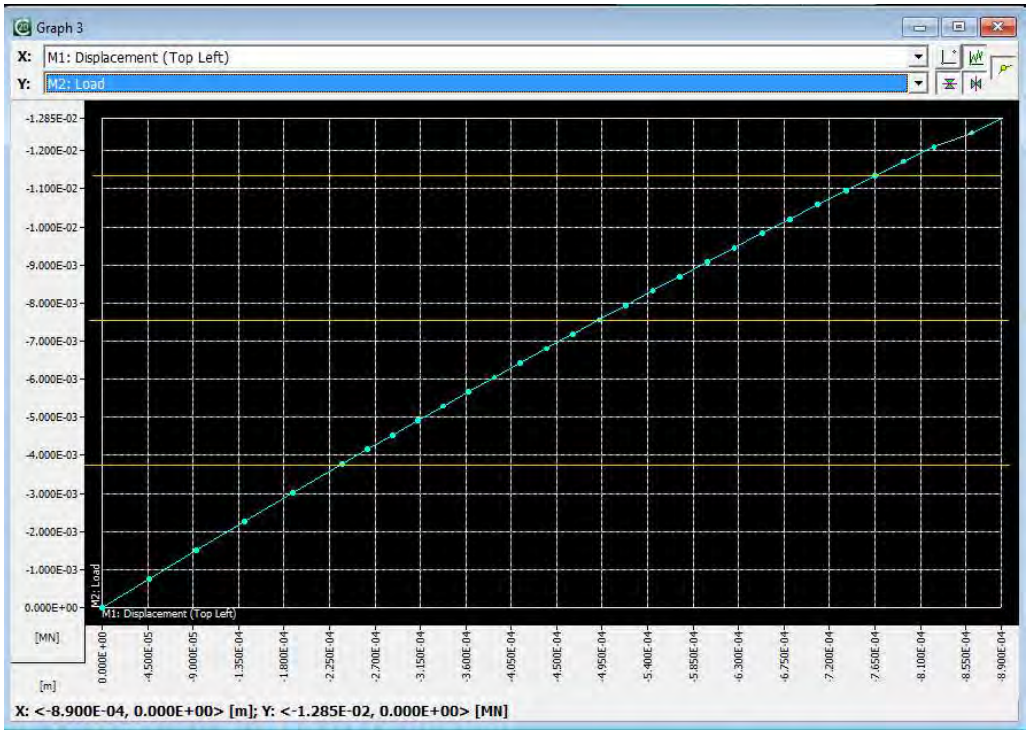

Figure D.6. Load-displacement curve of sectional wall of wall configuration 3 without connecting tie stones

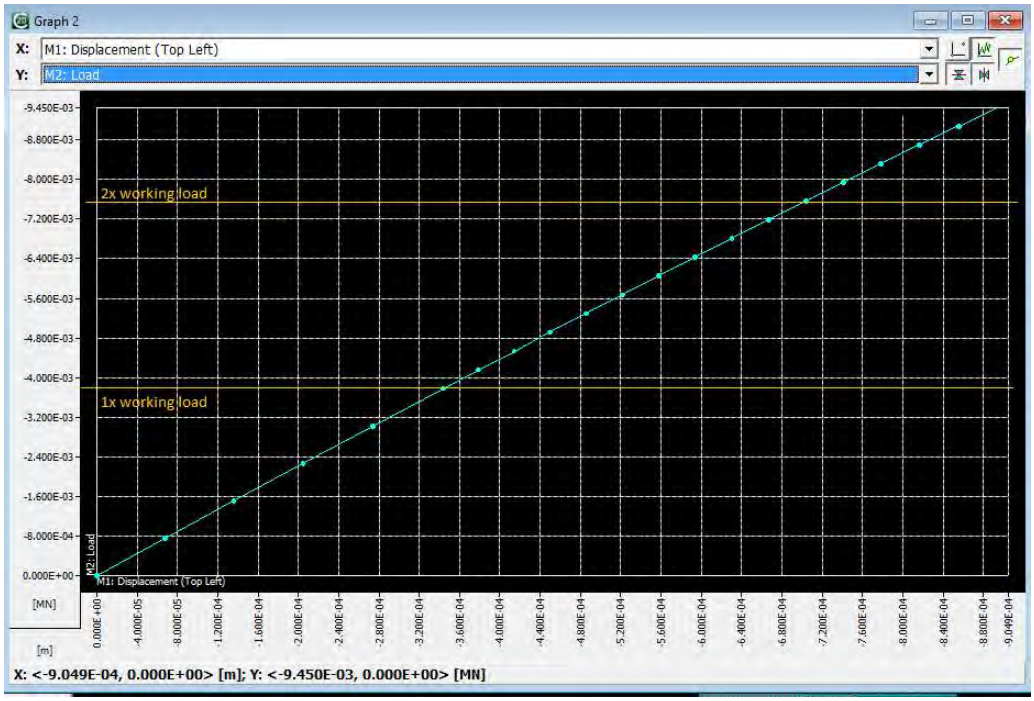

Figure D.7. Load-displacement curve of sectional wall of wall configuration 4 with connecting tie stones

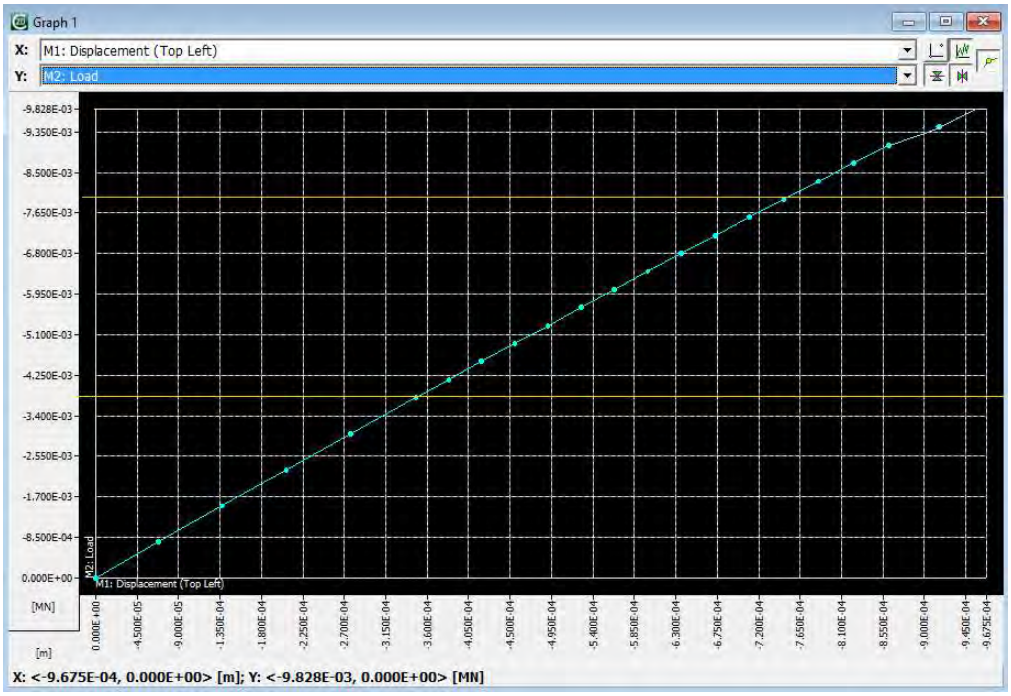

Figure D.8. Load-displacement curve of sectional wall of wall configuration 3 without connecting tie stones

E. APPENDIX E – APPLIED LOAD IN GEO5 AND ATENA-GID BREAKDOWNS

Table E.1. Breakdown of loads acting per meter span of the wall excluding its own self-weight for modelling in Geo5 and 3D ATENA-Gid Model

Element	Description	Load span (m)	Load area (m^2)	Unit Load (kN/m^2)	Unit Load (kN/m^3)	Total load (kN/m)	
Dead Load							
Roof	Pointed roof beam, bracing, cover and cladding	14.1		3		42.3	
Roof space	Access platform and beam supporting platform	10		2.5		25	
	Wooden ceiling and beam supporting it	10		2.5		25	
Wall	Ring beam		1.8		20	36	
						Total Dead Load	**128.3**
Live Load							
Roof space	Live load on roof space	10		0.4		4	
						Total Live Load	**4**
Snow Load							
Roof	Snow load above pointed roof	14.1		0.62		8.742	
						Total Snow Load	**8.742**
Wind Load							
Roof	Wind pressure acting on the roof	14.1		0.79		11.139	
						Total Wind Load	**11.139**

Table E.2. Load combinations assumed in modelling and the maximum ultimate surcharge on enclosure wall model for modelling in Geo5 and 3D ATENA Model

No	Load Combination	Total Load (kN/m)
1	1.35DL + 1.5LL + 1.5 (0.5SL + 0.2WL)	189.1032
2	1.35DL + 1.5LL + 1.5 (0.6WL + 0.2SL)	191.8527
3	1.35DL + 1.5WL + 1.5 (0.6SL)	197.7813
4	1.35DL + 1.5SL + 1.5 (0.5WL)	194.67225
	Maximum ULS Load	**197.7813**

This page is left blank on purpose.

F. APPENDIX F – GEO5 RESULTS

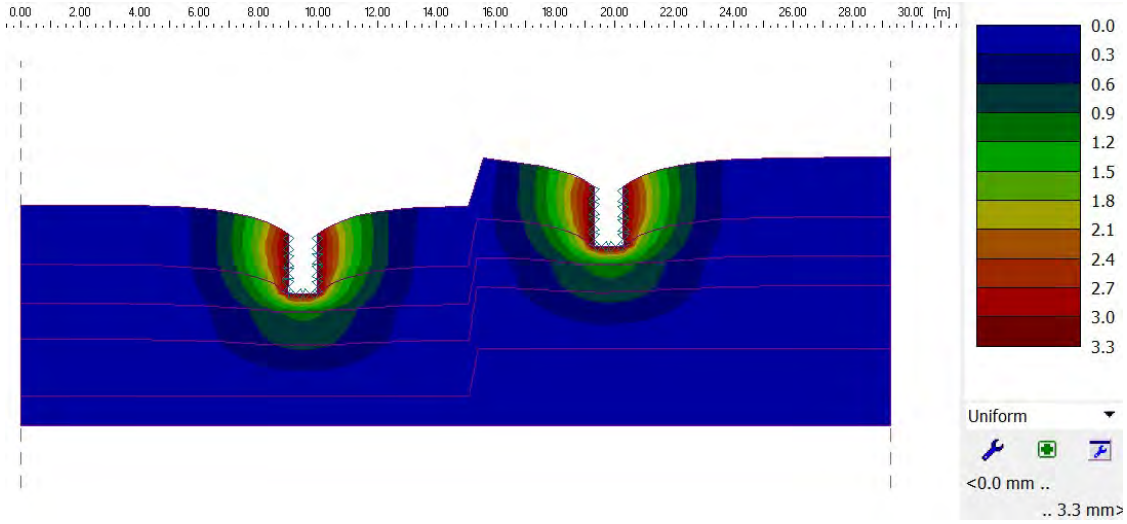

Figure F.1. Deformation of the soil under foundation due to the church load on the presumed original soil condition

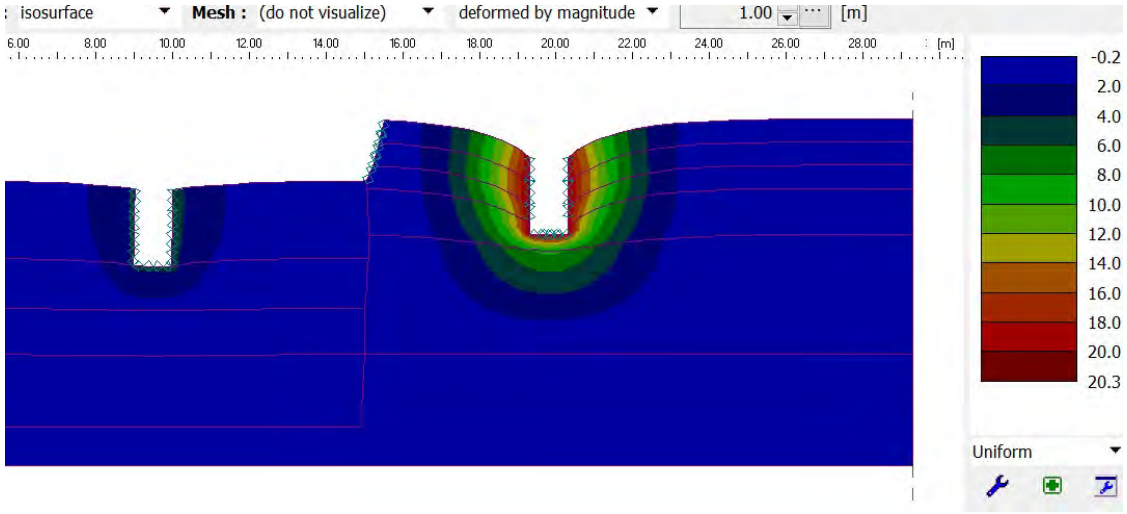

Figure F.2. Deformation of the soil under foundation due to the church load on the current soil condition

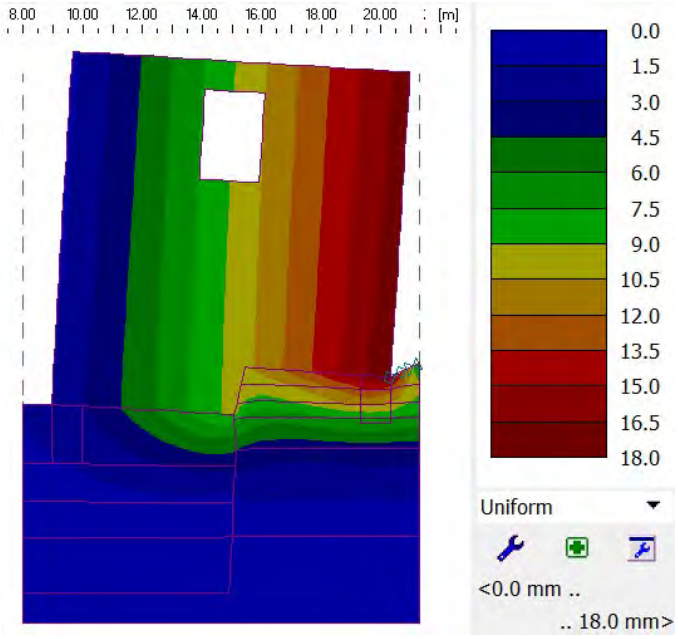

Figure F.3. imposed deformation of eastern facade with the altered load on the model to analyse the wall stresses

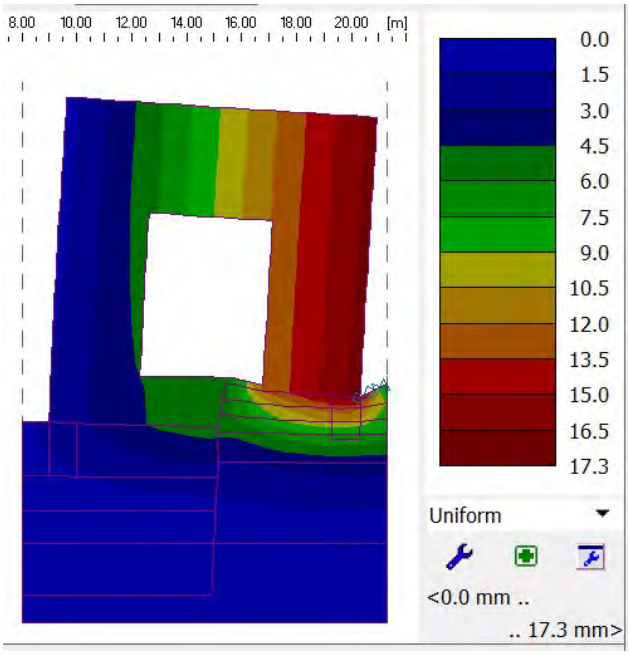

Figure F.4. Imposed deformation of western facade with the altered load on the model to analyse the wall stresses

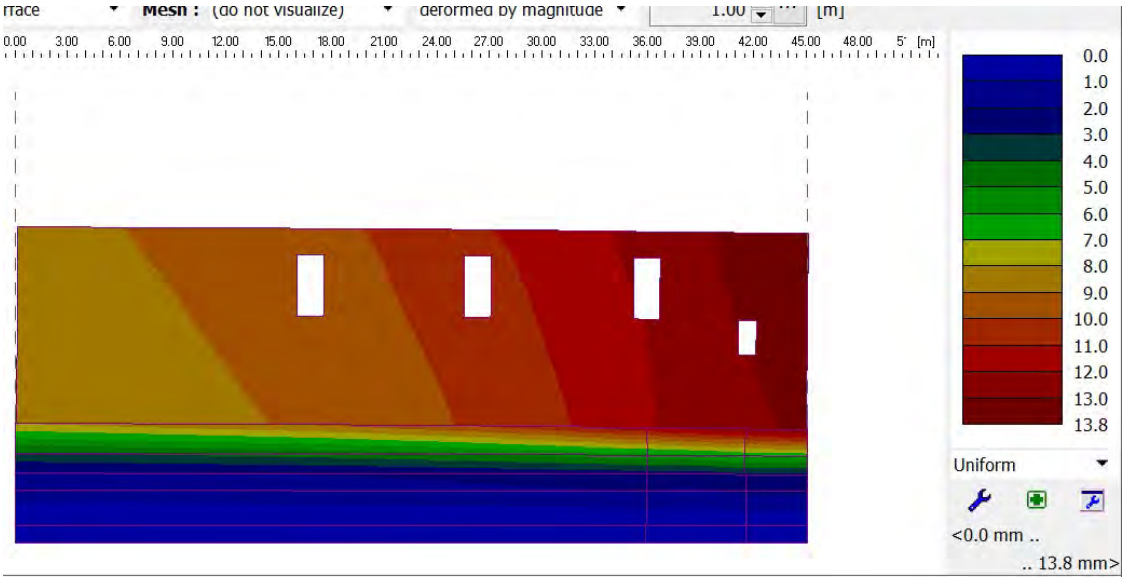

Figure F.5. Deformation of the southern longitudinal wall and the subsoil due to the church load on the current soil condition

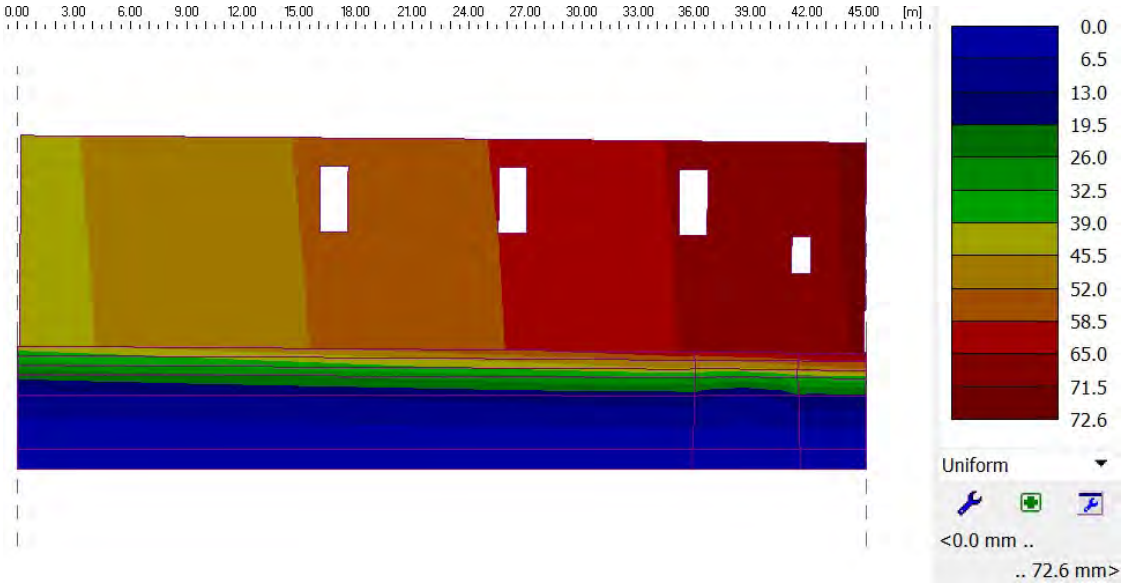

Figure F.6. Deformation of the northern longitudinal wall and the subsoil due to the church load on the current soil condition